NASA CR-112158

THREE-DIMENSIONAL COMPRESSIBLE BOUNDARY-LAYER COMPUTATIONS FOR A FINITE SWEPT WING

By J. F. Nash and R. M. Scruggs

Prepared under Contract No. NAS1-10823 by
LOCKHEED-GEORGIA COMPANY
Marietta, Georgia

for Langley Research Center

NATIONAL AERONAUTICS AND SPACE ADMINISTRATION

For sale by the Clearinghouse for Federal Scientific and Technical Information
Springfield, Virginia 22151 - Price

NASA CR-112158

THREE-DIMENSIONAL COMPRESSIBLE BOUNDARY-LAYER COMPUTATIONS FOR A FINITE SWEPT WING

By J. F. Nash and R. M. Scruggs

Prepared under Contract No. NAS1-10823 by
LOCKHEED-GEORGIA COMPANY
Marietta, Georgia

for Langley Research Center

NATIONAL AERONAUTICS AND SPACE ADMINISTRATION

For sale by the Clearinghouse for Federal Scientific and Technical Information
Springfield, Virginia 22151 - Price

FOREWORD

This work was performed under Contract NAS1-10823 for the National Aeronautics and Space Administration, Langley Research Center. The Technical Monitor was Dr. R. T. Whitcomb.

The authors wish to acknowledge the assistance of Dr. S. Y. Ruo in programming the laminar boundary-layer method, and the assistance of Mr. R. R. Whipkey in the analysis and presentation of the data.

CONTENTS

CONTENTS (Cont'd)

LIST OF TABLES

LIST OF FIGURES

LIST OF FIGURES (Cont'd)

THREE-DIMENSIONAL COMPRESSIBLE BOUNDARY-LAYER COMPUTATIONS FOR A FINITE SWEPT WING

By

J. F. Nash
R. M. Scruggs

SUMMARY

Three-dimensional, compressible turbulent boundary-layer calculations have been performed for the finite supercritical wing of the NASA modified F8 transonic research airplane.

Data on the boundary-layer thickness, displacement thickness, skin friction components, and integrated streamwise skin friction are presented for points along the streamwise stations at which the pressure measurements were previously made. Representative velocity profiles are shown, and boundary-layer-thickness contour plots and skin-friction vector plots are presented.

Results are given for a Reynolds number of 1.5 million per foot, and for Mach numbers of 0.50 and 0.99.

INTRODUCTION

Objective of the Work

This report describes the calculation of the three-dimensional, compressible turbulent boundary layer on the supercritical finite swept wing of the NASA modified F8 transonic research aircraft. The calculations are based on the surface pressure distributions measured in wind-tunnel tests, but a higher Reynolds number of 1.5 million per foot was assumed. Results are presented for two Mach numbers: 0.50 and 0.99.

The main objective was to generate data on the boundary-layer thickness, displacement thickness, and the magnitude and direction of the skin friction. Integrated streamwise skin friction data are presented for use in drag estimates, and three-dimensional velocity profiles are available at selected points on the wing. The results of the calculations are presented in detail herein. Also, a description is given of the turbulent boundary-layer calculation method and of the way in which the calculation was performed. The results are summarized and some remarks are made about the overall picture presented by the results. Finally, a few recommendations are made for further development work on the calculation method to facilitate its application to similar situations in the future.

Evolution of the Calculation Method

Very substantial advances have been made during the last four to five years in the technology associated with the calculation of three-dimensional turbulent boundary layers. The method of Nash (ref. 1) provided the capability of calculating detailed profiles of mean velocity and turbulent shear stress in a fully three-dimensional flow field with arbitrary pressure gradients and with no restriction to small crossflows. The method involved the numerical integration of the differential equations of motion together with an empirical equation, for the Reynolds stress, based on the turbulent kinetic-energy equation. This method was restricted to incompressible flow over plane or developable surfaces. It has since been extended to flow over a generally curved surface, the only restriction being that the principal radii of curvature must be large compared with the boundary-layer thickness (refs. 2 and 3) and a more accurate explicit numerical scheme has also been incorporated (ref. 4).

The method has been subjected to stringent tests for internal numerical precision, and in-depth comparisons with available experimental data have been made. The method has been applied to infinite swept wings (ref. 5) and, on a quasi-steady basis, to the rotor of a helicopter in forward flight (ref. 6). Very recently the method has been extended to unsteady flows over infinite yawed cylinders (ref. 7), with the aim of treating the rotor-blade case as a fully time-dependent flow.

In the present work the method is extended to compressible flows, and this is the first time that fully three-dimensional compressible turbulent boundary-layer calculations have been performed. The extension to compressible flow is made with the aid of the Crocco relation for temperature, and one would expect the method to be valid up to Mach numbers of at least two in the absence of heat transfer.

Method of Approach

It is a theorem of differential geometry that there is at least one orthogonal curvilinear coordinate system (x, y, z) which can be wrapped around any given body such that its (i.e. the body) surface is represented by $y = 0$. It would thus have been possible, in principle, to find a coordinate system in which $y = 0$ represented the surface of the wing, and in which the intersection $x = 0$, $y = 0$ represented the leading edge, and the intersection $x = 1$, $y = 0$ represented the trailing edge. One way to approach the present calculatous would have been to apply the method to this coordinate system, and integrate the equations from $x = 0$ to $x = 1$. It was decided not to do the calculations this way, partly, because of the practical problem of determining the coordinate system, and, partly, because the imposition of boundary conditions would have been difficult: it is easier to impose boundary conditions on surfaces $x =$ constant or $z =$ constant than on planes which cut across them. Instead, it was decided to segment the wing into an inboard and an outboard portion and fit a separate coordinate system to each. The calculation would then be done in two stages with appropriate matching along the interface between the two portions. Fortunately, the wing geometry lent itself well to segmentation, yielding a triangular delta planform inboard and a straight tapered planform outboard (Figure 1). A simple conical coordinate system could thus be fitted to each.

NOTATION

a_1, a_2	Empirical functions in Equations (9) and (10)
c	Local chord
c_{d_f}	Sectional skin-friction drag coefficient
C_{D_f}	Integrated streamwise skin friction (Equation 17)
C_p	Pressure coefficient
h_1, h_3	Metric coefficients
K_{13}, K_{31}	Curvature parameters
L	Dissipation length
M	Mach number
p	Static pressure
Q	Resultant velocity: $Q^2 = U^2 + W^2$, to the boundary-layer approximation
s	Length of a line in space
U, V, W	Mean velocity components in the x-, y-, z-directions, respectively
u, v, w	Fluctuating velocity components corresponding to U, V, W
X, Y, Z	Rectangular coordinates, with X lying along the aircraft centerline and Y measured spanwise
X_ℓ	Streamwise distance from the leading edge (local)
x, y, z	Orthogonal curvilinear coordinates, with y measured normal to the wing surface
Γ	Constant in Equations (11)
δ	Boundary-layer thickness
δ^*	Displacement thickness (see Equation 13)
Λ	Angle of sweep
ρ	Density of air

Φ_x, Φ_z	Functions appearing in Equations (9), (10)
τ_{w_x}, τ_{w_z}	Skin-friction components in the x-, z- directions, respectively
τ_{w_s}, τ_{w_n}	Skin-friction coefficients in the streamwise and (negative) spanwise directions, respectively

Subscripts

e	Value at the outer edge of the boundary layer
∞	Value in the free stream at infinity

OUTLINE OF THE CALCULATION METHOD

Governing Equations

An orthogonal curvilinear coordinate system (x, y, z) is chosen, with the body represented by the surface y = 0; h_1, h_3 are the metric coefficients for distances measured in the x-, z- directions, such that the length, ds, of a line element is given by

$$(ds)^2 = h_1^2(dx)^2 + (dy)^2 + h_3^2(dz)^2 \tag{1}$$

The curvature parameters K_{13}, K_{31} are defined by

$$K_{13} = \frac{1}{h_1 h_3}\frac{\partial h_1}{\partial z} \quad , \quad K_{31} = \frac{1}{h_1 h_3}\frac{\partial h_3}{\partial x} \tag{2}$$

and represent the geodesic curvatures of the lines x = constant, z = constant, respectively. The metric coefficient, h_2, associated with distances measured in the y-direction is chosen to be unity, with the result that the curvature parameters K_{21}, K_{23} are identically zero 3/.

The two momentum equations for flow in a compressible turbulent boundary layer, in terms of the above coordinate system, are

$$\frac{U}{h_1}\frac{\partial U}{\partial x} + V\frac{\partial U}{\partial y} + \frac{W}{h_3}\frac{\partial U}{\partial z} + (K_{13}U - K_{31}W)W + \frac{1}{\rho h_1}\frac{\partial p}{\partial x} + \frac{1}{\rho}\frac{\partial}{\partial y}(\rho\,\overline{uv}) = 0 \tag{3}$$

$$\frac{U}{h_1}\frac{\partial W}{\partial x} + V\frac{\partial W}{\partial y} + \frac{W}{h_3}\frac{\partial W}{\partial z} + (K_{31}W - K_{13}U)U + \frac{1}{\rho h_3}\frac{\partial p}{\partial z} + \frac{1}{\rho}\frac{\partial}{\partial y}(\rho\,\overline{vw}) = 0 \tag{4}$$

where U, V, W are the mean velocity components in the x-, y-, z-directions, respectively, u, v, w are the corresponding fluctuating components. A bar over products of fluctuating quantities denotes the time average. The continuity equation can be written

$$\frac{1}{h_1}\frac{\partial}{\partial x}(\rho U) + \frac{\partial}{\partial y}(\rho V) + \frac{1}{h_3}\frac{\partial}{\partial z}(\rho W) + \rho(K_{31}U + K_{31}W) = 0 \tag{5}$$

In equations (3) through (5), V is interpreted to mean

$$V + \frac{1}{\rho}(\overline{\rho' v}) \tag{6}$$

where ρ' is the fluctuating component of the density.

It is assumed that the temperature at any point in the flow can be related to the magnitude of the local velocity vector, Q, via the Crocco relation. Accordingly, the density at a point within the boundary layer is related to the density and to the Mach number at the outer edge of the boundary layer by

$$\frac{\rho_e}{\rho} = 1 + \frac{\gamma - 1}{2} r M_e^2 \left(1 - \frac{Q^2}{Q_e^2} \right) \tag{7}$$

where, r is the recovery factor (taken to be 0.89), and Q is given by

$$Q^2 = U^2 + W^2 \tag{8}$$

to the boundary-layer approximation. The assumption is made in Equation (7) that the wall is adiabatic.

The components $-\rho\overline{uv}$, $\rho\overline{vw}$ of the Reynolds stress are determined from a pair of rate equations 2/, 3/:

$$\frac{U}{h_1}\frac{\partial}{\partial x}(\overline{uv}) + V\frac{\partial}{\partial y}(\overline{uv}) + \frac{W}{h_3}\frac{\partial}{\partial z}(\overline{uv}) + (K_{13}U - K_{31}W)\overline{vw}$$
$$+ 2a_1\left[(\overline{uv}^2 + \overline{vw}^2)^{1/2}\frac{\partial U}{\partial y} + \Phi_x + \frac{\partial}{\partial y}(a_2\,\overline{uv})\right. \tag{9}$$
$$\left. + \frac{\overline{uv}}{L}(\overline{uv}^2 + \overline{vw}^2)^{1/4}\right] = 0$$

$$\frac{U}{h_1}\frac{\partial}{\partial x}(\overline{vw}) + V\frac{\partial}{\partial y}(\overline{vw}) + \frac{W}{h_3}\frac{\partial}{\partial z}(\overline{vw}) + (K_{31}W - K_{13}U)\overline{uv}$$
$$+ 2a_1\left[(\overline{uv}^2 + \overline{vw}^2)^{1/2}\frac{\partial W}{\partial y} + \Phi_z + \frac{\partial}{\partial y}(a_2\,\overline{vw})\right. \tag{10}$$
$$\left. + \frac{\overline{vw}}{L}(\overline{uv}^2 + \overline{vw}^2)^{1/4}\right] = 0$$

where Φ_x, Φ_z are given by

$$\Phi_x = \Gamma \left[(\overline{uv}^2 + \overline{vw}^2)^{1/2} \frac{\partial U}{\partial y} + \overline{uv} \left\{ \left(\frac{\partial U}{\partial y} \right)^2 + \left(\frac{\partial W}{\partial y} \right)^2 \right\}^{1/2} \right]$$

$$\Phi_z = \Gamma \left[(\overline{uv}^2 + \overline{vw}^2)^{1/2} \frac{\partial W}{\partial y} + \overline{vw} \left\{ \left(\frac{\partial U}{\partial y} \right)^2 + \left(\frac{\partial W}{\partial y} \right)^2 \right\}^{1/2} \right] \qquad (11)$$

in which Γ is some large number (from experience, any number greater than about 4. Equations (11) cause the shear-stress "vector" to be aligned everywhere with the rate-of-strain vector:

$$\overline{uv} \Big/ \frac{\partial U}{\partial y} = \overline{vw} \Big/ \frac{\partial W}{\partial y} \qquad (12)$$

Equations (9) through (11) are identical to their incompressible counterparts. The assumption is made that they can be carried over without modification to compressible flows, and the further assumption is made that the empirical constant a_1 (= 0.15) and the empirical functions a_2 and L (Figure 2) are the same as in incompressible flow 2/, 3/. There is no direct experimental support for these assumptions in compressible three-dimensional flow, however they are probably valid at least up to about M = 2. In two-dimensions, they appear to be approximately valid up to higher Mach numbers: comparisons between calculations, performed by us using this method, and experimental data at M = 4, were reported by Peake et. al 8/. Bradshaw and Ferriss 9/ have also compared their method, which was the two-dimensional forerunner of the present method, with measurements.

Method of Solution

Equations (3), (4), (5), (9), and (10) form a hyperbolic set, and were integrated in a three-dimensional domain (x, y, z)(Figure 3) by an explicit finite-difference scheme based on the one-step staggered-mesh scheme of Reference 4/. The calculation proceeds in the x-direction, and values of the five dependent variables U, V, W, $\overline{uv}$, $\overline{vw}$, are computed on successive surfaces x = constant. Twenty collocation points were used in the y-direction (normal to the surface of this wing) and either six or seven in the z-direction.

As in the method of References 2/, 3/, the numerical solution was matched, at $y = 0.05$ (approximately), to a separate solution for the inner layer of the boundary layer. In the inner layer, it was assumed the resultant velocity, Q, and resultant skin friction, τ_w, mutually satisfy the law of the wall, this assumption provides an equation for τ_w in terms of Q at the matching station. The direction of the skin-friction vector was determined, as in References 2/, 3/, from an extrapolation in the polar plane (U, W), making use of the correct limiting value of $\partial^2 W/\partial U^2$ as $U \to 0$.

The boundary conditions at the surface of the wing, and at the outer surface of the integration domain (at $y = 1.25$, approximately), were handled in precisely the same manner as in References 2/, 3/, and the details will not be repeated here. The boundary conditions on the sides of the integration domains, for the inboard and outboard calculations, called for special treatment, however, and details of the procedures adopted will be given in the section: "ORGANIZATION OF THE CALCULATIONS," below.

Calculation of Displacement Thickness

In a fully three-dimensional boundary layer, the displacement thickness, δ^*, cannot be related directly to an integral of the velocity profile at one position on the body surface 3/. Instead, it is determined, from the normal component of velocity at the edge of the boundary layer, by means of the partial differential equation.

$$\frac{U_e}{h_1}\frac{\partial \delta^*}{\partial x} + \frac{W_e}{h_3}\frac{\partial \delta^*}{\partial z} = \left\{ V - (y - \delta^*)\frac{\partial V}{\partial y} \right\}_{y>\delta} \tag{13}$$

Once the velocity field is calculated, this equation can be integrated over the body surface to provide values of δ^*.

Equation (13) is compatible with the "two-dimensional" definition of δ^*:

$$\delta^* = \int_0^\infty \left(1 - \frac{\rho Q}{\rho_e Q_e}\right) dy \tag{14}$$

either where the velocity profiles are collateral (W proportional to U), or where deviations with respect to x or z vanish, as on an infinite swept wing.

ORGANIZATION OF THE CALCULATIONS

General Assumptions

The calculations were performed for Mach numbers of 0.5 and 0.99, and for a Reynolds number of 1.5×10^6 per foot. At this Reynolds number, the leading-edge sweep of the inboard wing is great enough to support turbulent flow along the attachment line, according to the criterion of Cumpsty and Head 10/. The assumption was therefore made that there was no laminar region on the inboard wing.

On the outboard wing, a laminar region can be expected to exist on account of the lower sweep angle, and transition to turbulent flow was assumed to occur at $x/c = 0.1$, where both x and c are measured along arcs of the conical coordinate system (see below).

Segmentation of the Wing

As stated in the INTRODUCTION, above, the wing was segmented into an inboard and an outboard portion (Figure 1). The inboard wing is delta-shaped in planform, bounded by two straight lines, one of which is parallel to the aircraft center line, and one of which is coincident with the highly swept inboard leading edge. The outboard wing has a straight, tapered planform. The fairing at the leading-edge break point, on the real wing, and a similar fairing on the trailing edge, are omitted from consideration in this idealized representation.

Coordinate Systems

A conical coordinate system was fitted to each portion of the wing. On the inboard wing different conical coordinate systems were used on the upper and lower surfaces because of the presence of the wing-fuselage junction on the lower surface. On the upper surface (Figure 4), the apex of the coordinate system is the intersection of the streamwise station: 0.044 semi-span, with the leading edge. This is the furthest inboard station at which pressure data were measured. On the lower surface (Figure 5), the apex is the intersection of streamwise station: 0.081 semi-span, with the leading edge. This station is approximately coincident with the side of the fuselage.

In each of the inboard conical coordinate systems, x is measured radially in inches from the apex; z is the angle in degrees between the ray in question and the center line of the aircraft. Thus, for the upper surface, z = 0 represents the streamwise station: 0.044 semi-span, and z = 18 represents the leading edge. For the lower surface, z = 0 represents the wing-fuselage junction. In the calculation, seven z-stations were used, corresponding to angles of 0, 3°, 6°, 9°, 12°, 15°, 18°.

The coordinates x, z may be related to rectangular coordinates X, Z, where the X-axis lies along the aircraft center-line and Z is measured spanwise (Z replaces Y in the notation of Reference 11/):

$$\left.\begin{aligned} X &= x\cos z + 118.0 \\ Z &= x\sin z + 11.38 \end{aligned}\right\} \quad \text{Upper Surface}$$

$$\left.\begin{aligned} X &= x\cos z + 149.0 \\ Z &= z\sin z + 21.0 \end{aligned}\right\} \quad \text{Lower Surface}$$

The metric coefficients for both inboard conical coordinate systems are given by:

$$\begin{aligned} h_1 &= 1 \\ h_3 &= 0.01745\,x \end{aligned} \tag{15}$$

The outboard coordinate system is common to both surfaces (Figure 6). On the outboard wing, x is measured along an arc which is orthogonal to both the leading edge and the trailing edge; z is measured inwards from the apex of the outboard coordinate system, which is beyond the wing tip. z is measured in inches, and x is expressed as a ratio of local radial chord such that x = 1 represents the trailing edge. For the present outboard wing, which has a small taper ratio, the radial chord is nearly equal to the chord measured normal to the average line of sweep. Six z-stations were used in the outboard calculation (see Figure 6).

Referring to Figure 7, the appropriate transformation from x, z to rectangular coordinates: X, Z, is:

$$\begin{aligned} X &= 388.0 - z\,(.695\cos\Delta\Lambda - .719\sin\Delta\Lambda) \\ Z &= 403.0 - z\,(.719\cos\Delta\Lambda \quad .695\sin\Delta\Lambda) \end{aligned}$$

where $\Delta\Lambda = .166x$ (radians).

The local chord (arc) at each z is given by $c = .166z$.

The metric coefficients for the outboard coordinate system are:

$$\begin{aligned} h_1 &= 0.166z \\ h_3 &= 1. \end{aligned} \tag{16}$$

Surface Pressure Distributions

Pressure data, derived from wind-tunnel measurements, were taken from Tables III-28 and III-230 of Reference 11/. The pressures were measured along streamwise stations, parallel to the aircraft centerline, and it was necessary to interpolate the data so as to provide values of the pressure coefficient, C_p, along the lines, z = constant, of the various conical coordinate systems. Linear interpolation was used, first between measuring points on the same streamwise station, and then, along lines of constant percentage of local streamwise chord, between adjacent streamwise stations (Figure 8).

On the inboard wing, in particular, the interpolation process had a smoothing effect on the measured pressure distribution; however, the general character of the pressure field was preserved.

Boundary Conditions

On the inboard wing the calculations were started at the arc x = 50 (Figure 9). The correct initial boundary-layer profiles at this station were unknown, but it was found that the solution further downstream was sufficiently insensitive to the initial conditions for guessed values to be adequate. It was assumed that the boundary layer at x = 50 was about 0.07 in. thick, and that the velocity and shear-stress profiles, there, were collateral and of flat-plate form.

The line z = 0 was assumed to be a plane of symmetry, on both surfaces. On the upper surface, the aircraft center line would have been a true plane of symmetry; however, there were no pressure data on the center line and therefore the calculation had to start further outboard. Little convergence or divergence would be expected between the center line and the line z = 0, and so the plane-of-symmetry conditions probably represent a reasonable approximation to the real situation.

On the lower surface, the line z = 0 corresponds to the side of the fuselage. The calculation method is not capable of treating the flow near a wing-fuselage intersection, and so conditions along this line were somewhat artificial. However, it was felt that the imposition of plane-of-symmetry conditions along this line would provide approximately the right constraint on the flow elsewhere on the wing.

Plane-of-symmetry conditions were also assumed to exist along the part of the line z = 18 which corresponds to the leading edge. This is appropriate for a swept attachment line (Reference 3/).

On the outboard wing it was assumed that transition from laminar to turbulent flow occurred at x = 0.1, at least outboard of the arc z = 432 (Figure 10). Initial conditions for the turbulent boundary layer were determined from a separate calculation of the laminar boundary layer from x = 0 to x = 0.1. The assumption that transition occurs instantaneously, at x = 0.1, is, of course, only an approximation to conditions in the real flow.

The laminar boundary-layer growth along each arc: z = constant, was calculated by the method of Rott and Crabtree 12/, assuming (a) that this flow approximates locally to infinite-swept-wing conditions, and (b) that the principle of independence holds. The computed value of the parameter q, which appears in the method of Reference 12/, indicated that there was relatively little cross-flow in the laminar boundary layers at x = 0.1, and so it was assumed that the initial-profiles of the turbulent boundary layer were collateral; it was also assumed that the profiles were of flat-plate form. Their thickness was determined by matching the momentum thicknesses across the transition line.

It was not considered worthwhile using a more sophisticated method for calculating the laminar boundary-layer development while the criteria for matching conditions across the transition line were necessarily crude. However, for transition as far forward as 10-percent chord, one would expect the predicted boundary-layer development to be substantially correct for any reasonable set of initial conditions, regardless of the magnification of initial errors due to the pressure gradients. The magnitude of such magnifications is discussed in Reference 13/.

There is flow from the inboard to the outboard wing, and therefore the solution has to be matched along some interface common to both domains. The arc: z = 467, of the outboard coordinate system was chosen to be the interface. This arc cuts across six out of the seven rays: z = constant, of the inboard system. The complete three-dimensional velocity and shear-stress profiles (U, W, $\overline{uv}$, $\overline{vw}$ versus y) were matched at these six points of intersection. The boundary conditions along the arc: z = 467, for the outboard calculation, consisted of the profiles at the six stations and interpolated values in between.

No boundary conditions needed to be prescribed along the arc: z = 215, of the outboard system, because there was outflow, across this boundary, from the domain towards the wing tip.

Appropriate boundary conditions are required for the integration of Equation (13) for the displacement thickness, δ^*. These are provided by conditions at the various planes of symmetry (where $\partial\delta^*/\partial Z = 0$), and by the initial velocity profiles at x = 50 on the inboard wing and at x = 0.1 on the outboard wing. These initial profiles were all assumed to be collateral, and so the "two-dimensional" result (Equation (14)) could be invoked to determine δ^* along the initial lines.

The displacement thickness was matched along the interface between the inboard and outboard segments of the wing.

RESULTS

Presentation of the Data

The results of the calculations are presented in Tables 1 through 4 and Figures 11 through 23. In the tables, and in Figures 11 through 18, the following quantities:

Displacement thickness, δ^*

Boundary-layer thickness, δ

Spanwise component of skin friction (measured positive inboard), τ_{w_n}

Streamwise component of skin friction, τ_{w_s}

Integrated streamwise skin friction, C_{D_f}

are shown as functions of X_ℓ, the streamwise distance from the leading edge, measured along the particular streamwise station (Figure 7). There are seven streamwise stations on the upper surface: 0.044, 0.133, 0.307, 0.458, 0.653, 0.804, and 0.933 semispan, and six on the lower surface: 0.133 through 0.933 semispan (station 0.044 semispan being omitted because it lies within the fuselage).

The displacement thickness and boundary-layer thickness are in inches, and may be compared to the dimensions of the full-scale airplane. The skin-friction components are non-dimensionalized by division by $\rho_\infty Q_\infty^2$, where ρ_∞ is the density of the ambient air and Q_∞ is the forward speed of the airplane, C_{D_f} is the sectional integrated skin friction, from the leading edge to the point X_ℓ:

$$C_{D_f} = 2 \int_0^{X_\ell} \tau_{w_s} \, d X_\ell \tag{17}$$

and has the dimensions of inches. The skin-friction drag of one surface of the wing would be given by:

$$\frac{1}{A} \int_{0^-}^{(Z)_{tip}} (C_{D_f})_{T.E.} \, dZ$$

where A is the planform area. C_{D_f} includes the small component contributed by the laminar boundary layer, on the outboard wing, ahead of the transition line.

In Figure 19 the values of δ^* and δ, at the trailing edge, are plotted versus spanwise position, and in Figure 20 the integrated skin friction, C_{D_f}, (at the trailing edge) is plotted versus spanwise position. If these values of C_{D_f} are divided by the local streamwise chord, in inches, the local sectional skin-friction coefficients are obtained. The latter, denoted c_{d_f}, are plotted versus spanwise position in Figure 21.

In Figure 22 representative velocity profiles are shown for the upper and lower surfaces, respectively. These profiles are for 0.458 semispan at a Mach number of 0.99.

In Figure 23 contour plots are presented showing lines of constant boundary-layer thickness, δ for each surface of the wing, at the two Mach numbers. Figure 24 shows the skin-friction vectors at selected points on the wing. The vectors are drawn to scale, with an arrow one inch long representing a skin-friction vector of magnitude $0.005\ \rho_\infty Q_\infty^2$.

Discussion

The boundary layer thickness, δ, at the trailing edge is of order one inch on both surfaces of the wing, and at both Mach numbers (Figure 19). There is the expected appreciable variation of δ over the span, with thinner boundary layers near the tip than further inboard; however, on the upper surface δ, at the trailing edge, is a maximum at around 30% semispan, not at the root.

At $M = 0.99$ the boundary layer on the upper surface forms a steep ridge, roughly parallel to the aircraft center line at about 0.09 semispan (Figure 23). On this ridge, well forward of the trailing edge, δ reaches a maximum of just over 2 in., which is higher than at any other point on the wing. The accumulation of boundary-layer air in the ridge appears to be associated with the confluence of streamlines moving inboard from the highly swept leading edge and a second set of streamlines lying in the flight direction, close to the aircraft center line. The locally large boundary-layer thickness is not indicative of incipient separation. At $M = 0.50$ the ridge is not well defined; however, areas of locally high values of δ still occur on the inboard wing upper surface (Figure 23).

On the lower surface, there is no indication of a boundary layer build-up on the inboard wing. However, locally high values of δ occur just forward of the trailing edge on the outboard wing (Figure 23), and there is a rapid decrease of boundary-layer thickness as the trailing edge is approached (Figures 13 and 17). This decrease results from an acceleration of the flow in this region, and the "fullness" of the resultant velocity profile on the lower surface (Figure 22) reflects the favorable pressure gradient.

The displacement thickness, δ^*, follows substantially the same trend as the boundary-layer thickness, although there are significant variations in the ratio of δ^* to δ. It will be noted from some of the plots of δ^* and δ versus X_ℓ, Figures 11 and 15 for 0.044 and 0.133 semispan, that δ^* starts to decrease before δ reaches a maximum. The decrease of δ^* is indicative of a decrease of severity of the adverse pressure gardients, probably coupled with lateral movements of fluid in the boundary layer. Much larger influences of the same nature

are needed before δ starts to decrease. In a three-dimensional boundary layer, the displacement thickness tends to be a fairly volatile quantity, exhibiting large variations, and sometimes even going negative. These movements are not at all implausible, and locally negative displacement thickness can easily be explained in terms of divergent crossflow patterns.

At the trailing edge, δ^* is about 0.2 in. on the upper surface and about 0.15 in. on the lower surface, at M = 0.50, and some 50% larger at M = 0.99 (Figure 19). The increase in δ^*/δ with increasing Mach number results primarily from the reduction of density in the inner part of the boundary layer.

The skin-friction vectors on the lower surface (Figure 24) exhibit some deflection at around 85% chord, but the acceleration of the flow just ahead of the trailing edge has the effect of realigning them with the flight direction. At the trailing edge itself, there is little variation of flow direction through the boundary layer either (Figure 22). On the upper surface, there is considerably more deflection of the flow. The skin-friction vectors are inclined by more than 30° to the flight direction at some points on the wing. The strong inclination towards the airplane centerline, of the vectors at 0.133 semispan for M = 0.99 (Figure 24) is indicative of inflow which is directly related to the accumulation of boundary-layer air into the ridge mentioned earlier. On the outboard wing there is strong outflow towards the tip in two regions along the trailing edge, one close to the tip, and one near mid-semispan.

This outflow is associated with substantial crossflow in the boundary layer (Figure 22) and is indicative of the approach to three-dimensional separation, although actual separation was not predicted to occur anywhere on the wing under the conditions of the calculations.

The skin-friction drag of the wing can be determined approximately, from Figure 20, by estimating the area enclosed by the curves of C_{D_f} on the upper and lower surfaces. Our calculations indicate that the skin-friction drag coefficient is about 0.0063 at M = 0.50 and about 0.0071 at M = 0.99. These figures are based on partial wing areas of 24,900 sq. in. for the upper surface and 20,200 sq. in. for the lower surface. The lower-surface sectional skin-friction drag coefficients (Figure 21) are close to equivalent values for a two-dimensional flat plate (one with the same transition position and the same Reynolds number based on local chord). On the upper surface, the computed values of c_{d_f} are higher than the flat-plate values, reflecting the higher average velocities at the edge of the boundary layer. It will be noted that the flat-plate skin friction decreases with increasing Mach number, whereas the skin-friction drag of the wing increases with increasing Mach number, even before the sharp transonic drag rise occurs. This behavior, usually referred to as "drag creep," is typical of both finite wings and two-dimensional airfoils (Reference 14).

CONCLUSIONS AND RECOMMENDATIONS

The main objective of this program was to perform turbulent boundary-layer calculations for the particular wing geometry and pressure distribution, and to present data on the boundary-layer thicknesses and the skin friction. We have met this objective. In so doing, we can claim to have advanced the state of the art, because it is the first time that a calculation method of this degree of sophistication has been used to compute the three-dimensional, compressible, turbulent boundary layer on a real finite swept wing. A considerable amount of useful experience has been gained in performing calculations of this type, and it will be less difficult to do similar calculations in the future. We have developed some "feel" for the balance between scientific rigor and engineering judgment which must be struck in any complicated practical computation.

In advancing the state of the art in this way, the work has drawn attention to the strength and also the weaknesses of the calculation method. It has been demonstrated that the method is capable of calculating the boundary layer all the way from an attachment line or a transition "line" to the trailing edge, through a wide variety of pressure gradients, yielding results which look at least highly plausible. Subsequent experimental programs, in which boundary-layer explorations will be made, both in the wind tunnel and in flight, will show whether the results are also correct.

The main weakness of the method is apparent from the size of the present program which has yielded results for no more than two Mach numbers and one Reynolds number. The method is cumbersome and inflexible when attempts are made to apply it to even a moderately complex geometry like the present wing. This work has drawn attention to the gulf which lies between a set of equations containing all the appropriate terms for handling arbitrary geometries and a practical calculation method which can readily be used to generate engineering data.

There are three essential ingredients in a practical calculation tool: a set of reliable equations, a numerical scheme for integrating them, and a method of organizing the calculation in the particular real-life situation. In the context of three-dimensional turbulent boundary layers, the present method can be claimed to provide the first two ingredients, but there is an urgent need to develop a method for handling complex geometries so that practical calculations can be performed more readily. If three-dimensional boundary-layer calculations are to become a routine part of every aircraft design process -- and the adverse impact of an unfavorable boundary-layer development on aircraft performance should make this mandatory -- then results for a given configuration must be available, at low cost, within days rather than months. We believe that the technology for providing this capability is now within reach, and that a design tool of this nature could be developed for no more than it has cost to perform the calculations described to in this report. We believe that the development of such a tool would be a good investment.

REFERENCES

1. J. F. Nash, "The Calculation of Three-Dimensional Turbulent Boundary Layers in Incompressible Flow," J. Fluid Mech. 37, part 4, p. 625, July 1969.

2. J. F. Nash and V. C. Patel, "A Generalized Method for the Calculation of Three-Dimensional Turbulent Boundary Layers," Project SQUID Symposium, Georgia Institute of Technology, 1971.

3. J. F. Nash and V. C. Patel, "Three-Dimensional Turbulent Boundary Layers," SBC Technical Books, 1972.

4. J. F. Nash, "An Explicit Scheme for the Calculation of Three-Dimensional Turbulent Boundary Layers," J. Basic Eng. 94D, no. 1, p. 131, 1972.

5. J. F. Nash and R. R. Tseng, "The Three-Dimensional Turbulent Boundary Layer on an Infinite Yawed Wing," (to be published in the Aero. Quart.).

6. J. G. Hicks and J. F. Nash, "The Calculation of Three-Dimensional Turbulent Boundary Layers on Helicopter Rotors," NASA CR 1845, 1971.

7. R. E. Singleton, J. F. Nash, L. W. Carr and V. C. Patel, "Unsteady Turbulent Boundary-Layer Analysis," Final Report, Contract NAS2-6466, 1972.

8. D. J. Peake, G. Brakmann and J. M. Romeskie, "Comparisons Between Some High Reynolds Number Turbulent Boundary Layer Experiments at Mach 4, and Various Recent Calculation Procedures," AGARD Specialists' Meeting, London, England, 1971.

9. P. Bradshaw and D. H. Ferriss, "Calculation of Boundary-Layer Development Using the Turbulent Energy Equation: Compressible Flow on Adiabatic Walls," J. Fluid Mech. 46, part 1, p. 83, 1971.

10. N. A. Cumpsty and M. R. Head, "The Calculation of the Three-Dimensional Turbulent Boundary Layer. Part III: Comparison of Attachment - Line Calculations with Experiment," Aero. Quart. 20, p. 99, 1969.

11. C. D. Harris, "Wind-Tunnel Measurements of Aerodynamic Load Distribution on a NASA Supercritical-Wing Research Airplane Configuration," NASA TMX-2469, 1972 (Title unclassified, paper classified).

12. N. Rott and L. F. Crabtree, "Simplified Laminar Boundary Layer Calculations for Bodies of Revolution and for Yawed Wings," J. Aero. Sci. 19, p. 553, 1952.

13. J. F. Nash and P. Bradshaw, "The Magnification of Roughness Drag by Pressure Gradients," J. Roy. Aero. Soc., 71, p. 44, 1967.

14. J. F. Nash, T. H. Moulden, and J. Osborne, "On the Variation of Profile Drag Coefficient Below the Critical Mach Number," Aero. Res. Council, Current Paper 758, 1965.

TABLE 1 - UPPER SURFACE, M = 0.50

X_ℓ	δ^*	δ	τ_{w_n}	τ_{w_s}	$\frac{1}{2} C_{D_f}$
		0.044 Semispan			
50.00	.0113	.0649	0	.002409	.00000
56.16	.0253	.1519	0	.002125	.01421
63.46	.0400	.2459	0	.002025	.02932
69.71	.0533	.3292	0	.001994	.04185
75.28	.0666	.4101	0	.001981	.05293
80.54	.0845	.5025	0	.001869	.06313
85.64	.1047	.6046	0	.001751	.07235
90.65	.1230	.7044	0	.001657	.08087
95.62	.1369	.7962	0	.001581	.08892
100.00	.1435	.8643	0	.001526	.09572
104.73	.1430	.9169	0	.001476	.10282
109.81	.1319	.9349	0	.001434	.11020
115.37	.1114	.9129	0	.001399	.11807
121.34	.0871	.8582	0	.001372	.12634
127.68	.0638	.7834	0	.001349	.13496
134.32	.0411	.6902	0	.001406	.14410
141.30	.0276	.6092	0	.001453	.15408
148.60	.0217	.5490	0	.001484	.16482
155.78	.0207	.5079	0	.001508	.17554
163.77	.0223	.4798	0	.001543	.18775
172.55	.0262	.4683	0	.001567	.20141
183.44	.0316	.4679	0	.001617	.21865
197.85	.0400	.4861	0	.001716	.24271
216.06	.0666	.5774	0	.001524	.27318
237.86	.0898	.7197	0	.001305	.30322
250.02	.0891	.7664	0	.001283	.31897
256.49	.0891	.7874	0	.001267	.32721
		0.133 Semispan			
0.00	.0087	.0985	-.000620	.001665	.00000
5.13	.0088	.0973	.000114	.002097	.00975
10.12	.0090	.0982	.000863	.002475	.02115
15.00	.0104	.1109	.001534	.002775	.03410
19.85	.0237	.2145	.001365	.002576	.04707
24.65	.0439	.3238	.001146	.002371	.05894
29.13	.0550	.3844	.000932	.002099	.06862
33.93	.0560	.4202	.000878	.001991	.07842

TABLE 1 - UPPER SURFACE, M = 0.50 (Cont'd)

X_ℓ	δ^*	δ	τ_{w_n}	τ_{w_s}	$\frac{1}{2} C_{D_f}$
		0.133 Semispan (Cont'd)			
39.19	.0491	.4057	.000760	.001957	.08875
44.91	.0490	.4019	.000505	.001959	.09997
51.00	.0615	.4568	.000220	.001914	.11178
57.42	.0860	.5685	-.000089	.001821	.12380
64.15	.1176	.7302	-.000422	.001697	.13564
71.19	.1402	.9120	-.000776	.001574	.14715
79.31	.1205	.9758	-.000933	.001502	.15955
87.07	.0766	.9324	-.000966	.001464	.17104
95.32	.0390	.8416	-.000942	.001463	.18309
104.94	.0199	.7400	-.000880	.001471	.19721
117.36	.0198	.6517	-.000781	.001495	.21562
133.71	.0339	.6101	-.000616	.001520	.24028
153.50	.0592	.6574	-.000498	.001479	.27007
177.01	.0929	.8065	-.000443	.001292	.30272
183.45	.0983	.8435	-.000425	.001251	.31091
		0.307 Semispan			
10.20	.0142	.1015	.000469	.003096	.00484
11.14	.0156	.1070	.000450	.002940	.00764
12.30	.0175	.1155	.000434	.002775	.01095
13.66	.0199	.1273	.000428	.002636	.01463
15.20	.0235	.1449	.000397	.002496	.01860
17.07	.0279	.1691	.000390	.002410	.02318
19.44	.0333	.1985	.000374	.002304	.02876
22.46	.0400	.2342	.000350	.002183	.03553
26.34	.0483	.2782	.000317	.002058	.04374
31.34	.0603	.3498	.000280	.001934	.05369
37.60	.0733	.4348	.000265	.001855	.06552
43.33	.0831	.5073	.000271	.001820	.07604
52.88	.1001	.6260	.000264	.001748	.09302
61.26	.1117	.7202	.000279	.001732	.10763
73.89	.1319	.8607	.000273	.001663	.12909
88.10	.2188	1.1426	.000037	.001118	.14988

TABLE 1 - UPPER SURFACE, M = 0.50 (Cont'd)

X_ℓ	δ^*	δ	τ_{w_n}	τ_{w_s}	$\frac{1}{2} C_{D_f}$
		0.458 Semispan			
8.97	.0066	.0357	.000959	.003743	.00495
9.79	.0091	.0476	.000829	.003412	.00785
10.81	.0122	.0637	.000709	.003107	.01116
12.01	.0159	.0841	.000601	.002843	.01472
13.37	.0204	.1073	.000506	.002602	.01842
15.01	.0244	.1327	.000487	.002508	.02262
17.09	.0297	.1647	.000445	.002376	.02770
19.74	.0360	.2042	.000414	.002257	.03384
23.15	.0439	.2530	.000382	.002140	.04132
27.55	.0537	.3136	.000351	.002034	.05048
33.06	.0655	.3878	.000320	.001930	.06139
38.09	.0772	.4571	.000285	.001832	.07087
46.49	.0931	.5648	.000278	.001761	.08588
53.86	.1048	.6527	.000283	.001724	.09876
64.96	.1271	.7954	.000259	.001619	.11732
77.15	.2121	1.0792	.000029	.001114	.13504
		0.653 Semispan			
7.38	.0060	.0322	.001030	.003900	.00455
8.05	.0081	.0420	.000905	.003574	.00705
8.89	.0106	.0552	.000793	.003285	.00991
9.88	.0137	.0719	.000687	.003026	.01302
10.99	.0172	.0908	.000596	.002800	.01627
12.34	.0208	.1123	.000553	.002661	.01995
14.06	.0256	.1395	.000488	.002494	.02437
16.24	.0310	.1727	.000457	.002380	.02967
19.04	.0374	.2133	.000432	.002279	.03618
22.66	.0452	.2633	.000410	.002175	.04425
27.19	.0565	.3280	.000353	.002013	.05375
31.33	.0678	.3890	.000306	.001880	.06180
38.23	.0844	.4869	.000276	.001744	.07428
44.29	.0983	.5720	.000262	.001648	.08454
53.43	.1190	.6993	.000246	.001520	.09904
63.70	.1721	.8973	.000122	.001175	.11328

TABLE 1 - UPPER SURFACE, M = 0.50 (Cont'd)

X_ℓ	δ^*	δ	τ_{w_n}	τ_{w_s}	$\frac{1}{2} C_{D_f}$
		0.804 Semispan			
6.14	.0053	.0280	.001125	.004070	.00436
6.71	.0070	.0362	.001006	.003743	.00654
7.40	.0091	.0471	.000899	.003453	.00904
8.23	.0116	.0609	.000801	.003199	.01177
9.16	.0145	.0763	.000718	.002972	.01463
10.28	.0173	.0936	.000686	.002841	.01790
11.71	.0210	.1151	.000638	.002681	.02184
13.52	.0254	.1414	.000607	.002548	.02658
15.86	.0311	.1745	.000552	.002383	.03235
18.87	.0390	.2184	.000475	.002196	.03921
22.64	.0482	.2716	.000414	.002041	.04720
26.09	.0576	.3221	.000351	.001896	.05399
31.84	.0730	.4071	.000280	.001713	.06434
36.89	.0868	.4826	.000233	.001583	.07264
44.50	.0997	.5810	.000228	.001532	.08437
47.88	.1103	.6310	.000179	.001429	.08940
53.05	.1440	.7479	.000081	.001164	.09605
		0.933 Semispan			
5.09	.0048	.0256	.000690	.003926	.00378
5.56	.0064	.0329	.000616	.003669	.00553
6.13	.0082	.0426	.000542	.003402	.00757
6.82	.0104	.0547	.000475	.003171	.00980
7.59	.0129	.0682	.000418	.002971	.01217
8.52	.0154	.0833	.000398	.002848	.01487
9.70	.0186	.1021	.000367	.002706	.01816
11.20	.0225	.1254	.000336	.002570	.02212
13.14	.0275	.1547	.000294	.002422	.02695
15.64	.0341	.1922	.000246	.002267	.03279
18.76	.0427	.2396	.000185	.002100	.03962
21.62	.0530	.2880	.000102	.001905	.04536
26.38	.0683	.3675	.000047	.001721	.05393
30.56	.0848	.4438	-.000015	.001541	.06078
36.87	.0868	.5183	.000071	.001666	.07050
39.67	.1082	.5829	-.000070	.001377	.07479
43.95	.1587	.7376	-.000168	.001046	.07971

TABLE 2 - LOWER SURFACE, M = 0.50

X_ℓ	δ^*	δ	τ_{w_n}	τ_{w_s}	$\frac{1}{2} C_{Df}$
		0.133 Semispan			
.00	.0124	.0712	-.000520	.001870	.00000
5.05	.0189	.1125	-.000379	.001793	.00953
8.07	.0265	.1548	-.000268	.001710	.01535
14.52	.0388	.2389	-.000181	.001635	.02547
21.10	.0509	.3211	-.000104	.001590	.03605
28.28	.0619	.3993	-.000035	.001572	.04739
35.71	.0738	.4832	.000032	.001571	.05908
43.28	.0788	.5462	.000099	.001577	.07099
50.97	.0846	.6062	.000139	.001573	.08311
51.60	.0853	.6120	.000138	.001572	.08410
60.04	.0992	.6975	.000153	.001526	.09719
68.15	.1162	.8053	.000153	.001484	.10939
76.43	.1300	.9207	.000152	.001449	.12152
84.82	.1369	1.0151	.000151	.001418	.13355
93.30	.1454	1.1011	.000145	.001388	.14545
101.90	.1583	1.1994	.000133	.001356	.15724
106.58	.1696	1.2615	.000124	.001308	.16345
115.28	.1960	1.4024	.000097	.001218	.17446
124.19	.2218	1.5516	.000066	.001139	.18494
134.17	.2439	1.7021	.000040	.001064	.19593
139.83	.2525	1.7745	.000033	.001026	.20185
145.89	.2586	1.8408	.000027	.000988	.20796
152.16	.2614	1.8990	.000023	.000952	.21404
159.15	.2306	1.8798	.000020	.001045	.22102
166.97	.1977	1.8384	.000033	.001148	.22959
175.26	.1744	1.8117	.000061	.001243	.23950
		0.307 Semispan			
10.20	.0132	.1279	.000085	.002066	.00412
11.08	.0143	.1318	.000101	.002024	.00591
12.19	.0158	.1383	.000118	.001953	.00811
13.53	.0178	.1464	.000140	.001910	.01070
15.04	.0204	.1584	.000145	.001872	.01357
16.72	.0241	.1795	.000131	.001824	.01666
18.78	.0285	.2023	.000121	.001780	.02040
20.70	.0323	.2216	.000115	.001747	.02377
23.93	.0385	.2506	.000098	.001696	.02915
27.69	.0457	.2897	.000095	.001655	.03561

TABLE 2 - LOWER SURFACE, M = 0.50 (Cont'd)

X_ℓ	δ^*	δ	τ_{w_n}	τ_{w_s}	$\frac{1}{2} C_{D_f}$
		0.307 Semispan (Cont'd)			
32.63	.0548	.3531	.000103	.001608	.04367
38.61	.0658	.4287	.000104	.001551	.05315
43.78	.0756	.4944	.000098	.001519	.06111
52.55	.0931	.6072	.000083	.001447	.07407
60.40	.1144	.7199	.000042	.001338	.08513
66.54	.1620	.8772	-.000073	.001076	.09254
73.28	.2457	1.1053	-.000180	.000817	.09891
76.88	.2979	1.2338	-.000197	.000750	.10171
80.84	.3189	1.3444	-.000188	.000744	.10474
85.27	.2580	1.3230	-.000106	.000923	.10835
90.05	.1350	1.0774	.000165	.001482	.11411
		0.458 Semispan			
8.97	.0060	.0319	.000082	.002367	.00410
9.74	.0082	.0447	.000086	.002268	.00588
10.71	.0110	.0519	.000091	.002130	.00802
11.89	.0141	.0813	.000099	.002038	.01048
13.23	.0172	.1018	.000107	.001972	.01315
14.70	.0208	.1244	.000103	.001899	.01599
16.52	.0250	.1512	.000105	.001836	.01940
18.20	.0287	.1752	.000105	.001789	.02244
20.35	.0347	.2141	.000105	.001721	.02727
24.34	.0415	.2601	.000108	.001672	.03301
28.68	.0492	.3156	.000113	.001638	.04019
33.95	.0588	.3821	.000110	.001598	.04870
38.48	.0676	.4402	.000101	.001558	.05586
46.20	.0838	.5414	.000080	.001477	.06751
53.10	.1029	.6424	.000035	.001365	.07744
58.50	.1427	.7754	-.000082	.001122	.08416
64.43	.2214	.9890	-.000194	.000851	.09000
64.86	.2314	1.0130	-.000198	.000828	.09045
67.59	.2688	1.1175	-.000221	.000770	.09254
71.15	.3108	1.2503	-.000226	.000739	.09524
74.97	.2837	1.2910	-.000178	.000877	.09832
78.18	.1573	1.0887	.000072	.001432	.10319

TABLE 2 - LOWER SURFACE, M = 0.50 (Cont'd)

X_ℓ	δ^*	δ	τ_{w_n}	τ_{w_s}	$\frac{1}{2} C_{D_f}$
		0.653 Semispan			
7.38	.0051	.0267	.000041	.002438	.00388
8.01	.0070	.0377	.000049	.002348	.00550
8.81	.0093	.0523	.000063	.002217	.00732
10.05	.0125	.0726	.000084	.002113	.00999
11.15	.0151	.0899	.000089	.002047	.01231
12.43	.0186	.1104	.000077	.001954	.01488
14.04	.0226	.1353	.000070	.001873	.01792
15.50	.0261	.1573	.000073	.001828	.02062
17.88	.0312	.1921	.000078	.001776	.02482
20.84	.0372	.2338	.000083	.001731	.03009
24.57	.0437	.2825	.000100	.001703	.03651
26.75	.0471	.3082	.000111	.001704	.04023
29.02	.0511	.3375	.000110	.001682	.04408
33.17	.0612	.3958	.000082	.001594	.05030
37.99	.0740	.4672	.000057	.001506	.05836
41.57	.0837	.5206	.000038	.001448	.06365
45.87	.1033	.6018	-.000019	.001310	.06960
50.45	.1430	.7275	-.000111	.001088	.07513
53.45	.1834	.8356	-.000164	.000848	.07816
58.52	.2591	1.0367	-.000206	.000815	.08261
61.65	.2363	1.0667	-.000121	.000995	.08545
65.12	.1414	.9221	.000085	.001443	.08968
		0.804 Semispan			
6.14	.0050	.0262	.000063	.002424	.00335
6.98	.0075	.0400	.000076	.002290	.00534
7.73	.0097	.0544	.000087	.002178	.00700
8.59	.0119	.0685	.000100	.002101	.00885
9.54	.0142	.0833	.000109	.002040	.01080
10.98	.0175	.1049	.000123	.001971	.01369
12.47	.0208	.1258	.000133	.001922	.01659
14.35	.0246	.1518	.000145	.001869	.02015
16.67	.0291	.1821	.000158	.001822	.02444
18.65	.0343	.2191	.000168	.001784	.02980
23.25	.0408	.2632	.000167	.001751	.03620
26.36	.0477	.3040	.000144	.001682	.04154
31.64	.0601	.3751	.000107	.001577	.05013
36.37	.0725	.4424	.000068	.001480	.05740

TABLE 2 - LOWER SURFACE, M = 0.50 (Cont'd)

X_ℓ	δ^*	δ	τ_{w_n}	τ_{w_s}	$\frac{1}{2}C_{D_f}$
		0.804 Semispan (Cont'd)			
40.07	.0878	.5063	.000002	.001343	.06263
44.13	.1184	.6090	-.000097	.001122	.06761
44.50	.1216	.6193	-.000103	.001103	.06802
46.29	.1358	.6672	-.000129	.001039	.06995
48.74	.1560	.7345	-.000157	.000364	.07240
51.35	.1276	.7287	-.000035	.001215	.07524
54.23	.0968	.6805	.000109	.001506	.07916
		0.933 Semispan			
5.09	.0049	.0257	-.000101	.002438	.00293
5.53	.0063	.0337	-.000088	.002386	.00388
5.93	.0075	.0413	-.000074	.002294	.00482
6.57	.0095	.0537	-.000057	.002194	.00627
7.33	.0116	.0668	-.000039	.002122	.00789
7.90	.0130	.0763	-.000028	.002083	.00910
8.58	.0145	.0872	-.000015	.002047	.01050
9.69	.0171	.1039	.000004	.002006	.01274
10.69	.0192	.1185	.000016	.001977	.01475
12.34	.0225	.1416	.000035	.001943	.01797
14.38	.0262	.1684	.000059	.001820	.02191
16.36	.0316	.2030	.000056	.001858	.02678
19.47	.0372	.2375	.000045	.001797	.03136
22.85	.0445	.2834	.000036	.001738	.03741
27.47	.0558	.3487	.000005	.001635	.04514
31.55	.0705	.4194	-.000055	.001488	.05170
36.56	.1067	.5418	-.000190	.001176	.05825
38.36	.1222	.5936	-.000216	.001096	.06032
40.38	.1426	.6555	-.000246	.001007	.06245
42.54	.1143	.6482	-.000115	.001284	.06497
44.93	.0909	.6120	-.000004	.001515	.06828

TABLE 3 - UPPER SURFACE, M = 0.99

X_ℓ	δ^*	δ	τ_{w_n}	τ_{w_s}	$\frac{1}{2} C_{D_f}$
		0.044 Semispan			
50.00	.0143	.0698	.000000	.002356	.00000
57.52	.0317	.1713	.000000	.002140	.01679
67.59	.0456	.2672	.000000	.002081	.03794
76.89	.0535	.3332	.000000	.002102	.05737
85.06	.0530	.3818	.000000	.002121	.07462
92.67	.0640	.4237	.000000	.002149	.09035
99.96	.0693	.4642	.000000	.002178	.10662
106.82	.0751	.5045	.000000	.002197	.12163
113.23	.0810	.5437	.000000	.002213	.13577
119.55	.0869	.5824	.000000	.002231	.14981
125.88	.0926	.6212	.000000	.002251	.16400
132.25	.0997	.6601	.000000	.002209	.17828
138.68	.1069	.6987	.000000	.002149	.19227
145.18	.1134	.7362	.000000	.002099	.20608
150.00	.1176	.7641	.000000	.002067	.21611
155.00	.1215	.7934	.000000	.002039	.22638
161.85	.1260	.8330	.000000	.002015	.24027
169.34	.1312	.8760	.000000	.001989	.25526
178.21	.1391	.9279	.000000	.001955	.27276
189.19	.1542	.9996	.000000	.001865	.29377
201.38	.1729	1.0896	.000000	.001770	.31590
213.65	.1974	1.1899	.000000	.001575	.33661
225.69	.2164	1.2818	.000000	.001379	.35436
237.80	.2019	1.3191	.000000	.001381	.37061
249.87	.1720	1.3184	.000000	.001476	.38788
255.92	.1608	1.3204	.000000	.001513	.39693
		0.133 Semispan			
2.83	.0130	.1431	-.000327	.001827	.00498
10.78	.0128	.1432	.000522	.002323	.02149
18.18	.0167	.1831	.001047	.002545	.03991
25.28	.0236	.2468	.001144	.002533	.05792
33.55	.0324	.3019	.001200	.002456	.07868
39.89	.0374	.3735	.001204	.002382	.09400
46.14	.0374	.4625	.001203	.002326	.10870
52.39	.0392	.5252	.001206	.002289	.12313

TABLE 3 - UPPER SURFACE, M = 0.99 (Cont'd)

X_ℓ	δ^*	δ	τ_{w_n}	τ_{w_s}	$\frac{1}{2}C_{D_f}$
		0.133 Semispan (Cont'd)			
58.69	.0457	.5684	.001209	.002226	.13738
65.04	.0553	.5979	.001189	.002161	.15130
71.47	.0673	.6227	.001150	.002106	.16501
76.30	.0654	.6874	.001122	.002067	.17510
80.71	.0602	.7380	.001109	.002048	.18417
84.04	.0581	.7804	.001096	.001997	.19092
90.97	.0577	.8308	.001049	.001913	.20445
94.69	.0583	.8368	.001007	.001883	.21150
98.70	.0599	.8323	.000950	.001858	.21898
108.05	.0689	.8036	.000783	.001815	.23615
119.36	.0871	.7847	.000589	.001768	.25643
125.50	.0886	.7989	.000497	.001738	.26720
131.66	.1106	.9085	.000412	.001704	.27731
137.77	.1207	.8343	.000340	.001706	.28822
143.81	.1307	.8679	.000288	.001705	.29851
149.85	.1420	.9115	.000236	.001699	.30879
155.79	.1538	.9650	.000179	.001684	.31886
161.82	.1638	1.0187	.000128	.001646	.32891
167.85	.1707	1.0688	.000084	.001605	.33871
179.87	.1770	1.1571	.000025	.001540	.35760
182.88	.1777	1.1776	.000016	.001526	.36222
		0.307 Semispan			
10.20	.0166	.0987	.000960	.004252	.00556
11.52	.0193	.1064	.000924	.004026	.01099
13.19	.0229	.1202	.000890	.003789	.01749
15.25	.0284	.1412	.000814	.003536	.02504
17.59	.0359	.1699	.000695	.003286	.03301
20.09	.0445	.2022	.000548	.003042	.04095
23.17	.0544	.2430	.000445	.002890	.05008
26.92	.0662	.2957	.000373	.002799	.06067
31.63	.0796	.3656	.000363	.002748	.07374
37.25	.0959	.4467	.000337	.002653	.08895
42.23	.1128	.5173	.000254	.002458	.10173
50.02	.1442	.6308	.000125	.002115	.11944
56.91	.1711	.7369	.000078	.001957	.13342

TABLE 3 - UPPER SURFACE, M = 0.99 (Cont'd)

X_ℓ	δ^*	δ	τ_{w_n}	τ_{w_s}	$\frac{1}{2}C_{D_f}$
		0.307 Semispan (Cont'd)			
66.35	.2030	.8853	.000082	.001889	.15155
74.51	.2334	1.0214	.000085	.001830	.16687
81.05	.2801	1.1433	-.000054	.001439	.17758
84.60	.3146	1.2215	-.000108	.001242	.18235
90.06	.3633	1.3432	-.000137	.001063	.18861
		0.458 Semispan			
8.97	.0097	.0378	.001493	.005224	.00572
10.13	.0138	.0539	.001386	.004889	.01154
11.60	.0188	.0773	.001286	.004561	.01844
13.41	.0246	.1046	.001205	.004290	.02645
15.46	.0308	.1337	.001157	.004087	.03504
17.67	.0372	.1639	.001118	.003923	.04387
20.37	.0448	.1991	.001065	.003742	.05421
23.67	.0539	.2400	.000992	.003527	.06623
27.81	.0653	.2903	.000863	.003244	.08024
32.75	.0794	.3502	.000713	.002923	.09550
37.12	.0958	.4056	.000493	.002520	.10748
43.97	.1217	.5046	.000333	.002220	.12339
50.00	.1391	.5945	.000283	.002125	.13651
56.08	.1549	.6861	.000266	.002062	.14925
64.96	.1808	.8195	.000227	.001911	.16698
68.37	.2254	.8960	.000025	.001439	.17267
71.25	.2642	.9727	-.000059	.001222	.17651
74.38	.3112	1.0650	-.000127	.001026	.18002
79.18	.3815	1.2266	-.000170	.000889	.18459
		0.653 Semispan			
7.38	.0084	.0333	.001353	.005051	.00512
8.33	.0118	.0469	.001283	.004776	.00978
9.54	.0159	.0666	.001216	.004506	.01536
11.03	.0207	.0898	.001158	.004273	.02188
12.72	.0259	.1143	.001106	.004060	.02891
14.53	.0312	.1398	.001066	.003900	.03613

TABLE 3 - UPPER SURFACE, M = 0.99 (Cont'd)

X_ℓ	δ^*	δ	τ_{w_n}	τ_{w_s}	$\frac{1}{2} C_{D_f}$
		0.653 Semispan (Cont'd)			
16.75	.0377	.1699	.000996	.003688	.04455
19.47	.0456	.2054	.000900	.003445	.05426
22.87	.0554	.2488	.000794	.003177	.06549
26.93	.0662	.3007	.000732	.002989	.07797
30.53	.0746	.3465	.000728	.002917	.08856
36.16	.0884	.4171	.000680	.002757	.10462
41.15	.1048	.4797	.000543	.002457	.11769
47.97	.1317	.5688	.000361	.001999	.13300
53.87	.1740	.6638	.000114	.001401	.14301
56.23	.2105	.7228	-.000002	.001106	.14595
58.60	.2362	.7846	-.000015	.001032	.14849
61.17	.2618	.8487	-.000030	.000954	.15104
65.12	.2973	.9585	-.000022	.000910	.15471
		0.804 Semispan			
6.14	.0075	.0298	.001346	.004958	.00464
6.94	.0103	.0412	.001293	.004707	.00846
7.94	.0138	.0576	.001224	.004408	.01302
9.18	.0178	.0770	.001167	.004159	.01832
10.59	.0221	.0974	.001114	.003938	.02401
12.10	.0266	.1185	.001070	.003756	.02982
13.95	.0319	.1434	.001001	.003537	.03656
16.21	.0382	.1727	.000938	.003344	.04432
19.05	.0455	.2087	.000880	.003187	.05354
22.43	.0536	.2505	.000840	.003068	.06413
25.43	.0604	.2864	.000817	.002991	.07319
30.12	.0710	.3407	.000765	.002850	.08694
34.27	.0835	.3876	.000634	.002531	.09820
39.95	.1139	.4612	.000334	.001765	.11043
41.62	.1260	.4864	.000196	.001493	.11315
44.87	.1484	.5461	.000073	.001218	.11748
46.83	.1531	.5777	.000069	.001222	.11986
50.94	.1712	.6609	.000011	.001119	.12472
54.23	.1975	.7499	-.000044	.000977	.12817

TABLE 3 - UPPER SURFACE, M = 0.99 (Cont'd)

X_ℓ	δ^*	δ	τ_{w_n}	τ_{w_s}	$\frac{1}{2}C_{D_f}$
		0.933 Semispan			
5.09	.0062	.0252	.000594	.004567	.00416
5.94	.0093	.0392	.000605	.004335	.00797
6.81	.0123	.0546	.000613	.004147	.01163
7.88	.0158	.0719	.000614	.003981	.01596
9.12	.0197	.0909	.000604	.003829	.02081
10.39	.0234	.1097	.000608	.003731	.02562
11.99	.0278	.1323	.000617	.003654	.03151
13.98	.0337	.1598	.000554	.003479	.03863
16.44	.0409	.1928	.000502	.003319	.04697
19.38	.0489	.2312	.000458	.003176	.05653
21.95	.0554	.2640	.000435	.003095	.06460
26.05	.0709	.3178	.000189	.002599	.07648
28.40	.0890	.3563	-.000116	.001991	.08185
29.38	.1016	.3781	-.000255	.001663	.08365
31.83	.1348	.4426	-.000408	.001170	.08696
34.49	.1504	.5044	-.000333	.001160	.08995
36.87	.1525	.5555	-.000256	.001248	.09281
38.80	.1447	.5892	-.000194	.001392	.09537
40.43	.1434	.6215	-.000173	.001434	.09768
42.21	.1568	.6694	-.000236	.001314	.10012
44.93	.2159	.7901	-.000394	.000923	.10318

TABLE 4 - LOWER SURFACE, M = 0.99

X_t	δ^*	δ	τ_{w_n}	τ_{w_s}	$\frac{1}{2}C_{D_f}$
		0.133 Semispan			
.00	.0147	.0743	-.000531	.001910	.00000
9.84	.0310	.1750	-.000248	.001834	.01848
23.15	.0560	.3281	-.000004	.001787	.04258
38.33	.0784	.5073	.000189	.001839	.06993
51.60	.0818	.5870	.000378	.001932	.09499
61.73	.0888	.6603	.000450	.001925	.11455
74.08	.0974	.7727	.000468	.001904	.13820
86.10	.1089	.8908	.000453	.001827	.16068
97.87	.1220	1.0013	.000437	.001763	.18179
101.90	.1263	1.0394	.000430	.001748	.18887
110.98	.1458	1.1309	.000394	.001537	.20379
123.15	.1681	1.2461	.000342	.001319	.22112
130.10	.1856	1.3013	.000318	.001218	.22992
133.96	.1987	1.3304	.000293	.001176	.23454
138.03	.2168	1.3557	.000260	.001137	.23925
146.93	.1679	1.3690	.000202	.001184	.24967
156.89	.1346	1.3871	.000131	.001180	.26128
162.15	.1276	1.4033	.000108	.001200	.26754
167.67	.1304	1.4338	.000092	.001204	.27418
173.37	.1368	1.4738	.00081	.001206	.28105
		0.307 Semispan			
10.20	.0132	.1062	.000385	.002592	.00437
11.24	.0152	.1126	.000396	.002537	.00702
12.55	.0179	.1234	.000404	.002448	.01029
14.18	.0214	.1379	.000408	.002372	.01423
16.09	.0265	.1620	.000367	.002277	.01866
18.11	.0321	.1884	.000307	.002194	.02317
20.09	.0376	.2131	.000260	.002121	.02745
22.97	.0451	.2464	.000211	.002049	.03345
26.68	.0547	.2878	.000158	.001958	.04089
31.37	.0662	.3514	.000141	.001868	.04984
37.23	.0796	.4289	.000134	.001806	.06057
42.41	.0926	.4989	.000106	.001735	.06977
50.58	.1154	.6129	.000059	.001608	.08338
57.48	.1342	.7077	.000019	.001522	.09427
68.64	.2691	1.0164	-.000248	.000875	.10743
77.77	.3699	1.3072	-.000278	.000737	.11467

TABLE 4 - LOWER SURFACE, M = 0.99 (Cont'd)

X_ℓ	δ^*	δ	τ_{w_n}	τ_{w_s}	$\frac{1}{2} C_{D_f}$
		0.307 Semispan (Cont'd)			
80.76	.3896	1.3977	-.000280	.000724	.11686
83.72	.3642	1.4472	-.000244	.000808	.11913
87.97	.2230	1.3086	-.000053	.001255	.12351
90.06	.1658	1.2226	.000088	.001578	.12647
		0.458 Semispan			
8.97	.0075	.0339	.000291	.003044	.00459
9.88	.0106	.0484	.000274	.002903	.00729
11.03	.0144	.0687	.000259	.002732	.01054
12.47	.0188	.0924	.000248	.002591	.01436
14.15	.0241	.1190	.000205	.002429	.01858
15.93	.0302	.1479	.000153	.002262	.02275
17.67	.0362	.1764	.000110	.002128	.02657
20.20	.0441	.2169	.000076	.002024	.03182
23.46	.0535	.2685	.000064	.001949	.03826
27.58	.0622	.3276	.000100	.001951	.04626
32.73	.0711	.3938	.000143	.001968	.05637
37.28	.0839	.4570	.000098	.001858	.06515
44.46	.1091	.5665	.000024	.001676	.07771
60.35	.2893	.9885	-.000326	.000834	.09903
68.37	.4168	1.3089	-.000353	.000716	.10527
71.00	.4520	1.4201	-.000352	.000709	.10715
73.60	.4446	1.4942	-.000321	.000783	.10909
77.34	.2903	1.3386	-.000127	.001255	.11290
79.18	.2232	1.2664	.000017	.001604	.11553
		0.653 Semispan			
7.38	.0066	.0291	.000316	.003192	.00439
8.13	.0091	.0412	.000315	.003083	.00674
9.08	.0122	.0580	.000316	.002915	.00958
10.26	.0158	.0775	.000321	.002794	.01294
11.64	.0199	.0989	.000313	.002678	.01672
13.10	.0241	.1212	.000302	.002570	.02055
14.53	.0281	.1423	.000296	.002502	.02417
16.61	.0340	.1725	.000272	.002385	.02925
19.29	.0418	.2112	.000234	.002252	.03548
22.68	.0520	.2610	.000183	.002106	.04285

TABLE 4 - LOWER SURFACE, M = 0.99 (Cont'd)

X_ℓ	δ^*	δ	τ_{w_n}	τ_{w_s}	$\frac{1}{2}C_{D_f}$
		0.653 Semispan (Cont'd)			
26.92	.0631	.3218	.000181	.002039	.05157
30.66	.0724	.3746	.000174	.002001	.05915
36.57	.0894	.4597	.000124	.001864	.07067
41.56	.1134	.5440	.000004	.001613	.07942
49.63	.2312	.7969	-.000243	.001040	.08974
56.23	.3346	1.0337	-.000310	.000824	.09596
58.39	.3779	1.1318	-.000325	.000757	.09767
60.53	.3896	1.2087	-.000300	.000783	.09932
63.60	.2721	1.0789	-.000112	.001207	.10238
65.12	.2133	1.0368	.000026	.001534	.10445
		0.804 Semispan			
6.14	.0061	.0274	.000250	.003053	.00374
6.77	.0082	.0375	.000272	.002991	.00563
7.56	.0108	.0515	.000287	.002853	.00793
8.54	.0137	.0679	.000307	.002758	.01068
9.69	.0169	.0855	.000318	.002668	.01380
10.91	.0202	.1038	.000327	.002594	.01700
12.10	.0232	.1205	.000335	.002545	.02006
13.83	.0282	.1450	.000308	.002421	.02436
16.07	.0339	.1756	.000305	.002332	.02965
18.99	.0399	.2121	.000340	.002314	.03618
22.42	.0463	.2549	.000386	.002336	.04439
25.54	.0541	.2940	.000331	.002235	.05157
30.46	.0701	.3598	.000207	.001978	.06196
34.61	.0856	.4190	.000120	.001796	.06978
41.33	.1204	.5321	-.000063	.001449	.08114
46.83	.2014	.7032	-.000271	.000917	.08758
48.63	.2474	.7852	-.000319	.000745	.08907
50.41	.2555	.8490	-.000276	.000805	.09045
52.97	.1974	.7990	-.000144	.001138	.09294
54.23	.1696	.7891	-.000055	.001332	.09450

TABLE 4 - LOWER SURFACE, M = 0.99 (Cont'd)

X_ℓ	δ^*	δ	τ_{w_n}	τ_{w_s}	$\frac{1}{2}C_{D_f}$
		0.933 Semispan			
5.09	.0058	.0258	.000010	.002934	.00318
5.61	.0076	.0348	.000039	.002892	.00469
6.26	.0098	.0472	.000065	.002763	.00653
7.08	.0124	.0618	.000094	.002673	.00875
8.03	.0152	.0774	.000110	.002595	.01126
9.04	.0180	.0934	.000124	.002528	.01384
10.03	.0207	.1084	.000137	.002481	.01631
11.46	.0245	.1295	.000146	.002414	.01982
13.31	.0289	.1554	.000172	.002387	.02425
15.65	.0337	.1861	.000219	.002387	.02984
18.57	.0396	.2227	.000258	.002391	.03682
21.16	.0463	.2561	.000209	.002302	.04292
25.23	.0584	.3105	.000138	.002132	.05197
28.68	.0681	.3570	.000108	.002041	.05912
34.25	.0905	.4394	-.000072	.001708	.07037
37.21	.1458	.5408	-.000311	.001114	.07453
40.29	.2634	.7178	-.000468	.000585	.07719
41.77	.2554	.7792	-.000373	.000782	.07820
43.89	.1950	.7400	-.000293	.001093	.08018
44.93	.1845	.7432	-.000264	.001116	.08132

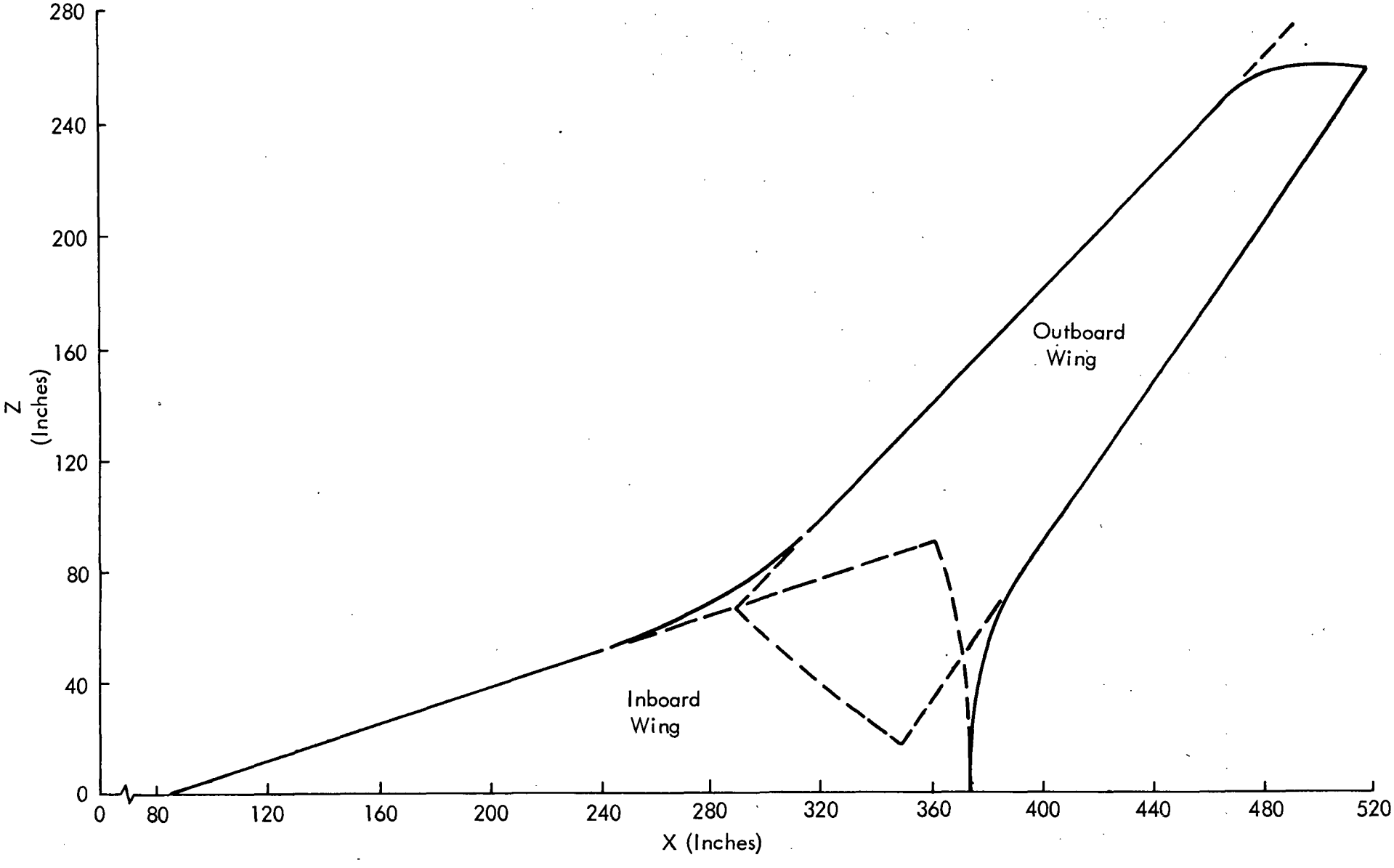

Figure 1. Segmentation of the Wing

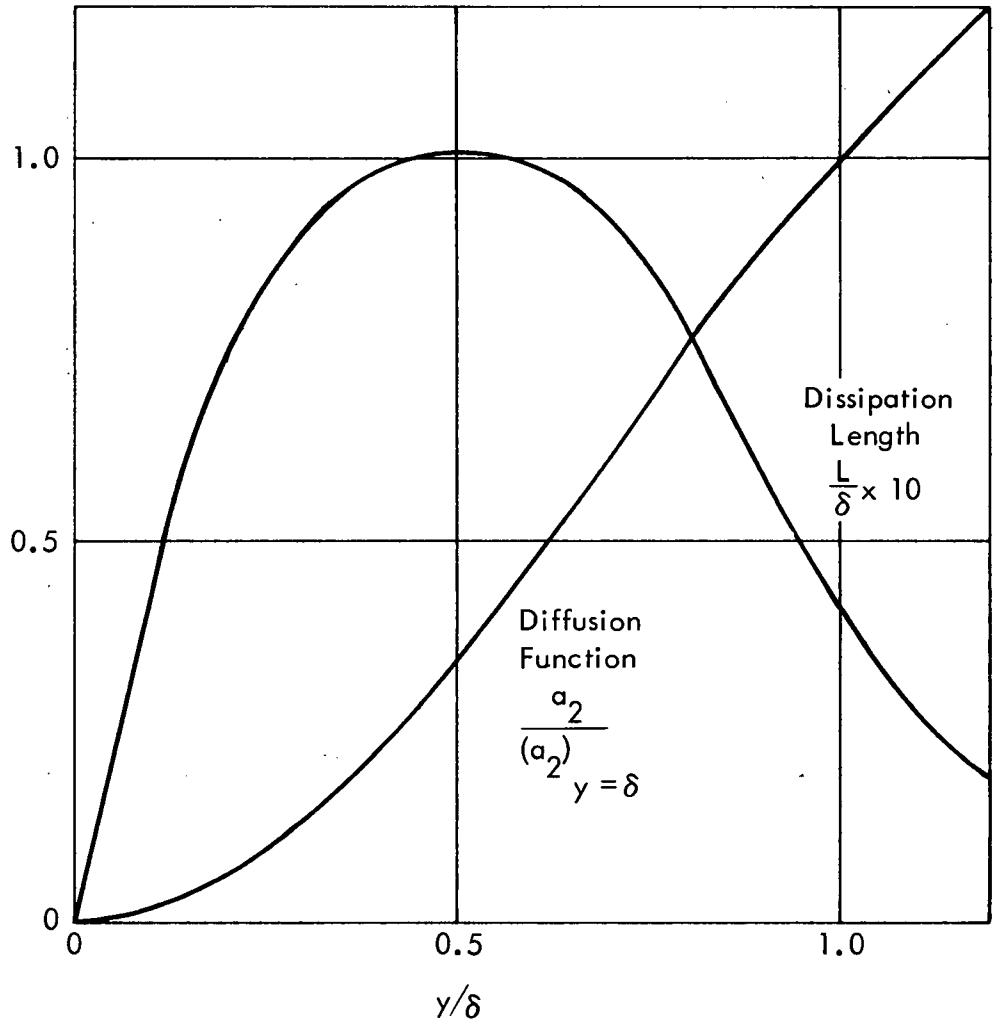

Figure 2. Empirical Functions in the Calculation Method

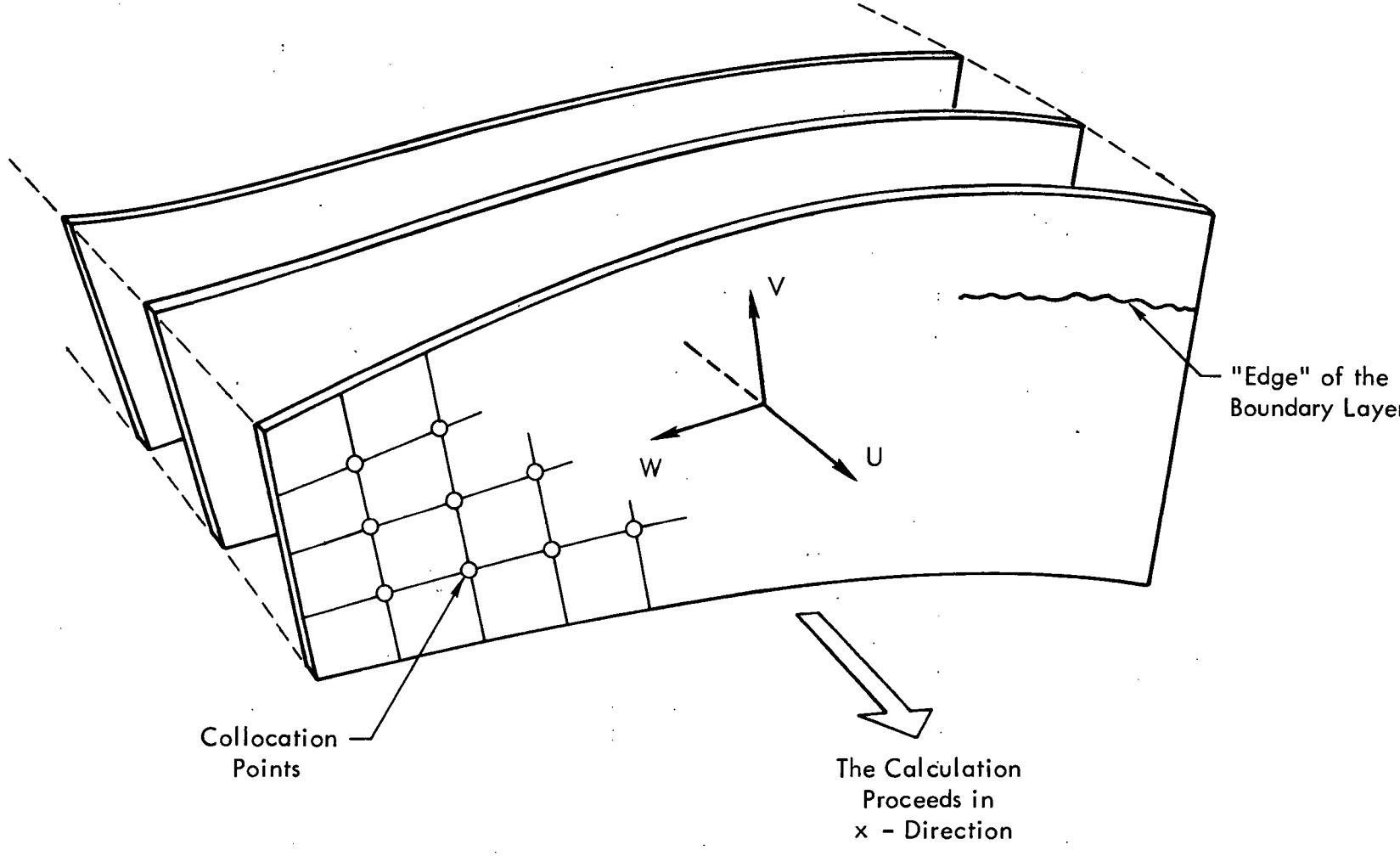

Figure 3. Integration Domain

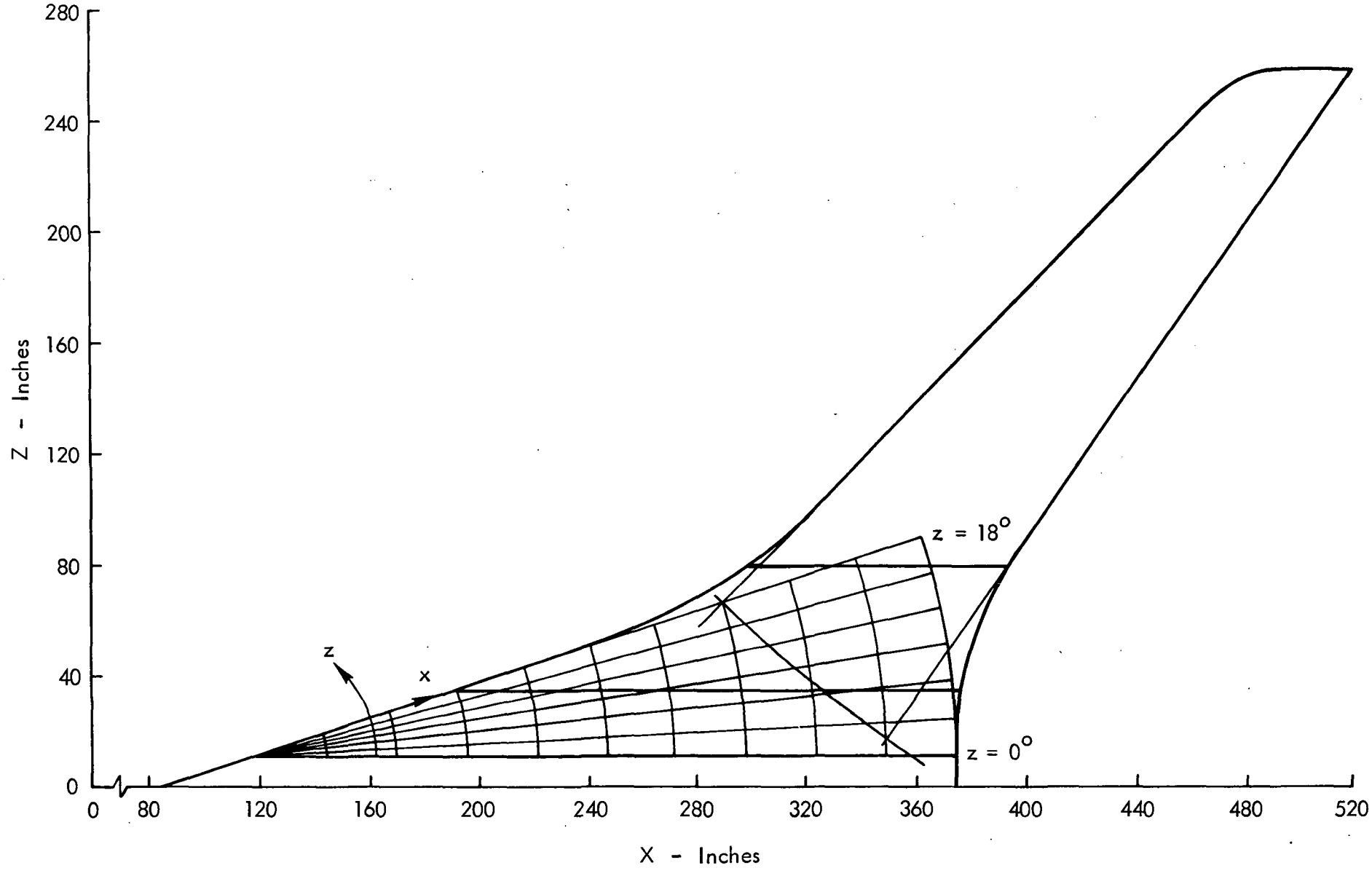

Figure 4. Upper Surface Inboard Coordinate System

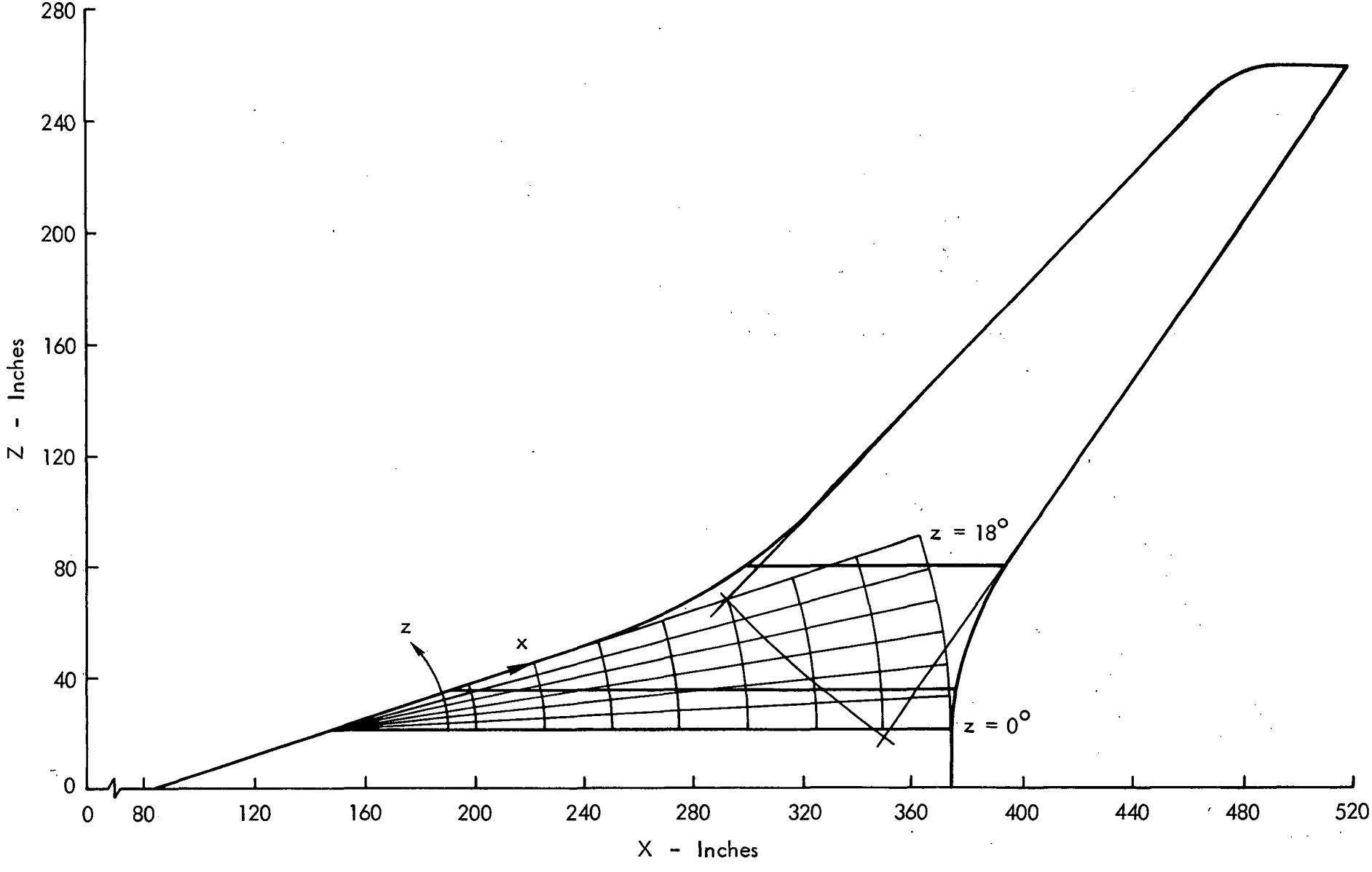

Figure 5. Lower Surface Inboard Coordinate System

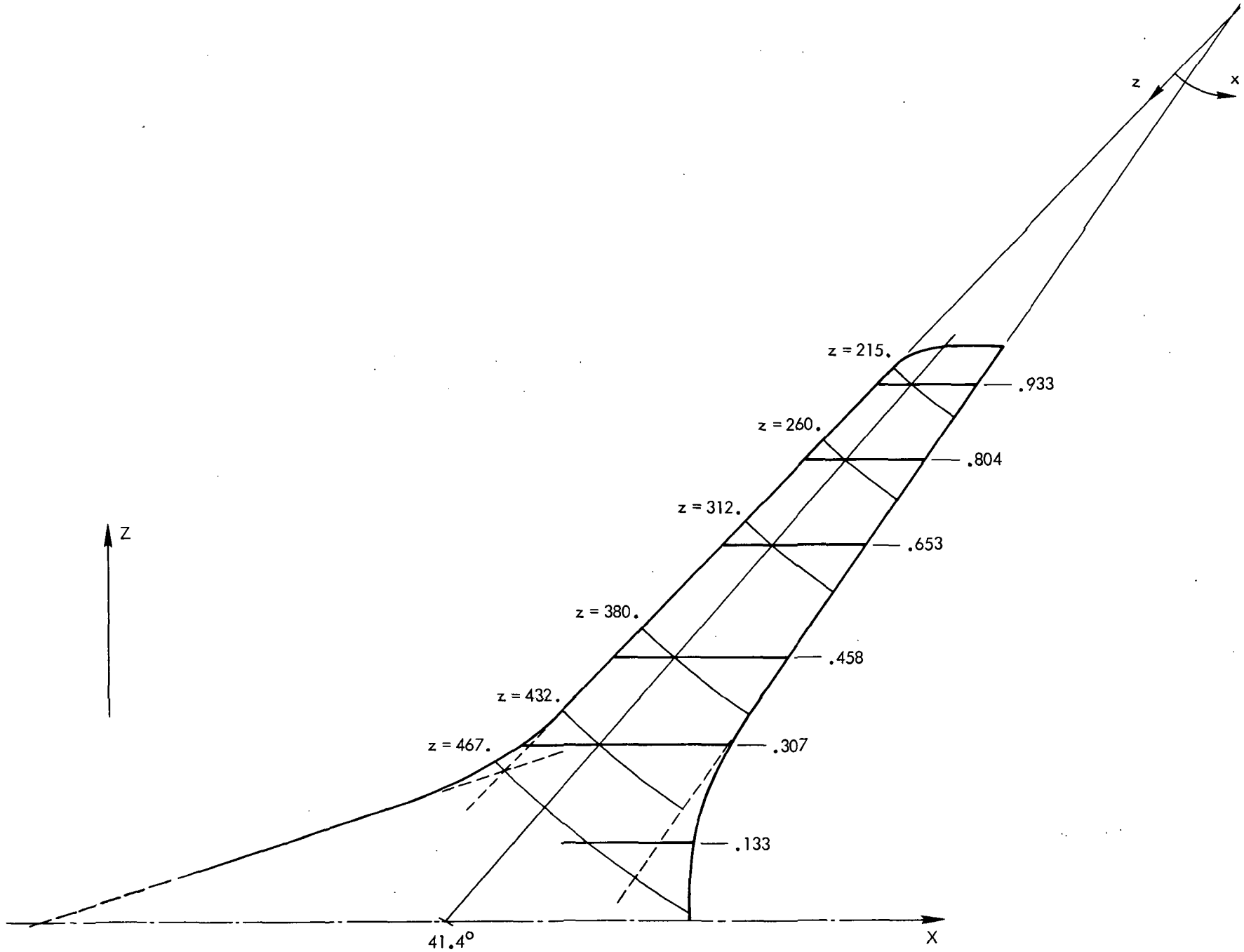

Figure 6. Outboard Coordinate System

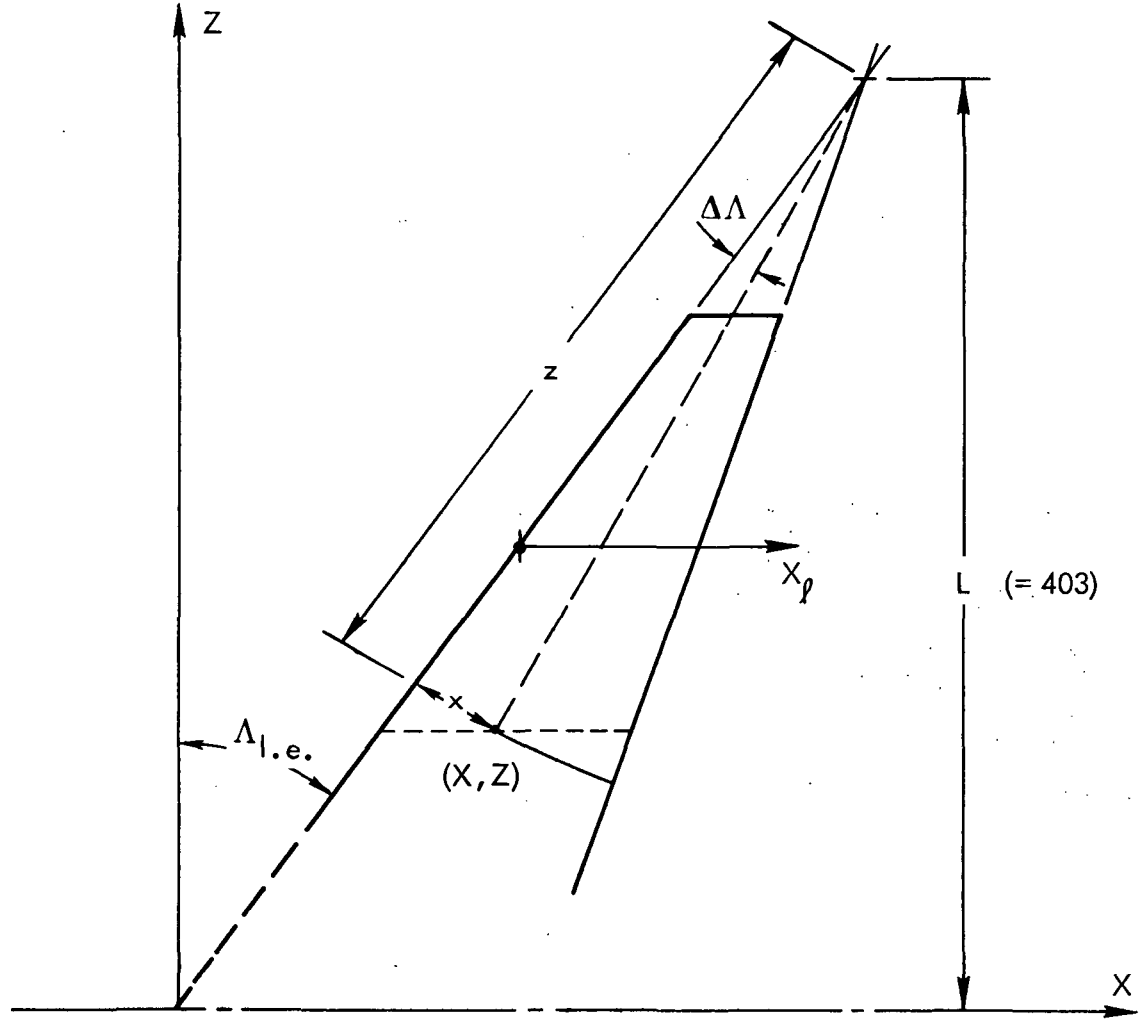

Figure 7. Relation Between Streamwise and Outboard Coordinates

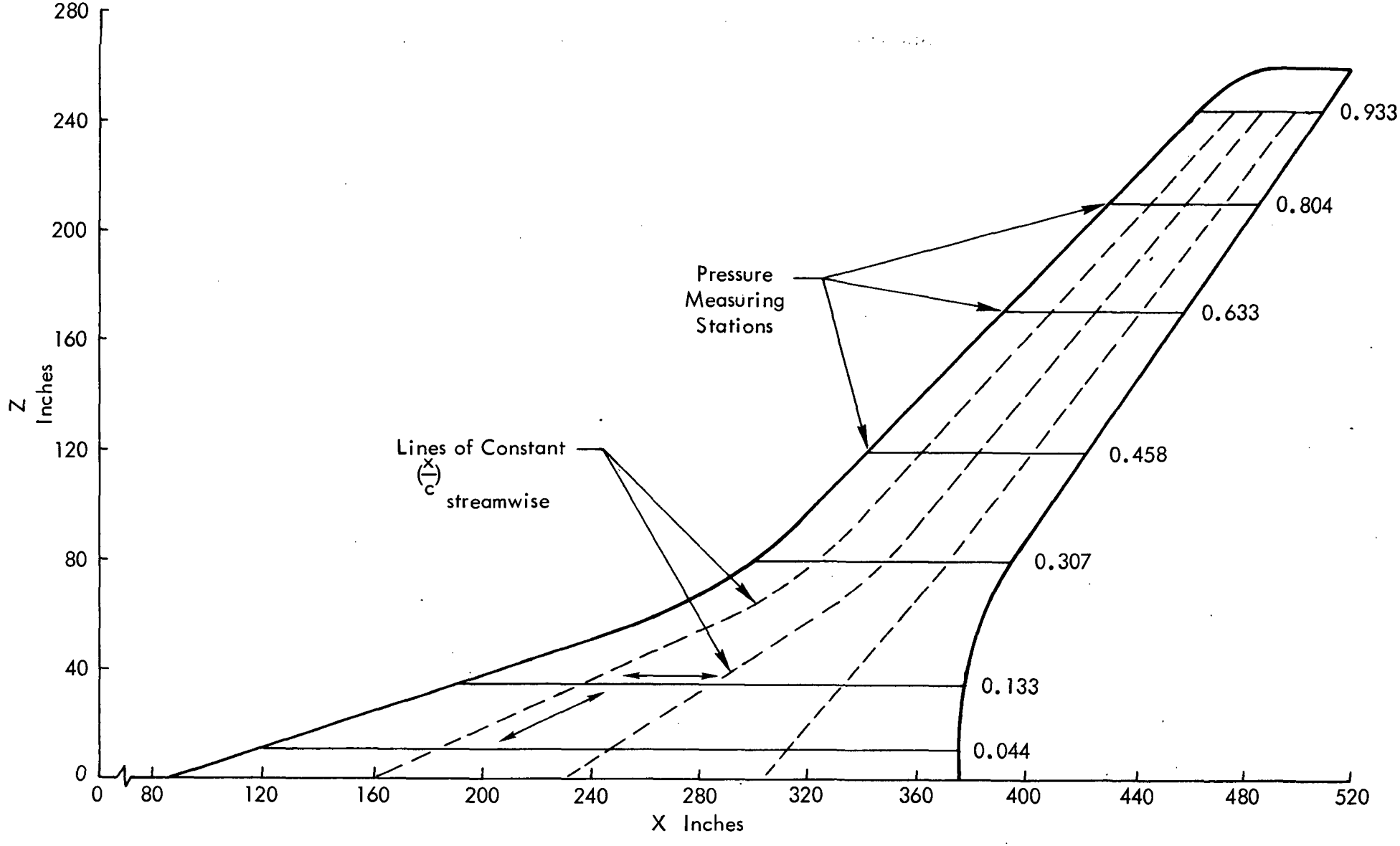

Figure 8. Method of Interpolating the Pressure Data

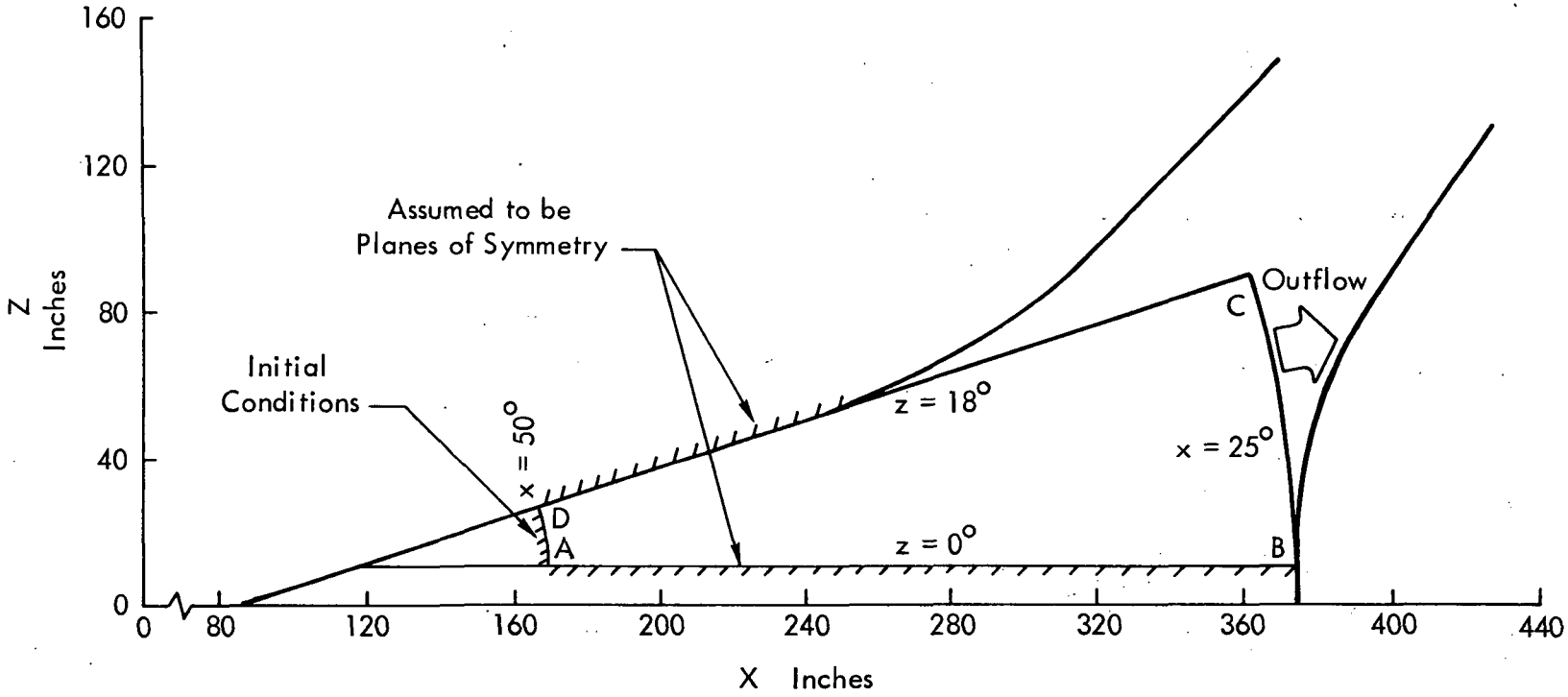

Figure 9. Boundary Conditions for the Inboard Calculation

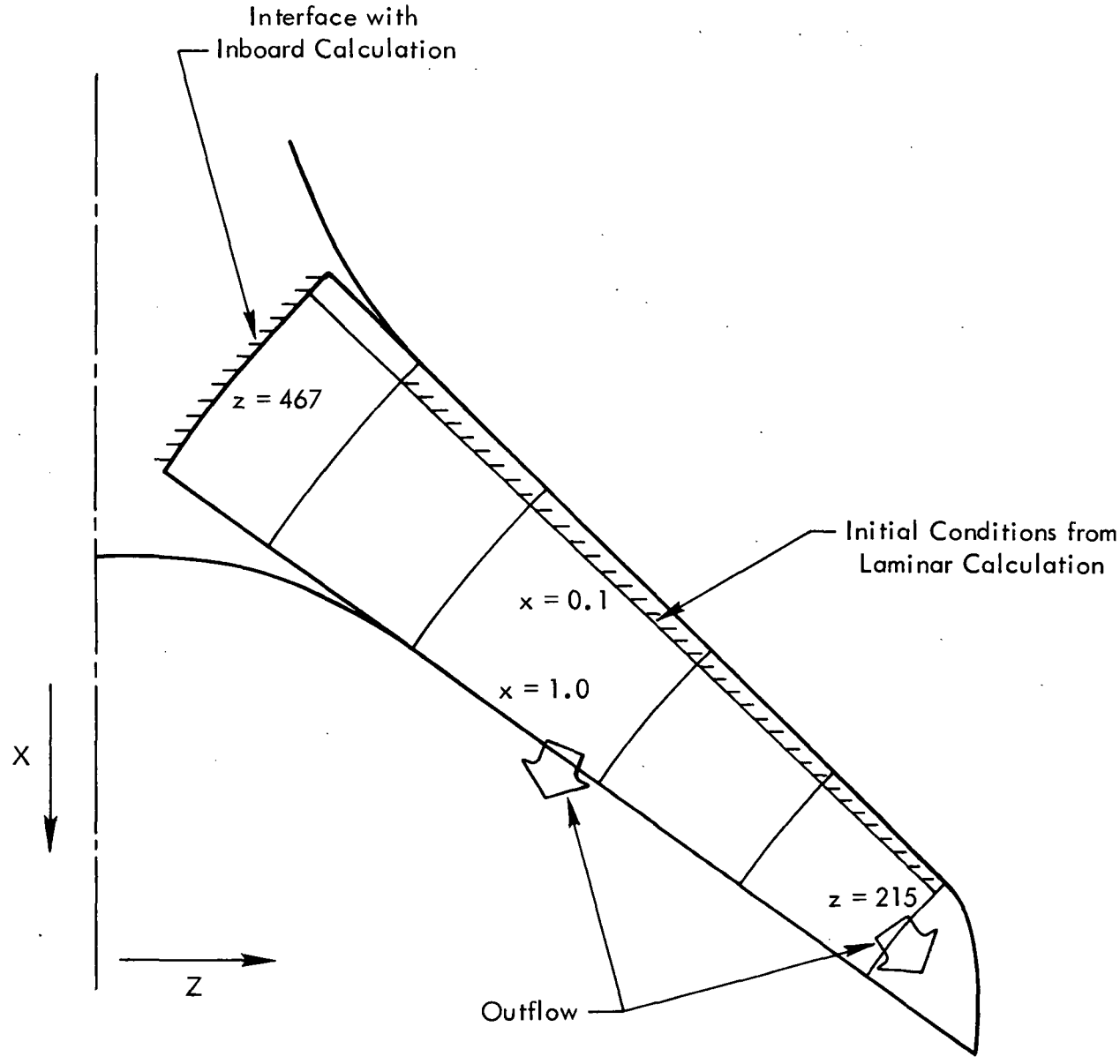

Figure 10 Boundary Conditions for the Outboard Calculation

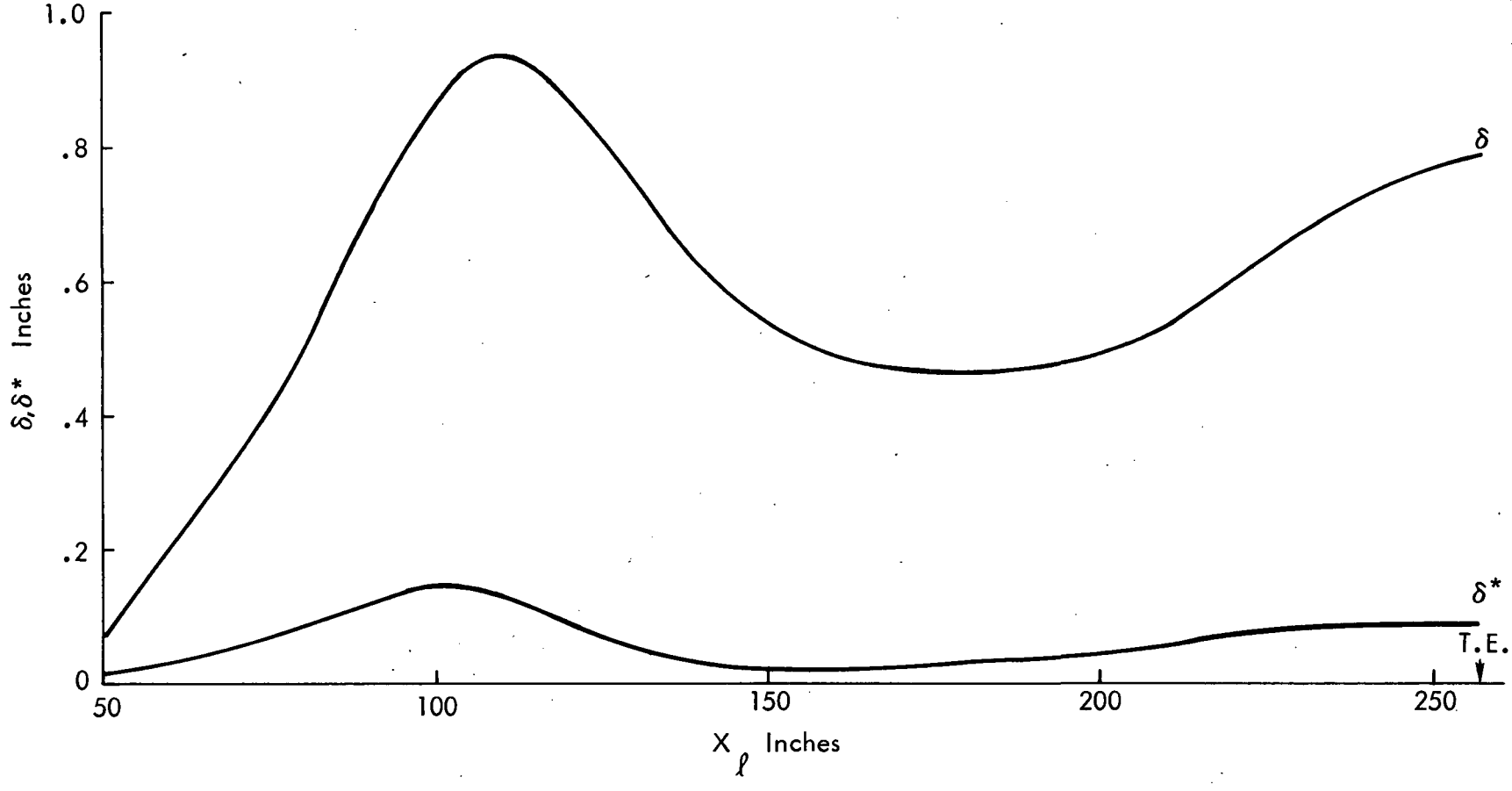

Figure 11. Boundary-Layer Thickness and Displacement Thickness, M = 0.5, Upper Surface: 0.044 Semispan

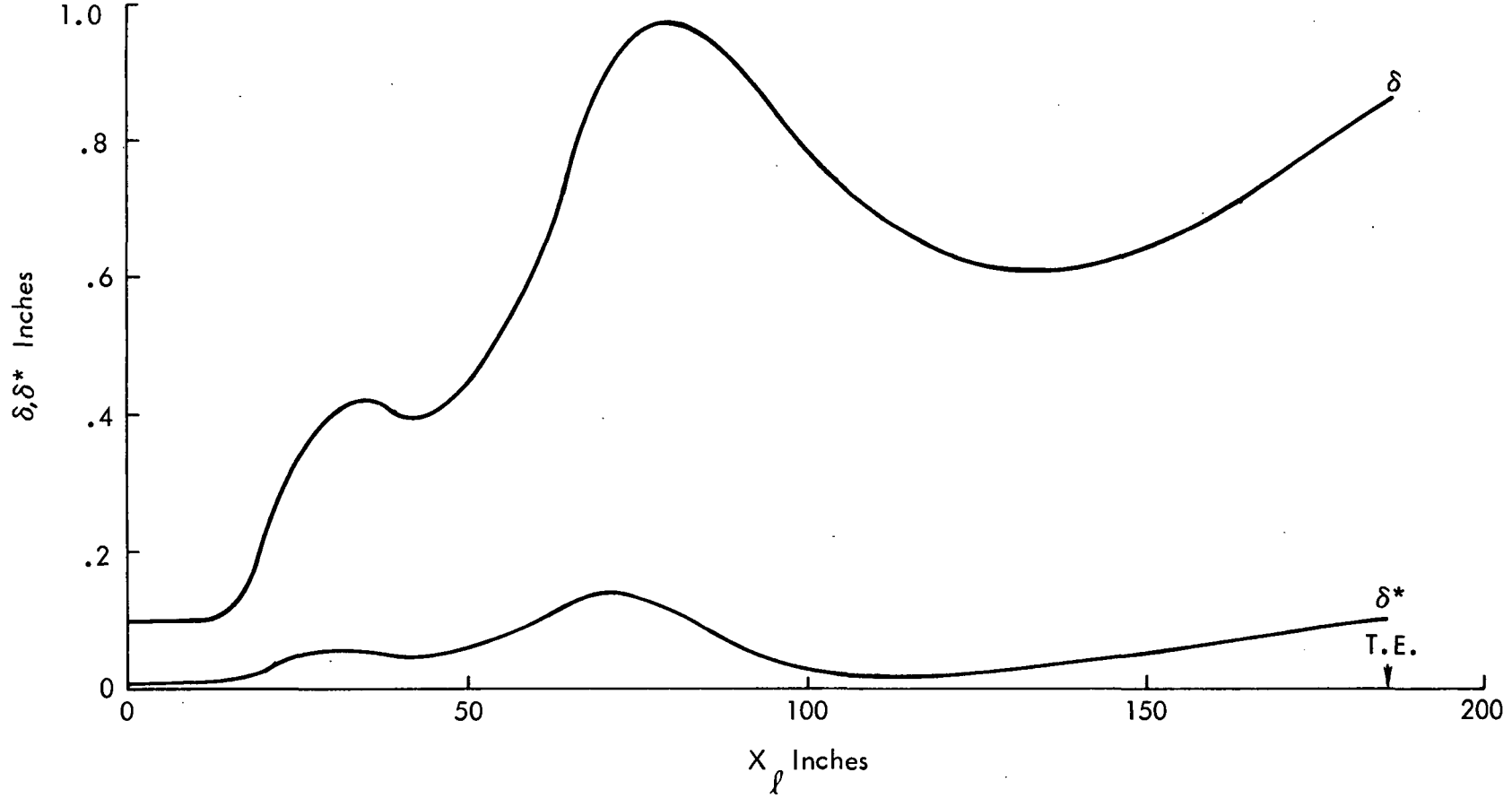

Figure 11. (Contd.) 0.133 Semispan

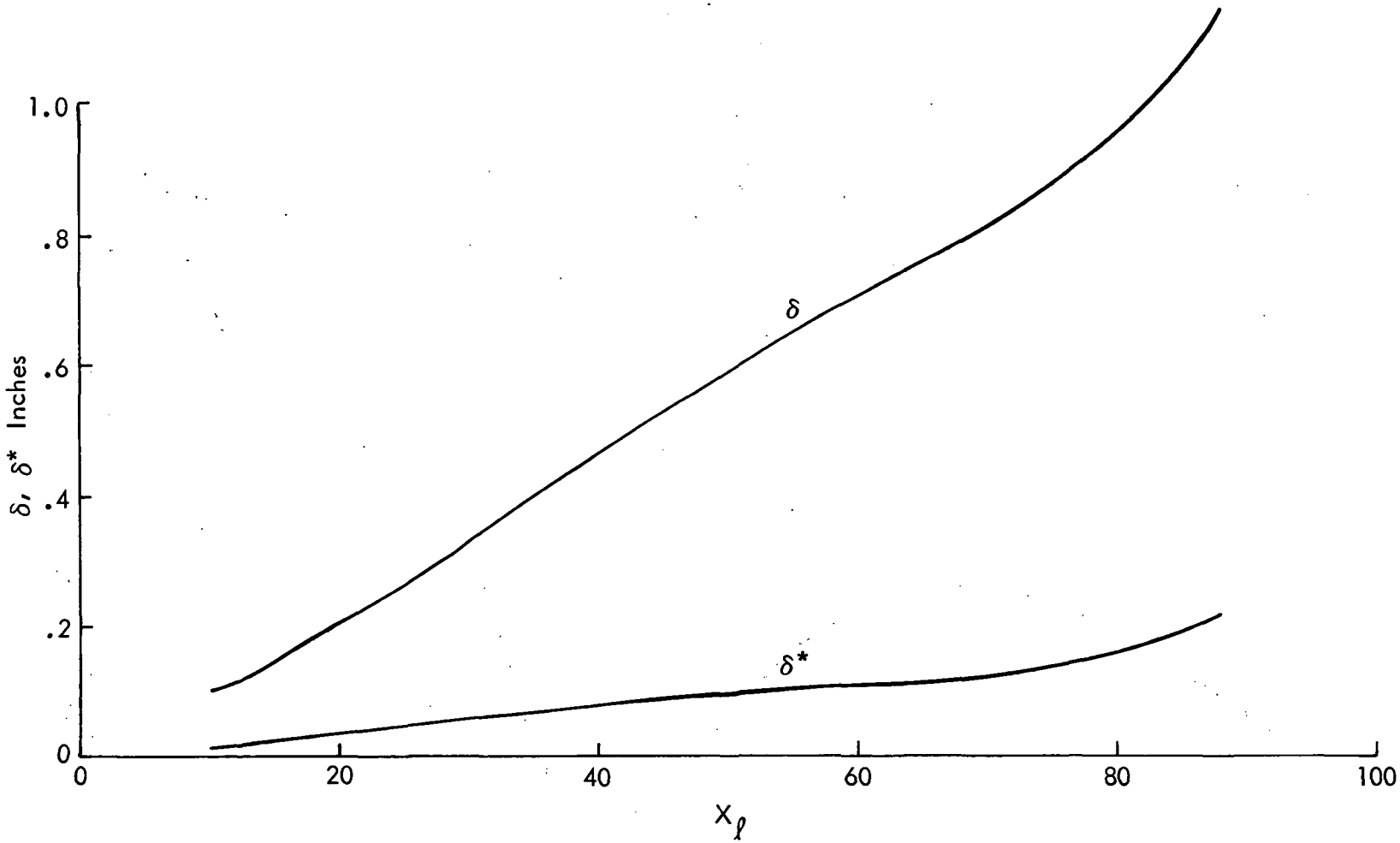

Figure 11. (Cont'd.) .307 Semispan

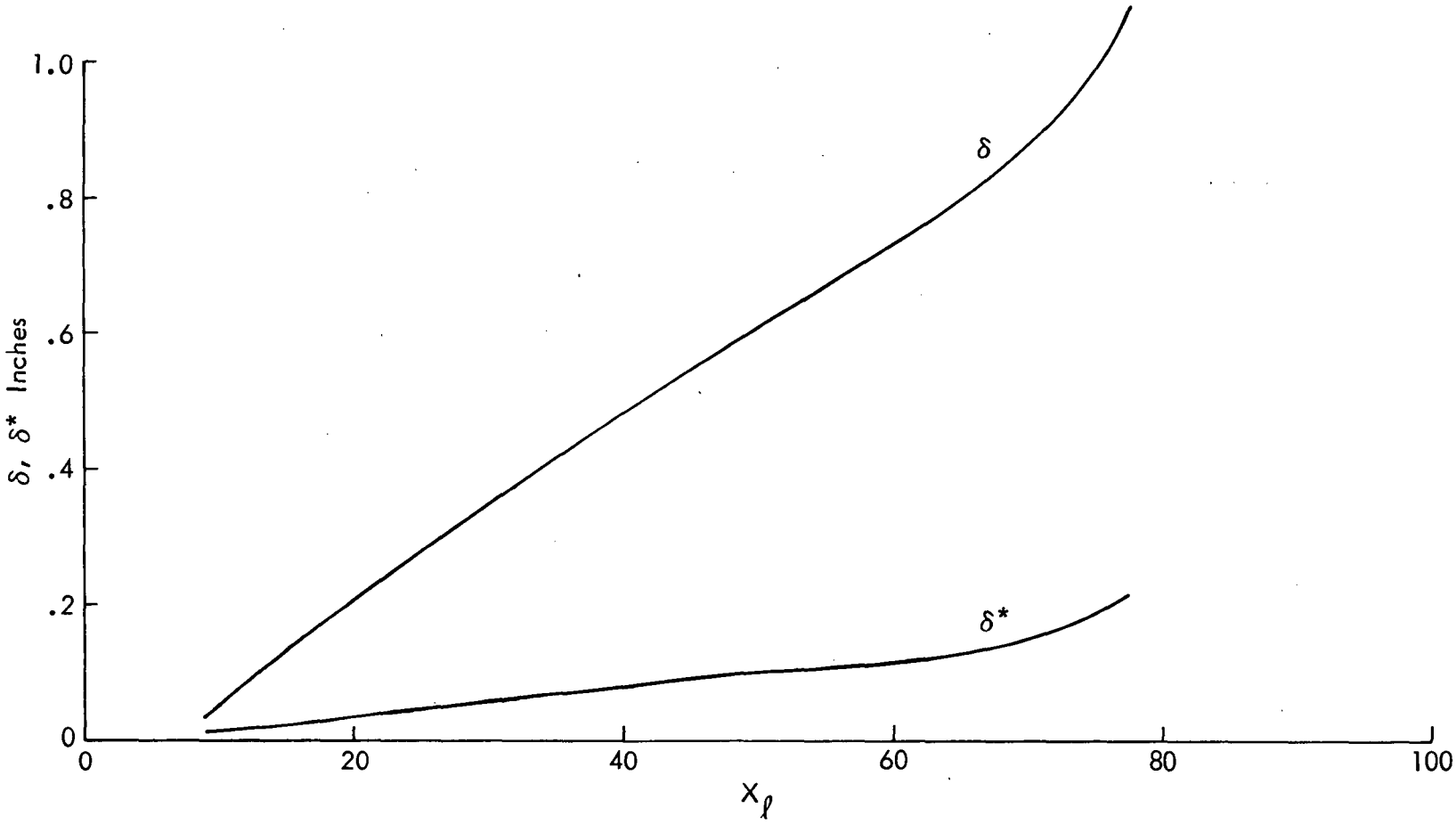

Figure 11. (Cont'd.) .458 Semispan

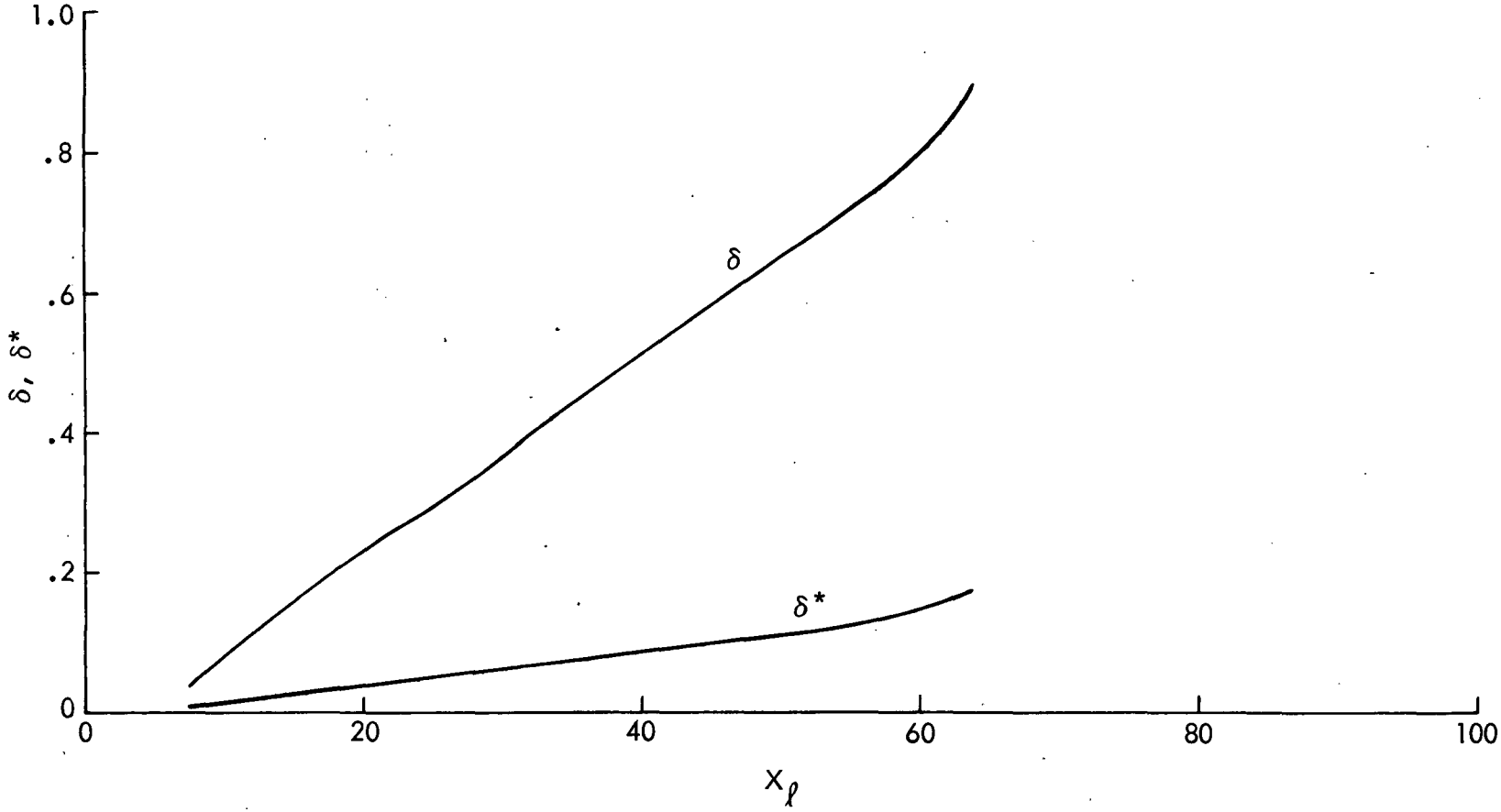

Figure 11. (Cont'd.) .653 Semispan

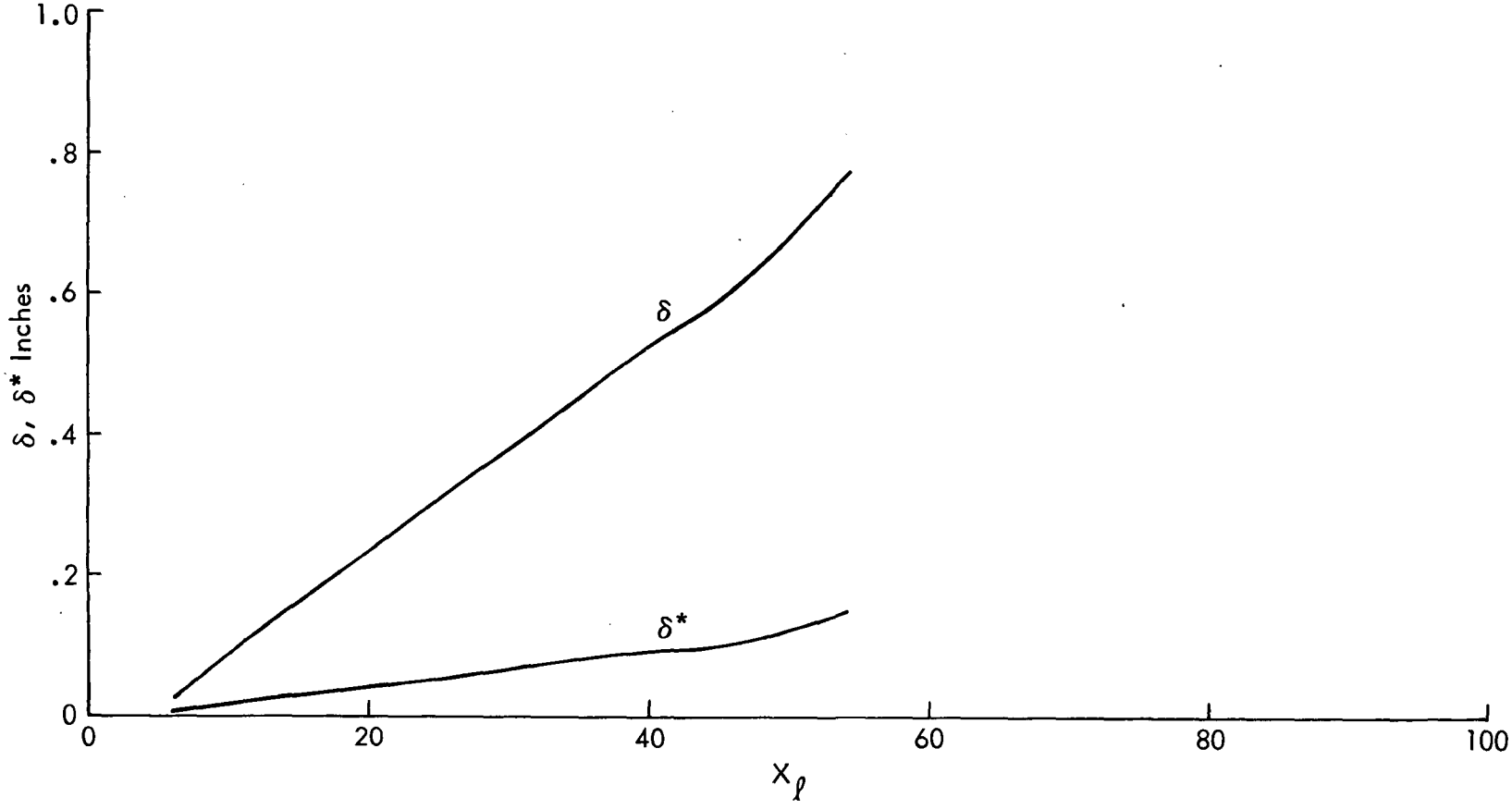

Figure 11. (Cont'd.) .804 Semispan

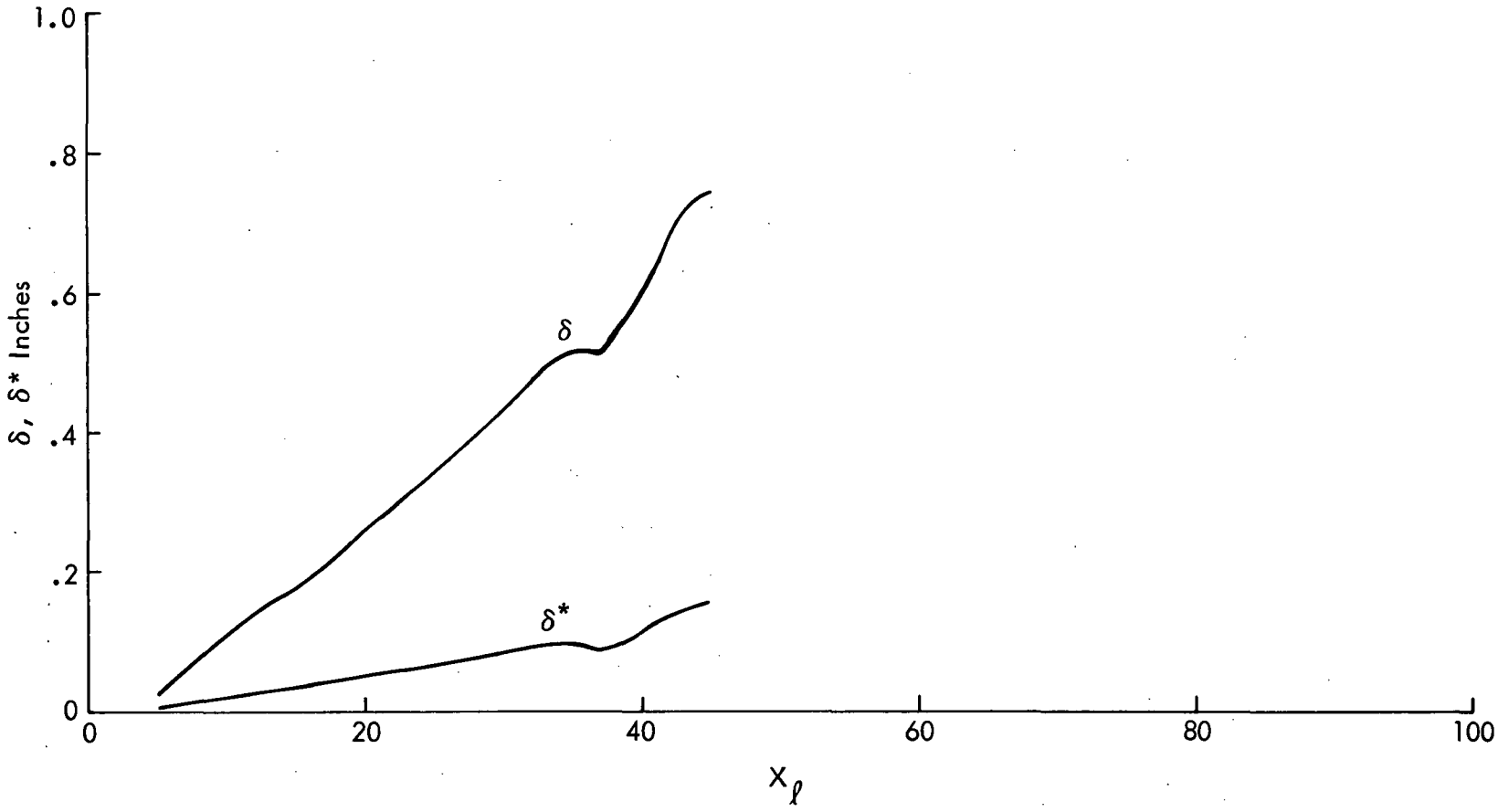

Figure 11. (Cont'd.) .933 Semispan

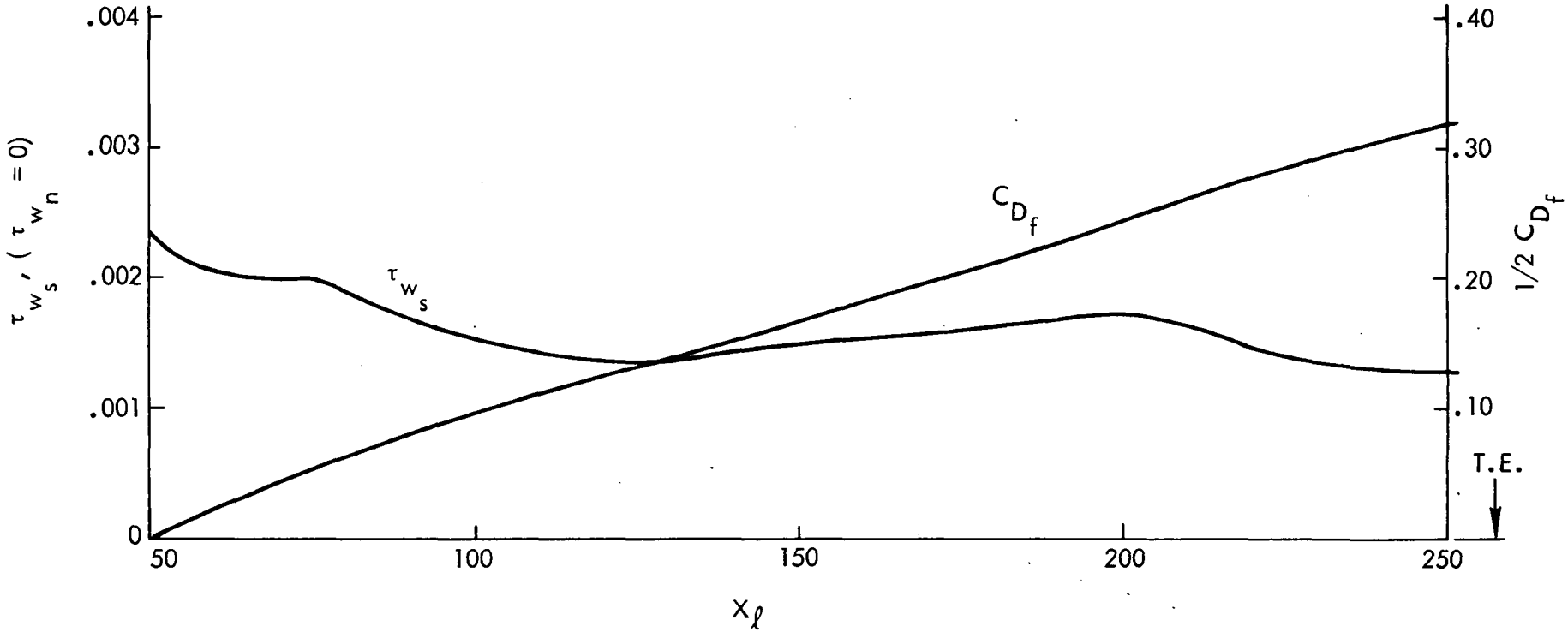

Figure 12. Skin Friction and Integrated Skin Friction
M = 0.50, Upper Surface, .044 Semispan

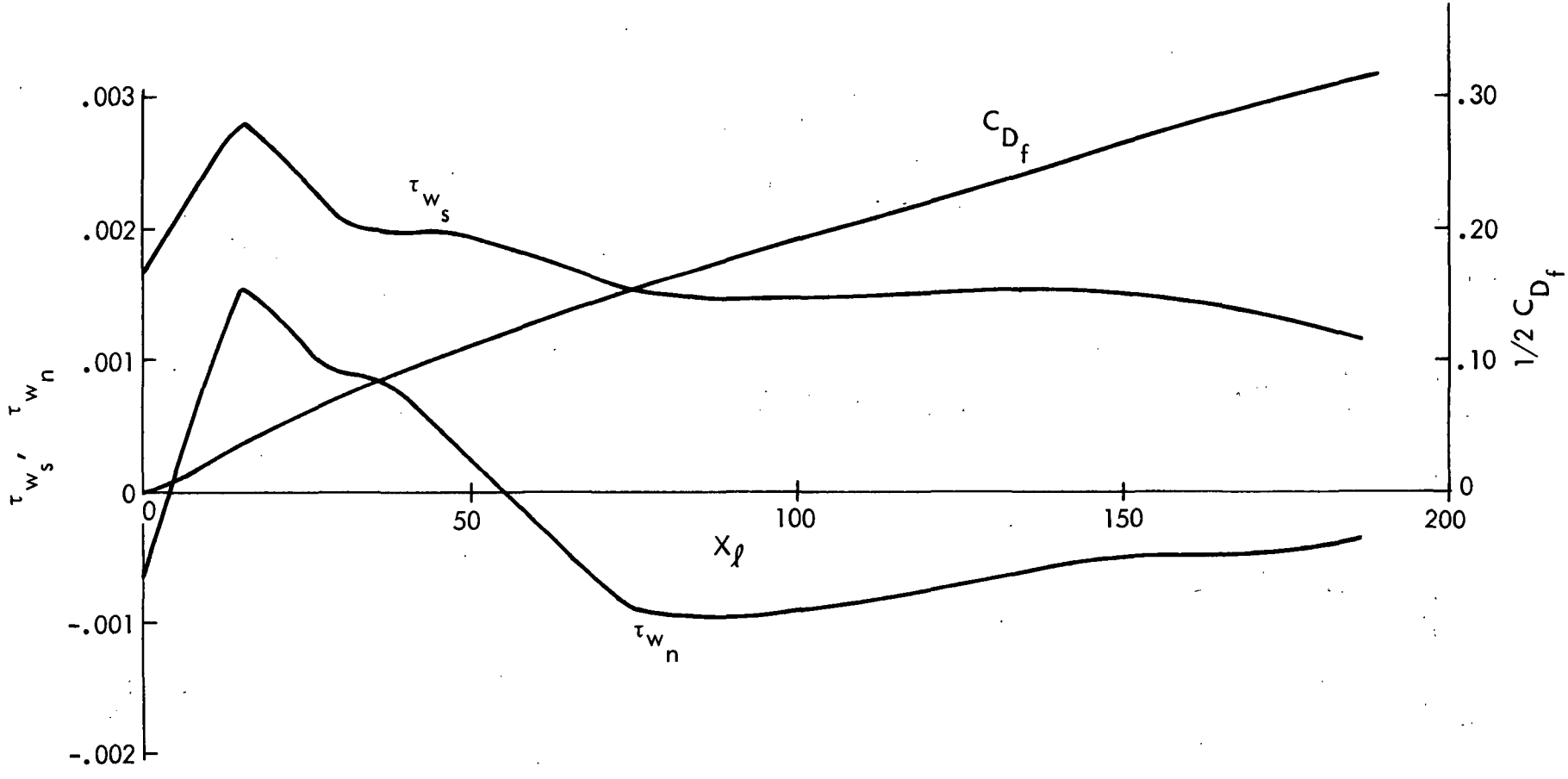

Figure 12. (Cont'd.) .133 Semispan

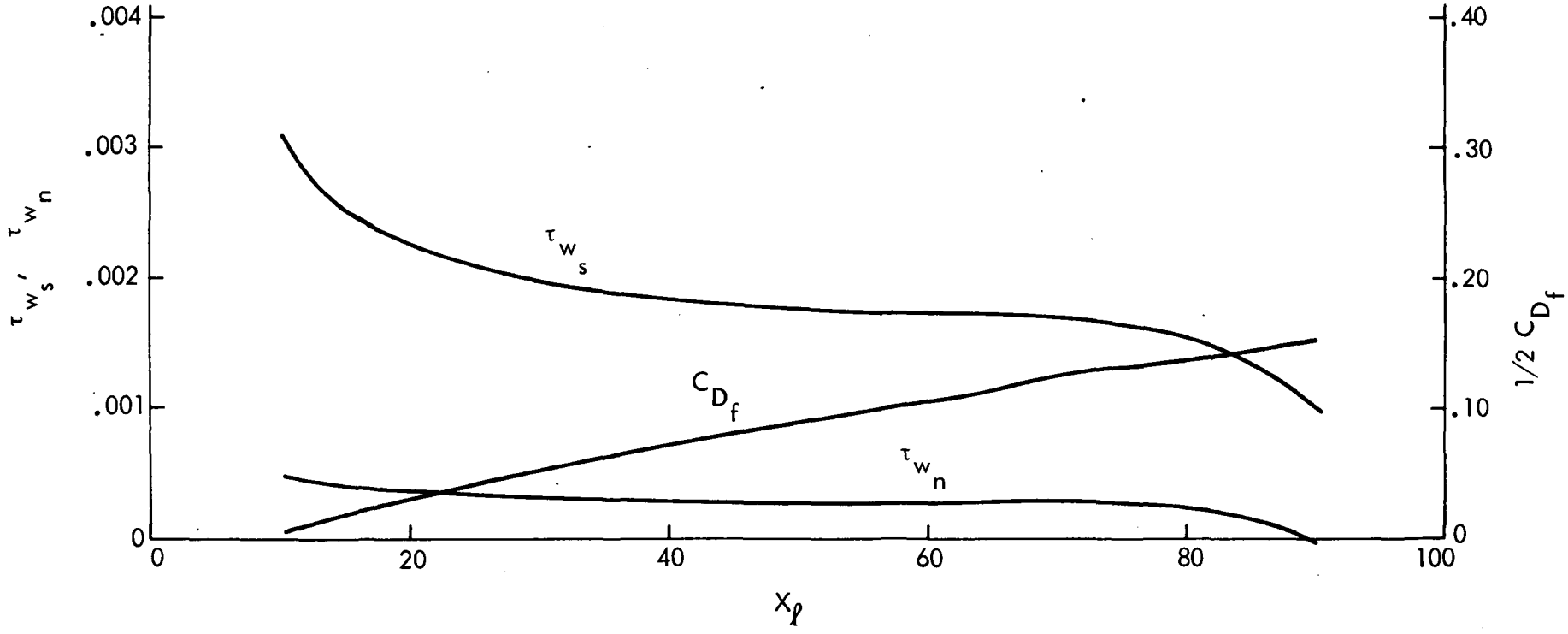

Figure 12. (Cont'd.) .307 Semispan

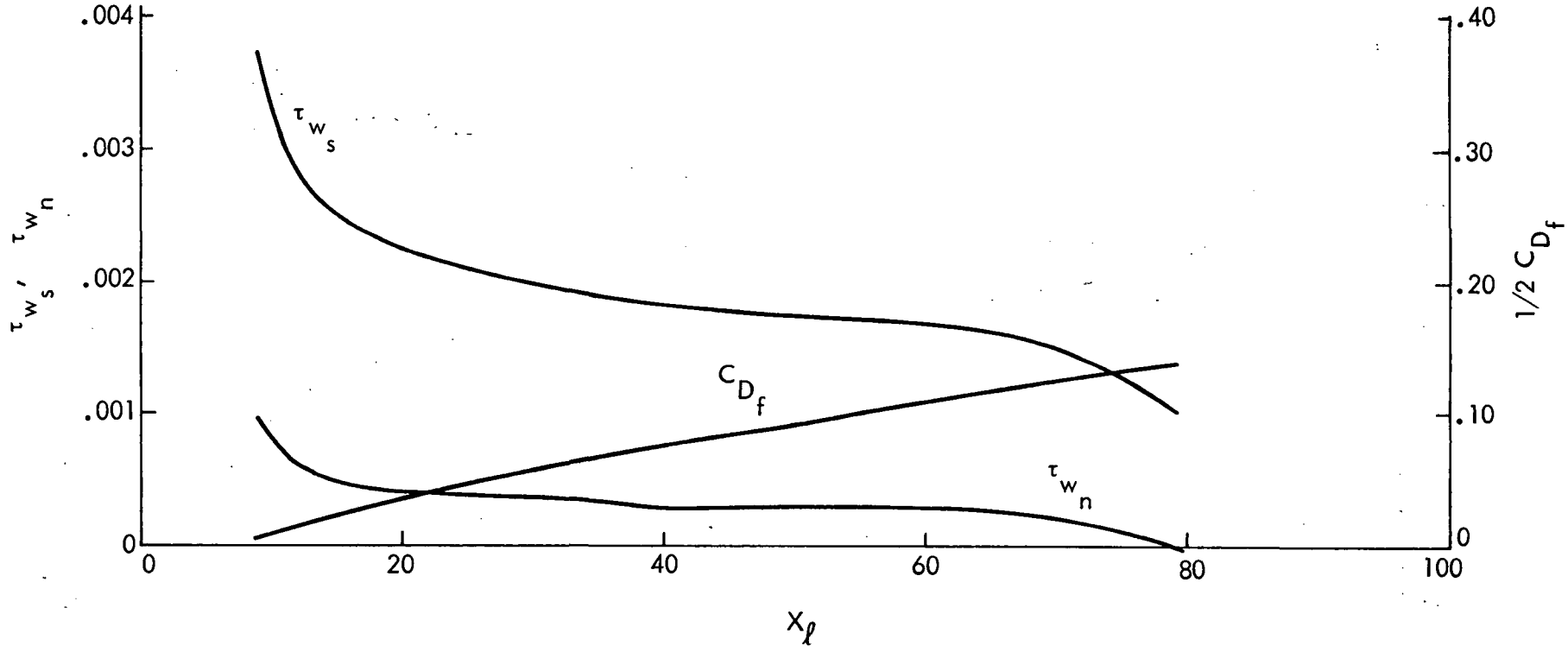

Figure 12. (Cont'd.) .458 Semispan

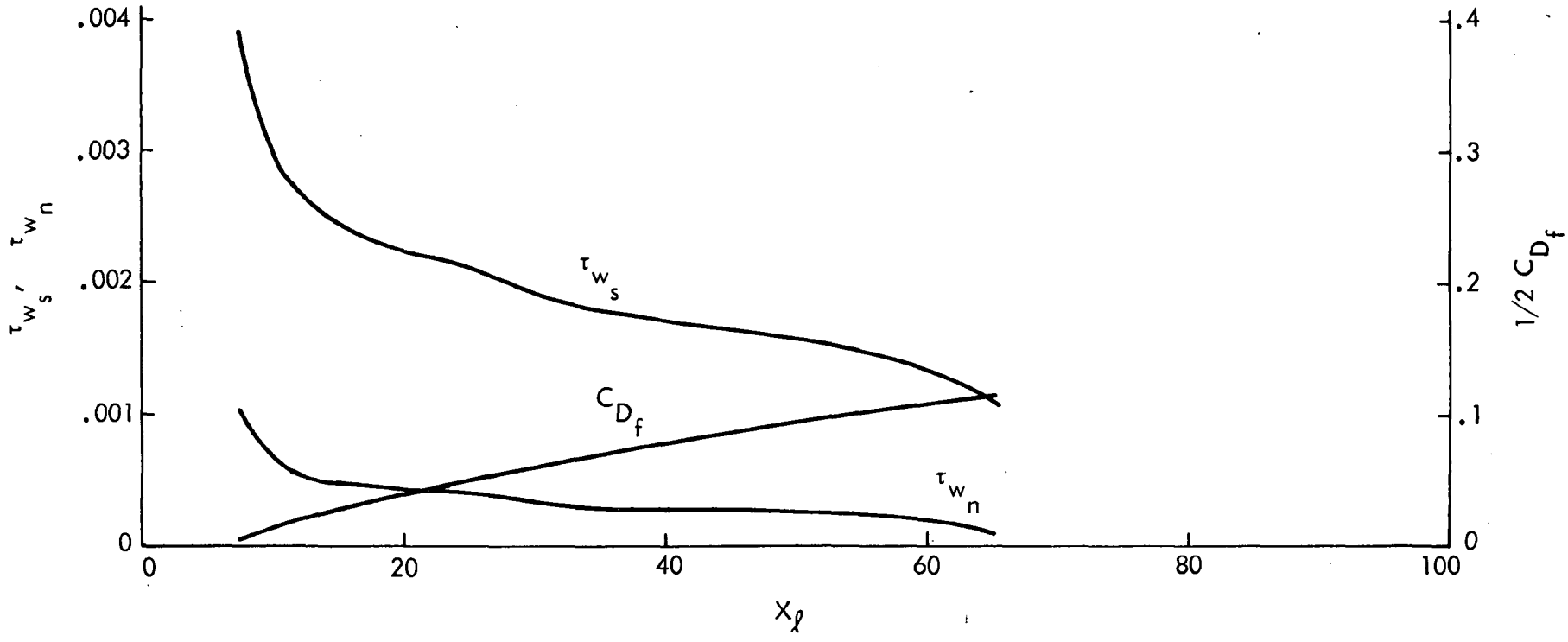

Figure 12. (Cont'd.) .653 Semispan

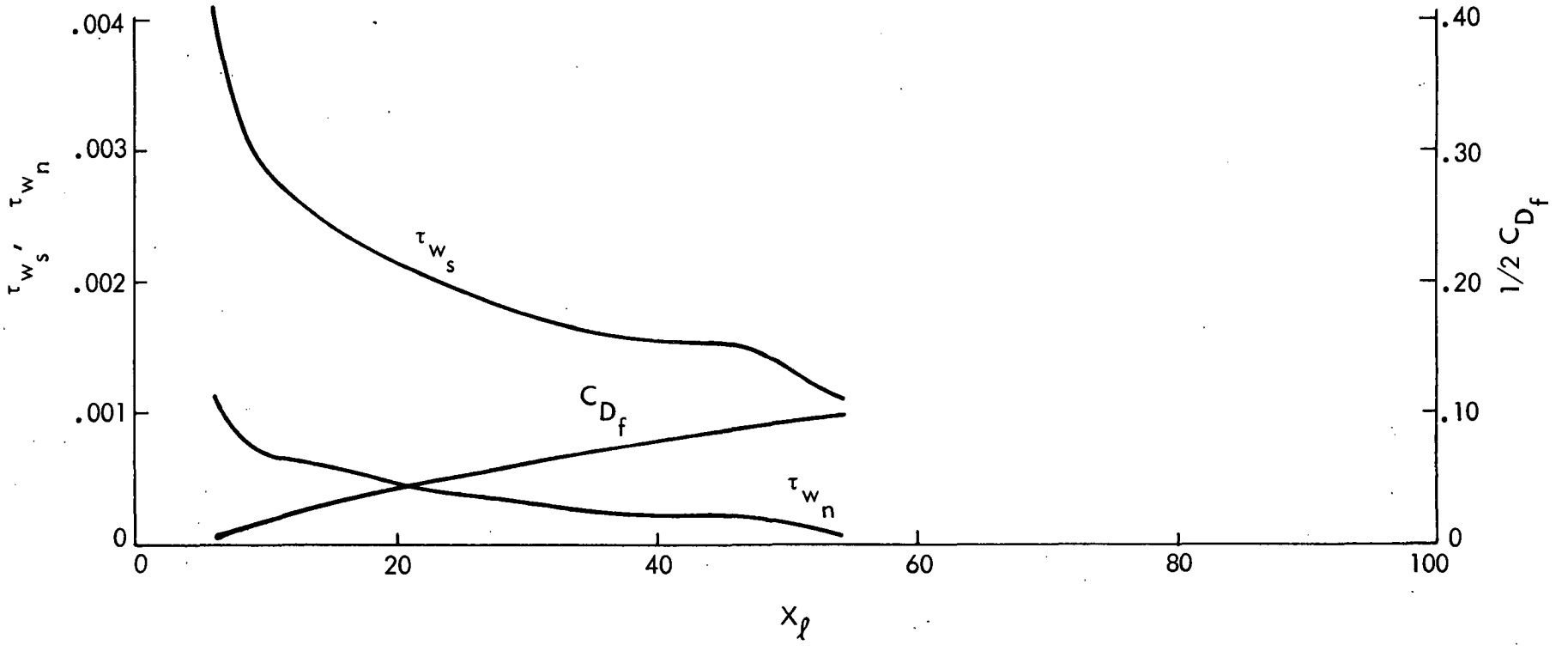

Figure 12. (Cont'd.) .804 Semispan

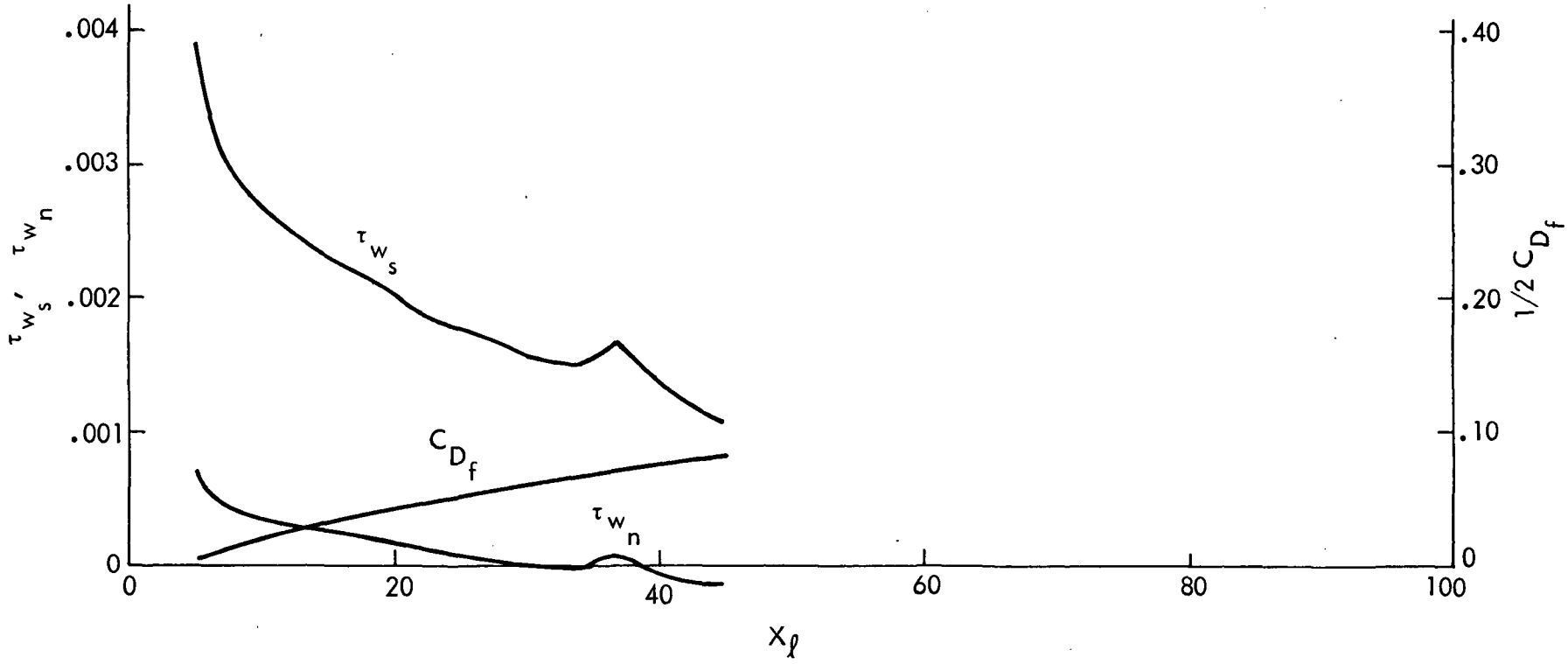

Figure 12. (Cont'd.) .933 Semispan

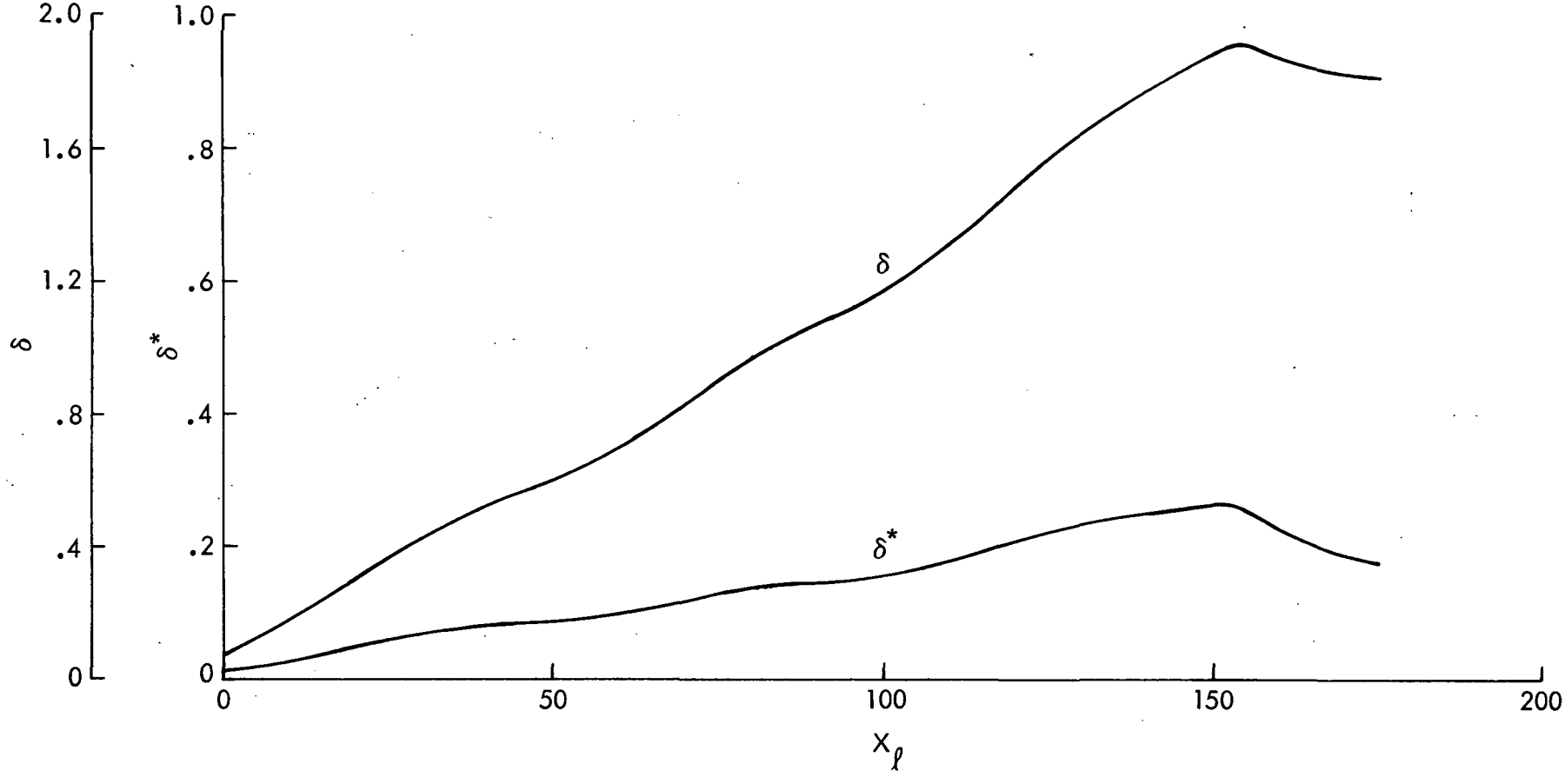

Figure 13. Boundary Layer Thickness and Displacement Thickness, M = 0.50, Lower Surface: .133 Semispan

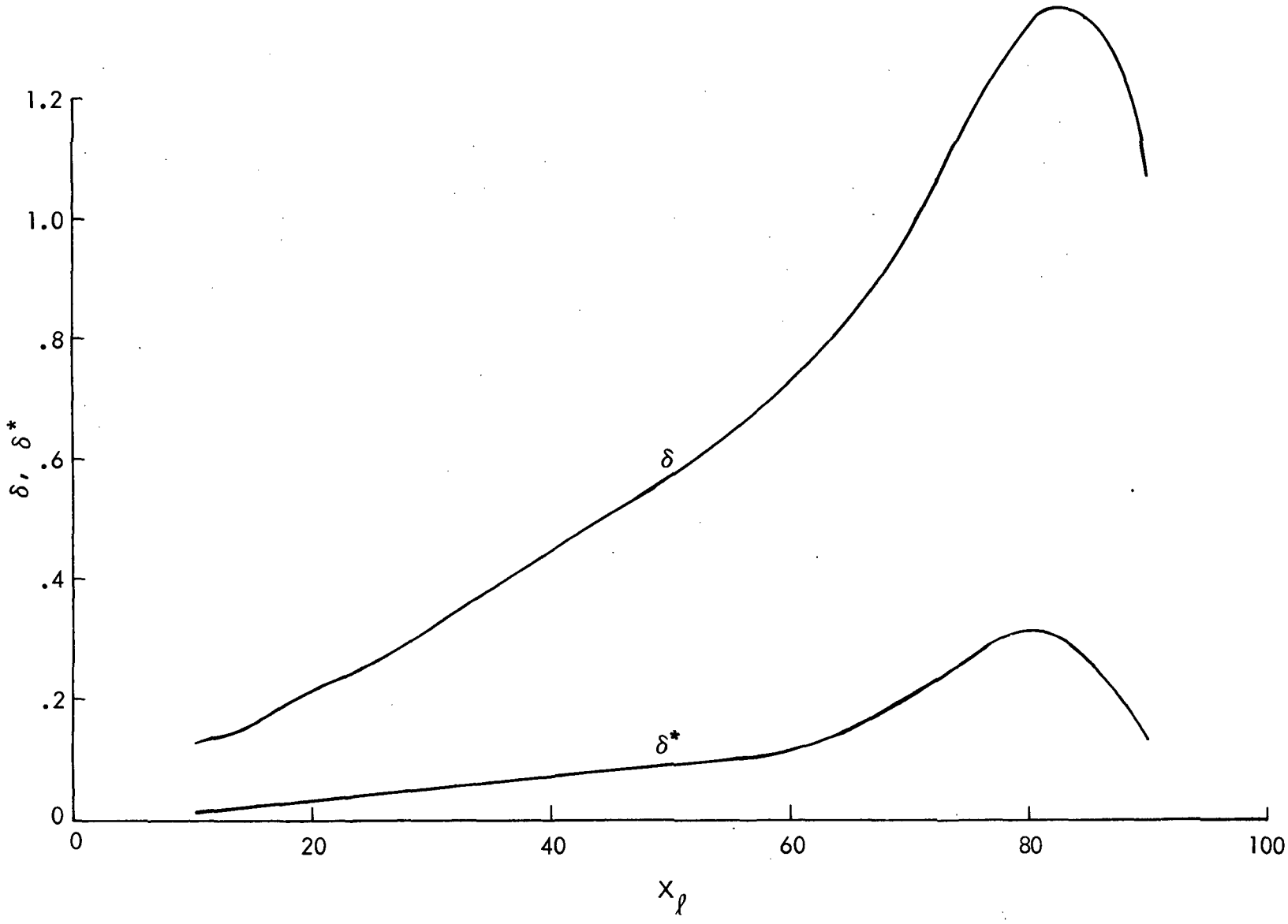

Figure 13. (Cont'd.) .307 Semispan

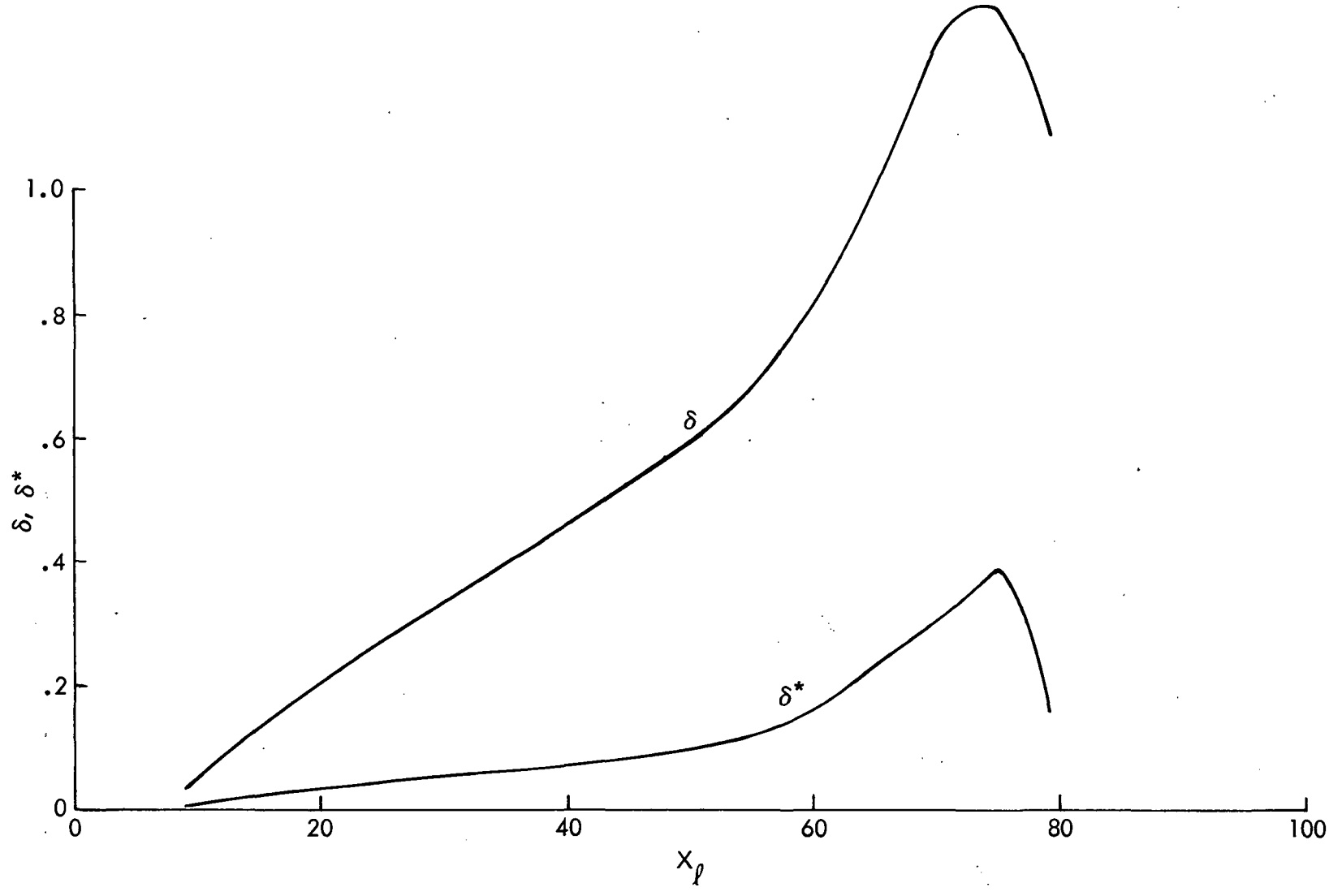

Figure 13. (Cont'd.) .458 Semispan

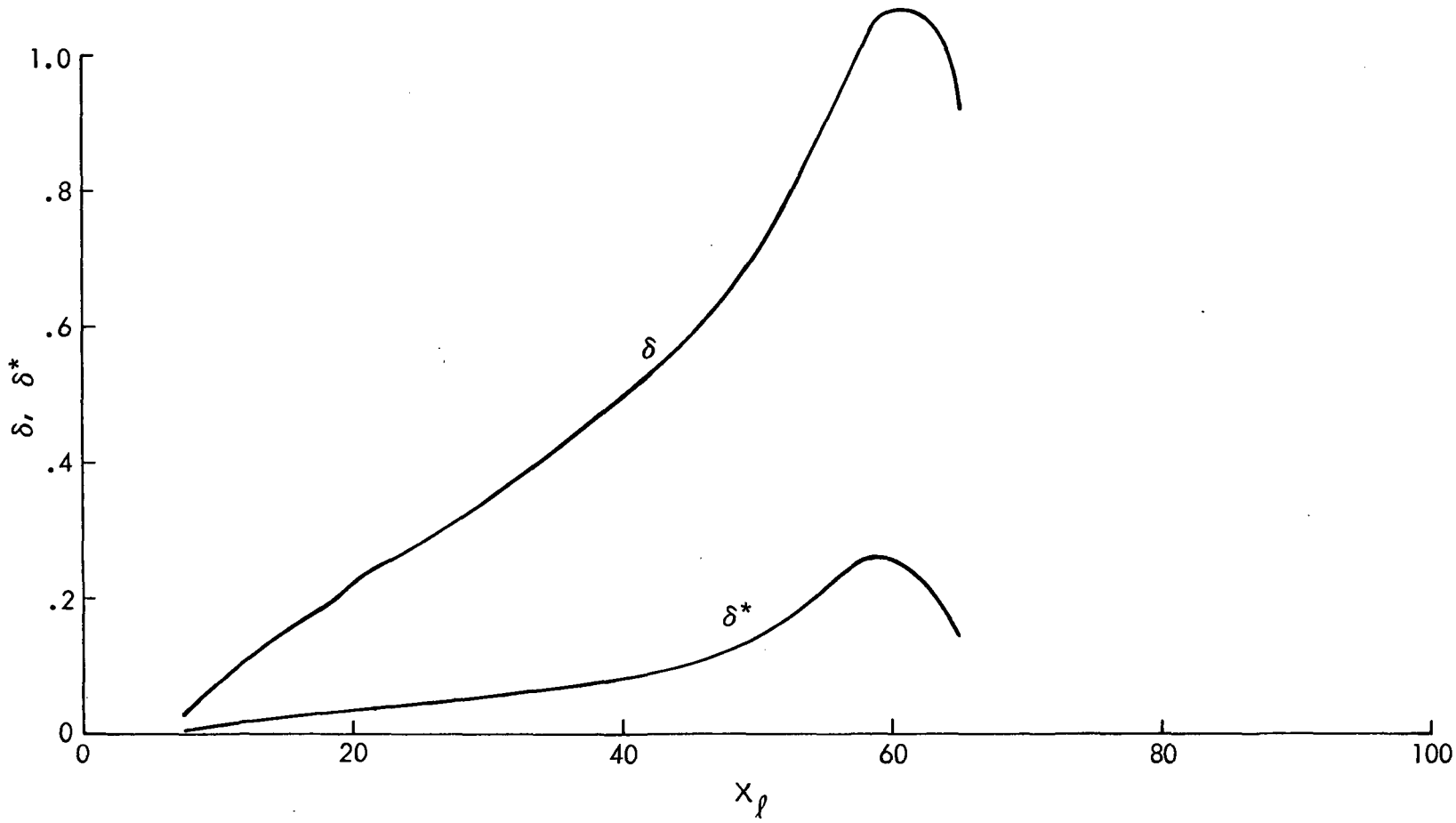

Figure 13. (Cont'd.) .653 Semispan

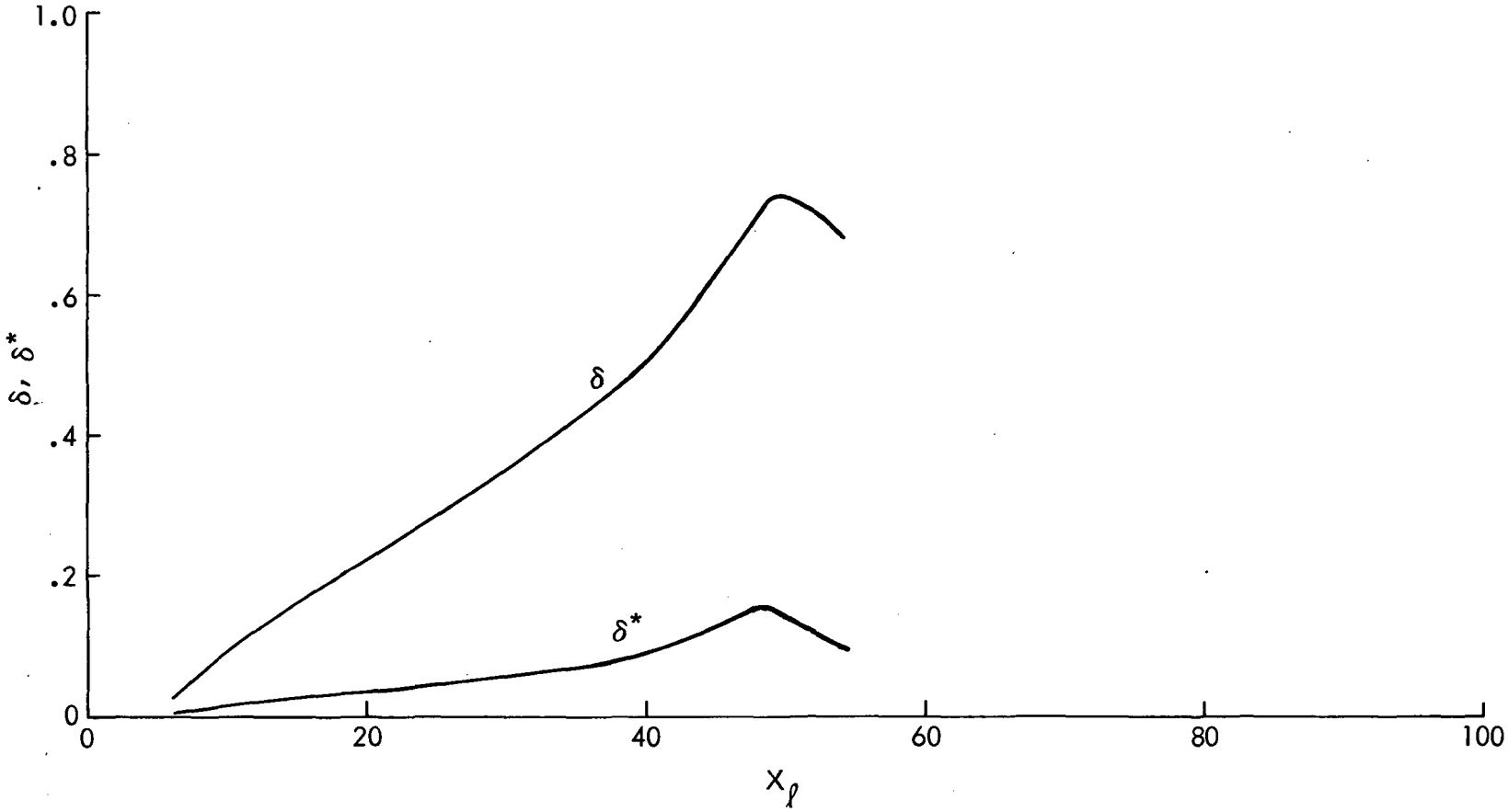

Figure 13. (Cont'd.) .804 Semispan

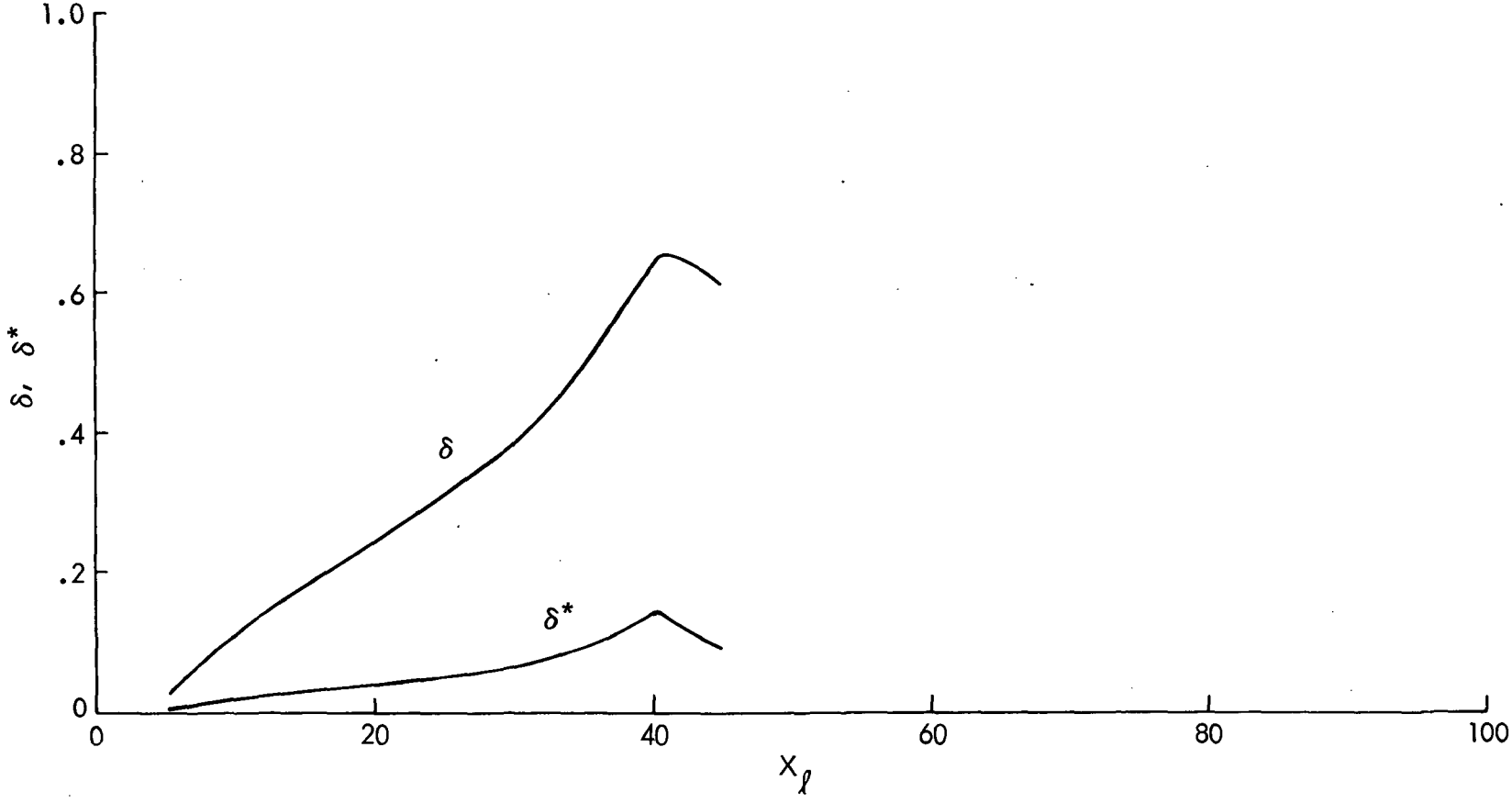

Figure 13. (Cont'd.) .933 Semispan

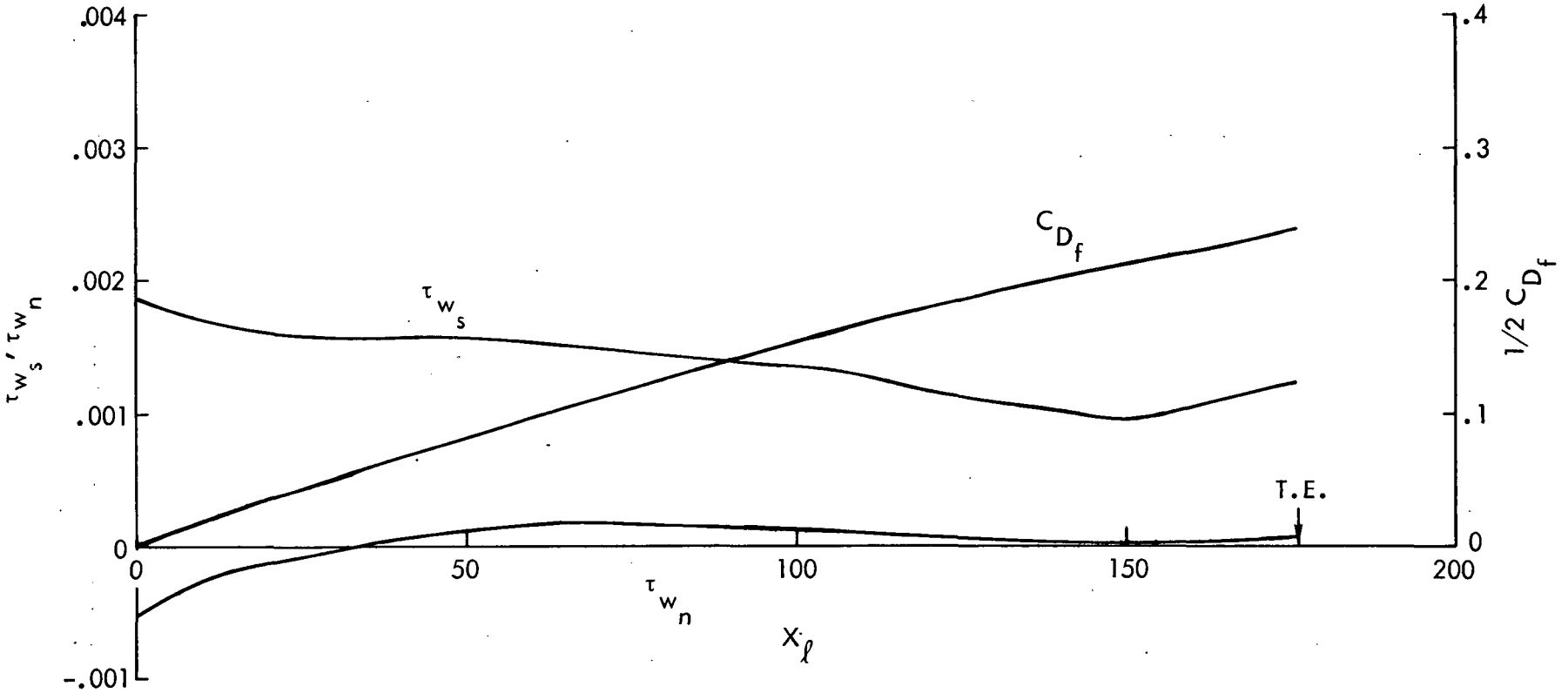

Figure 14. Skin Friction Components and Integrated Skin Friction
M = 0.50, Lower Surface, .133 Semispan

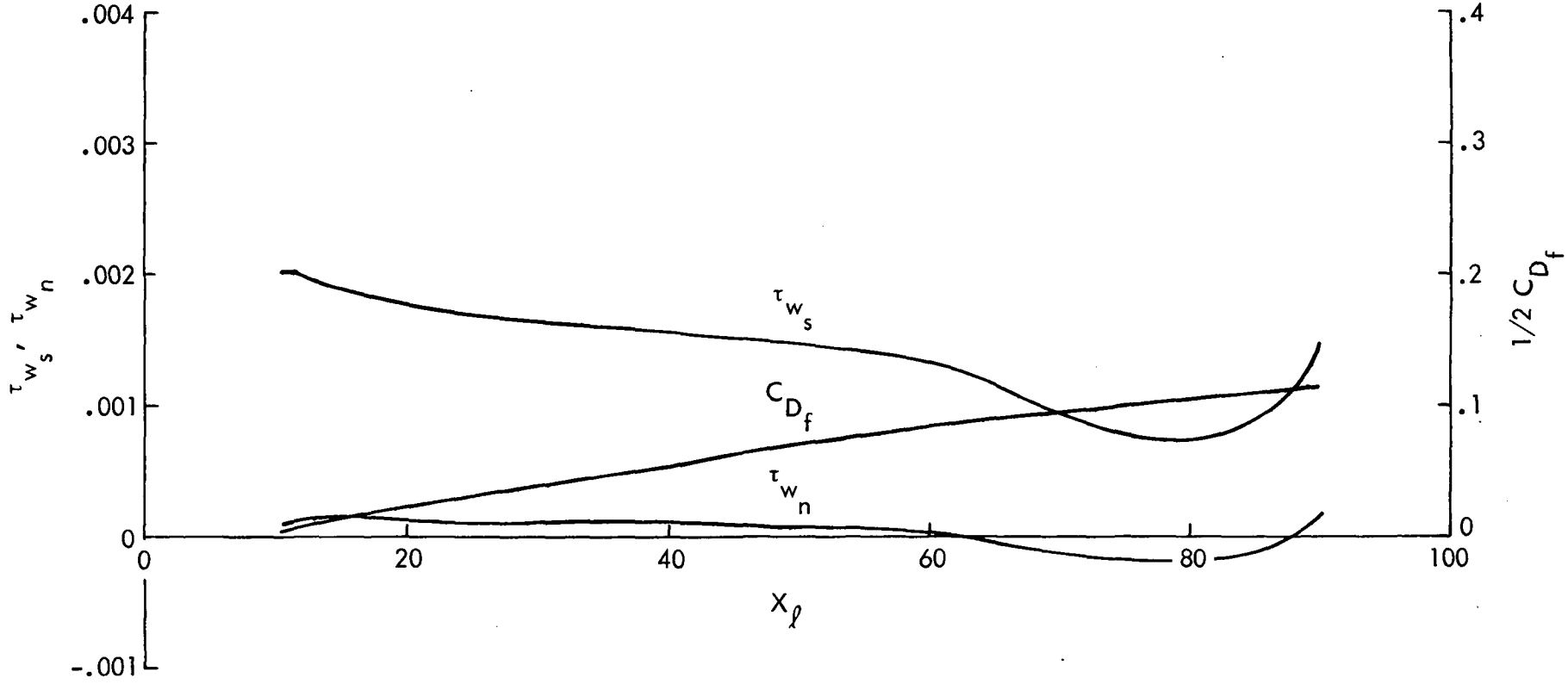

Figure 14. (Cont'd.) .307 Semispan

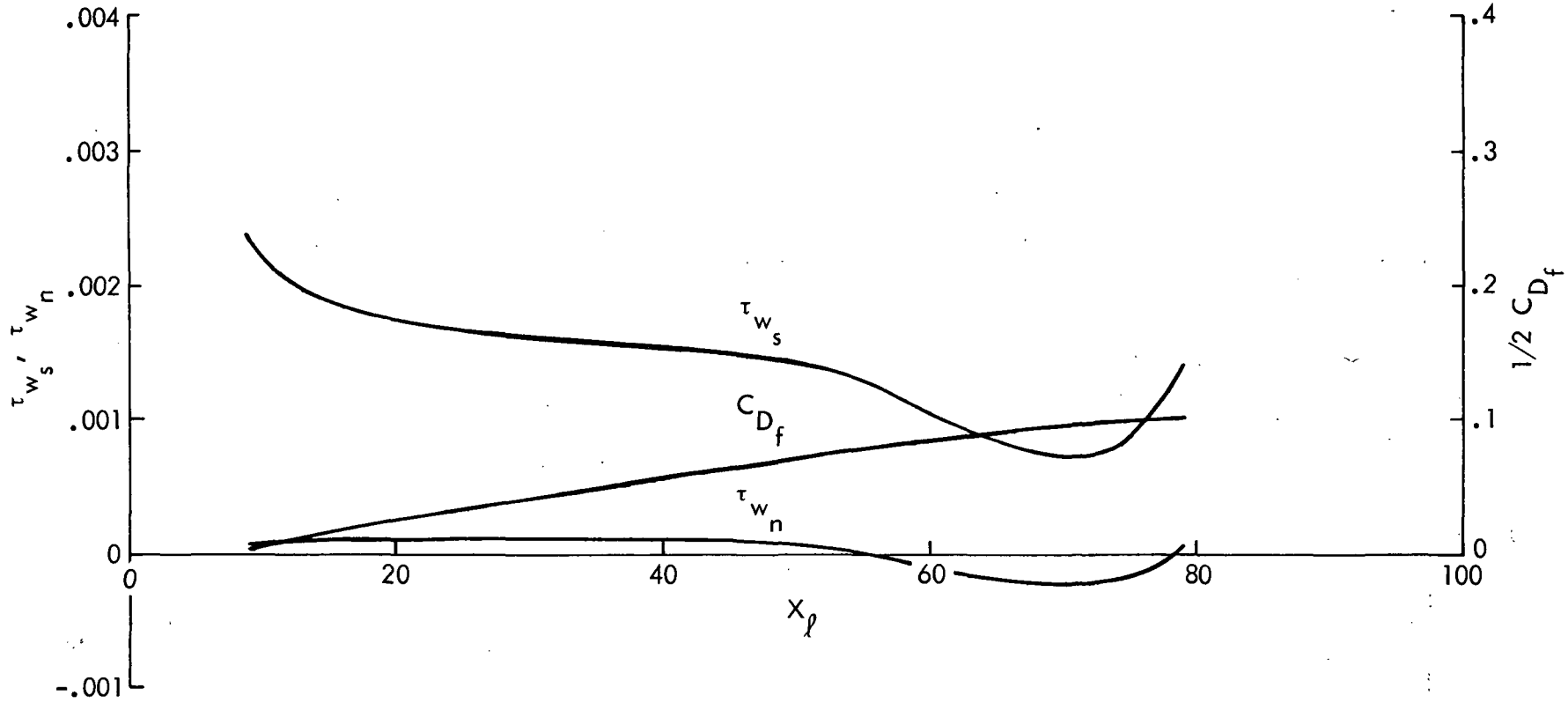

Figure 14. (Cont'd) .458 Semispan

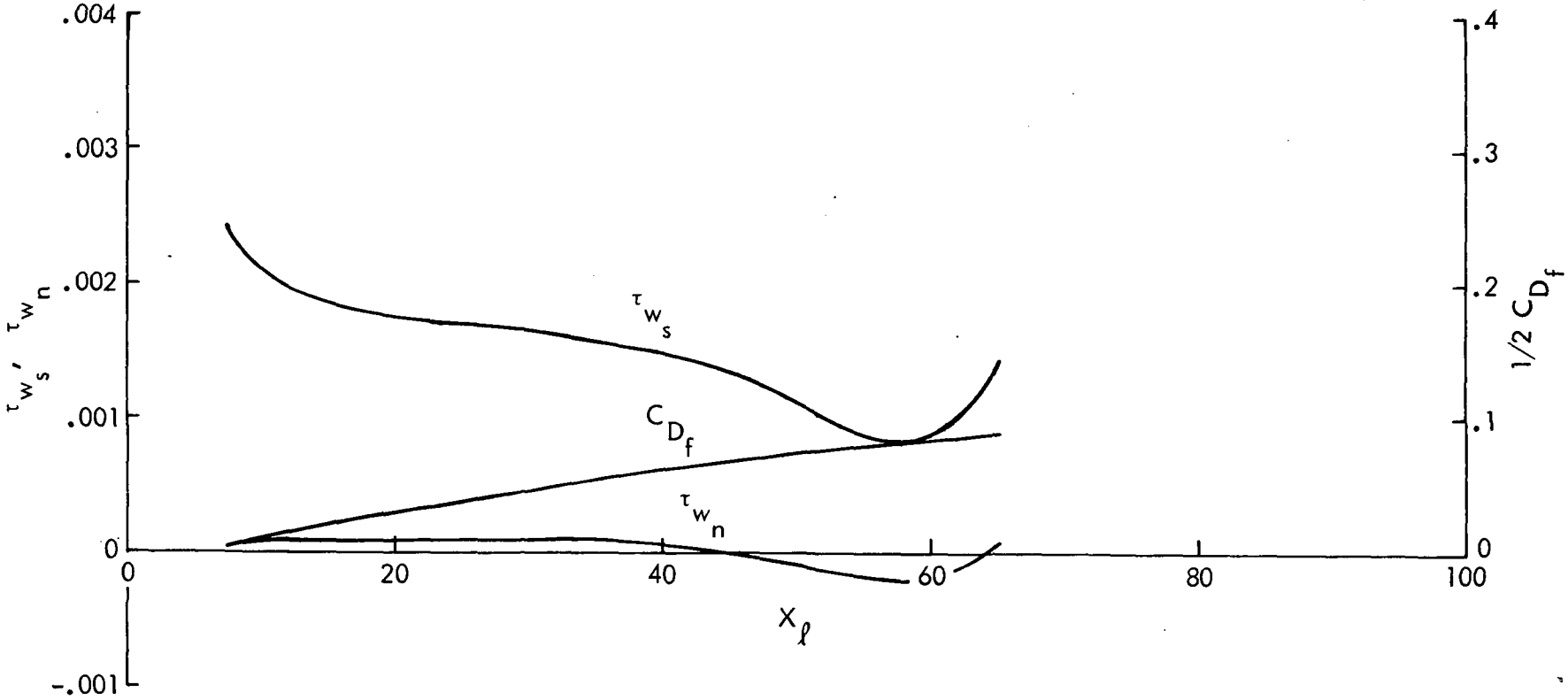

Figure 14. (Cont'd.) .653 Semispan

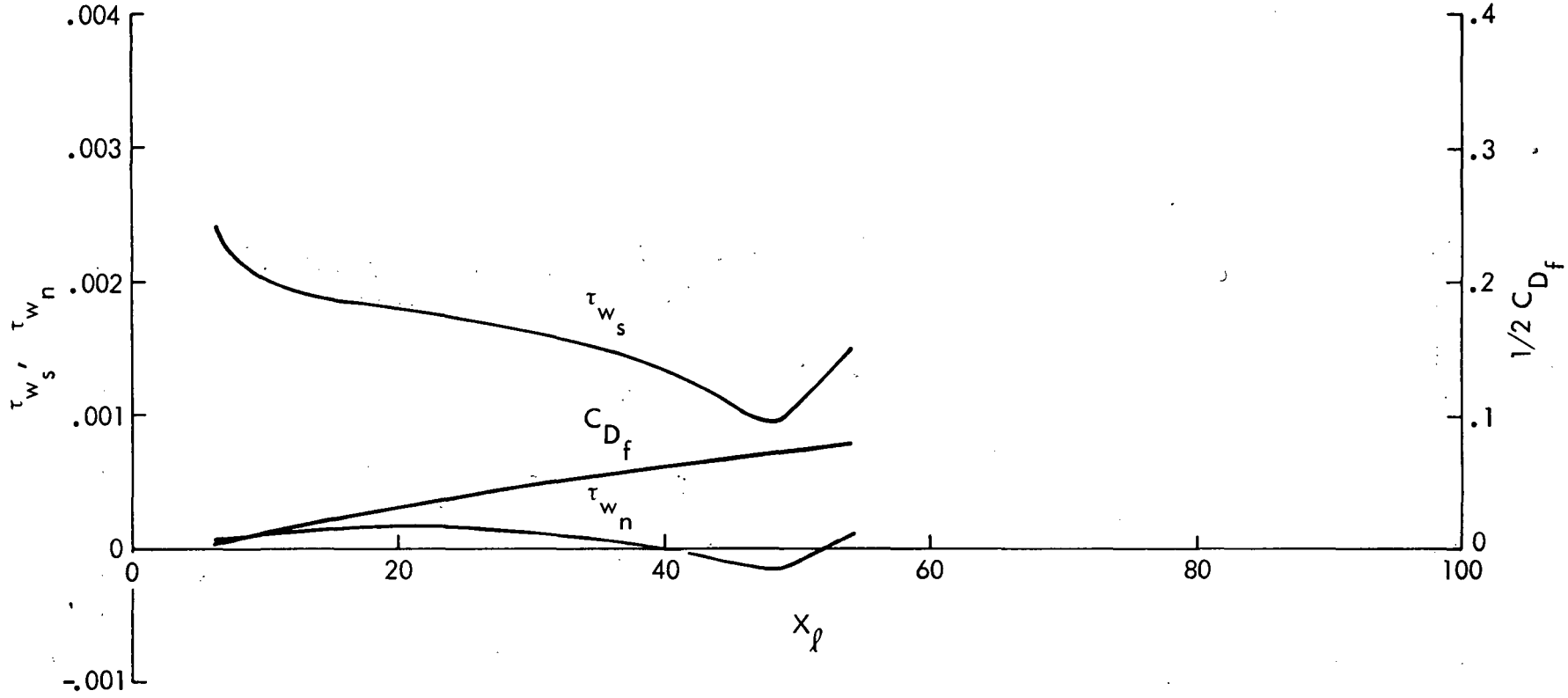

Figure 14. (Cont'd.) .804 Semispan

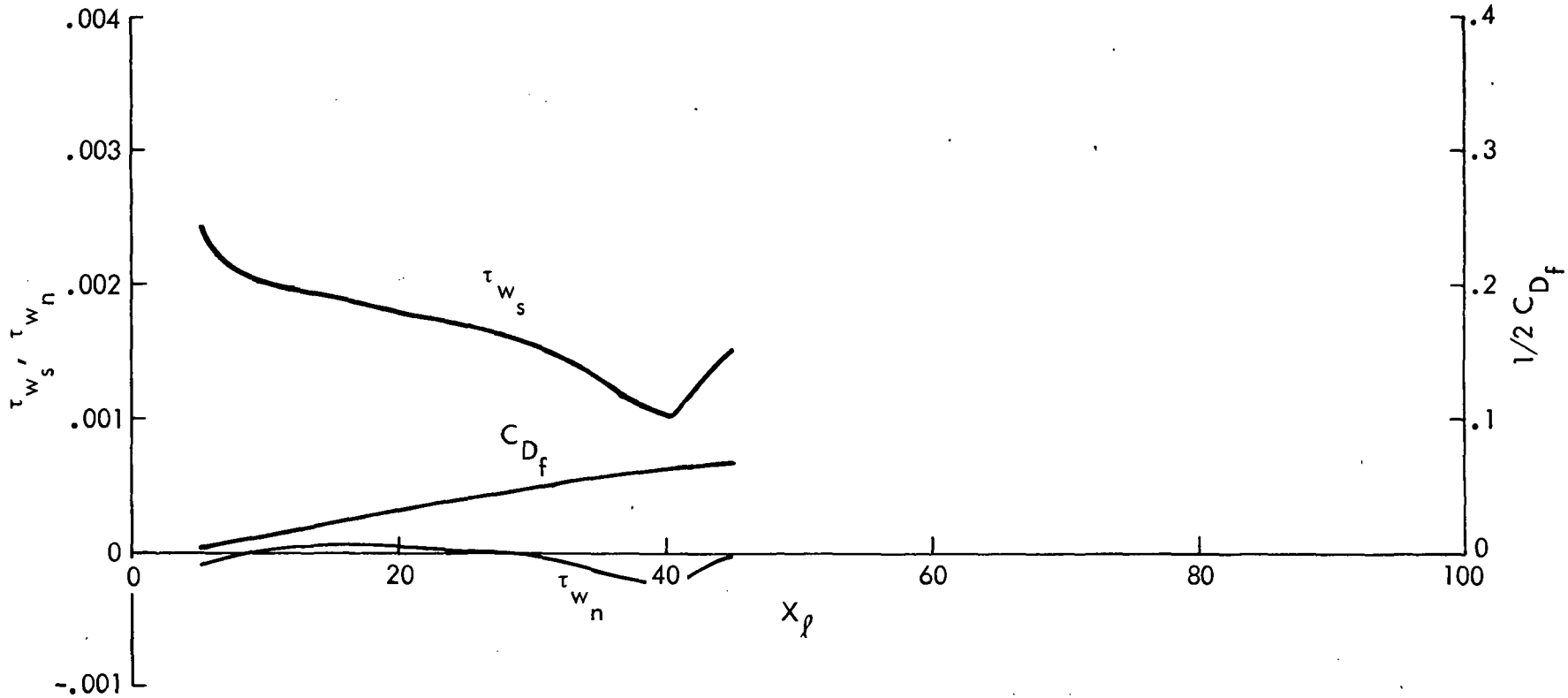

Figure 14. (Cont'd.) .933 Semispan

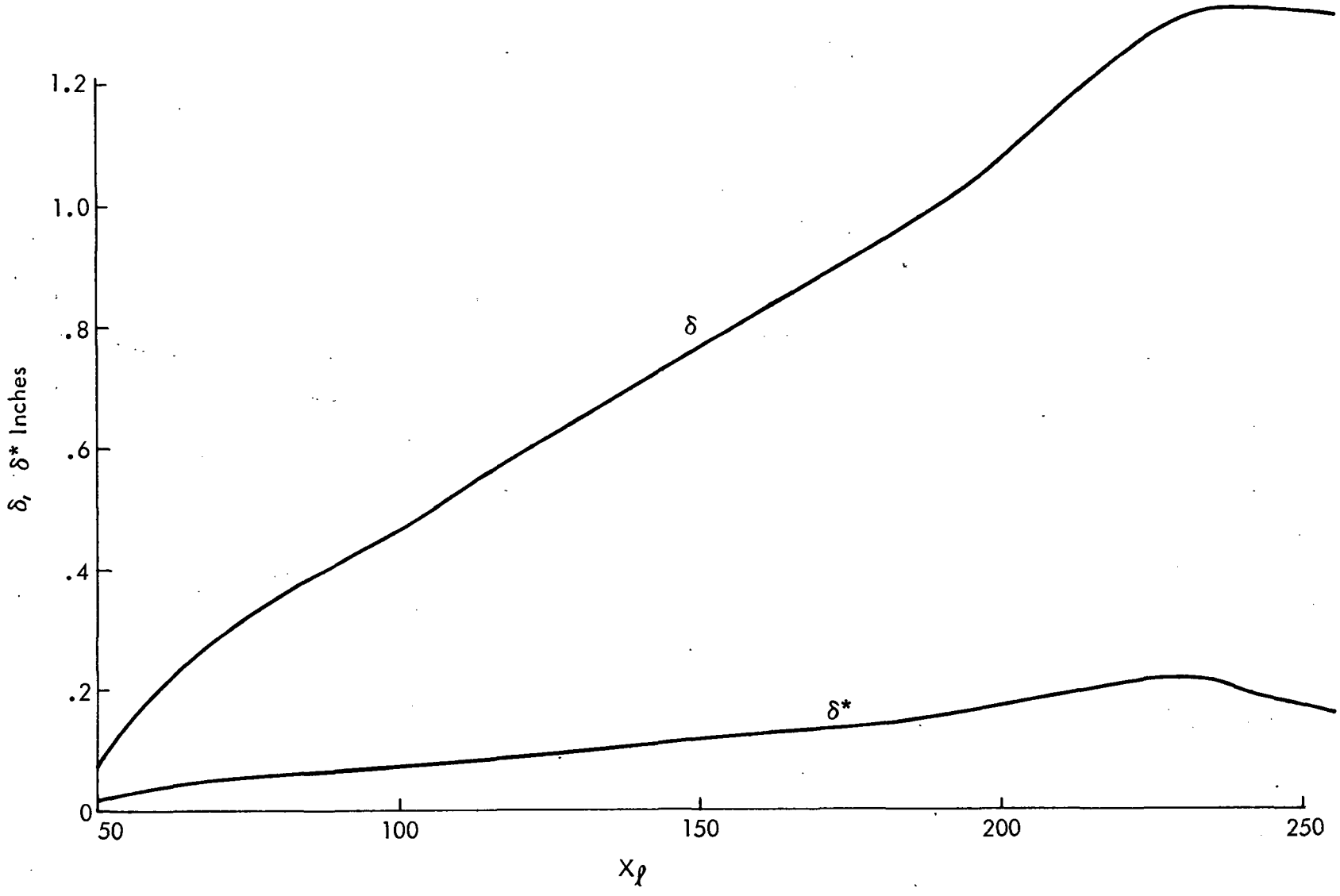

Figure 15. Boundary Layer Thickness and Displacement Thickness, M = 0.99, Upper Surface, .044 Semispan

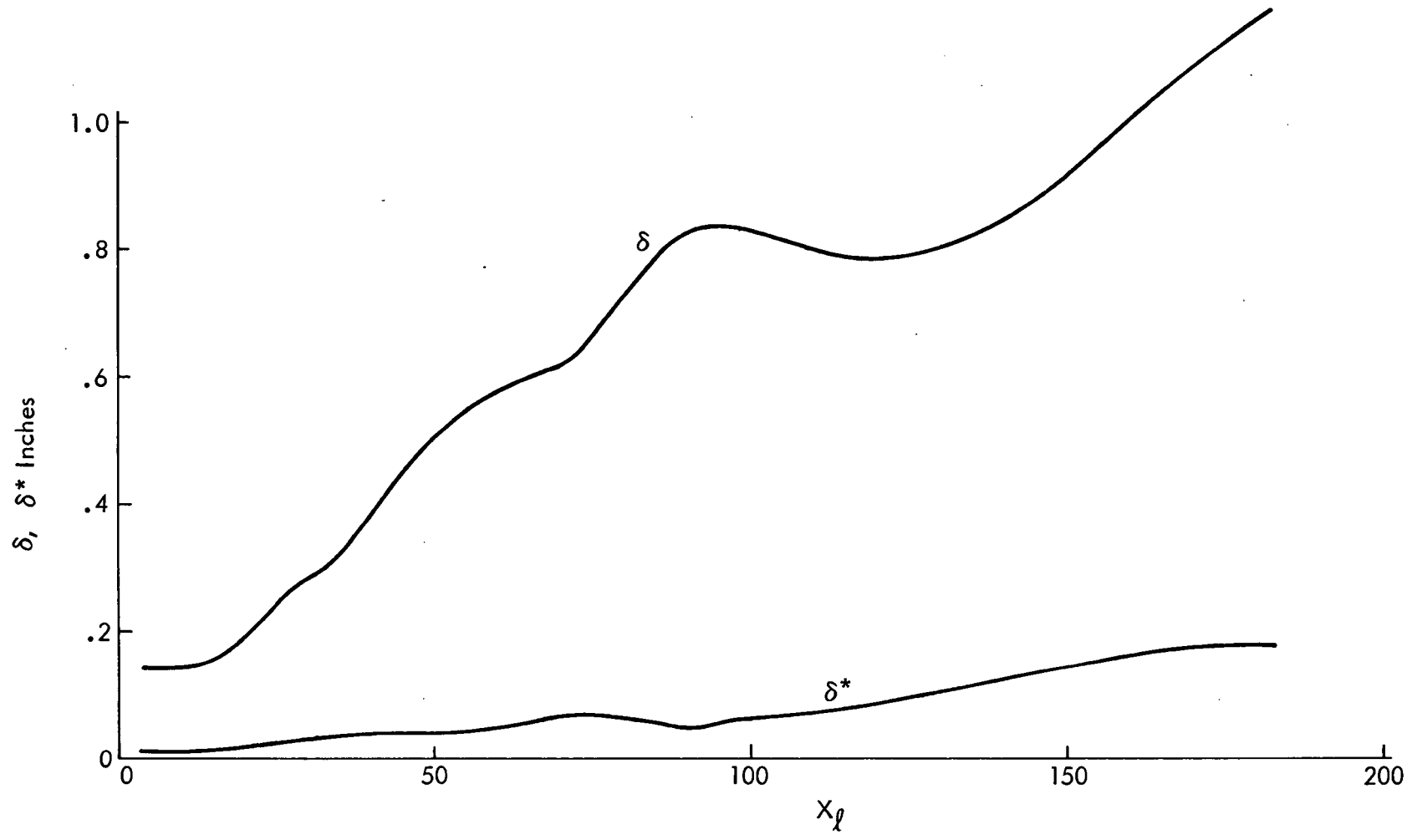

Figure 15. (Cont'd.) .133 Semispan

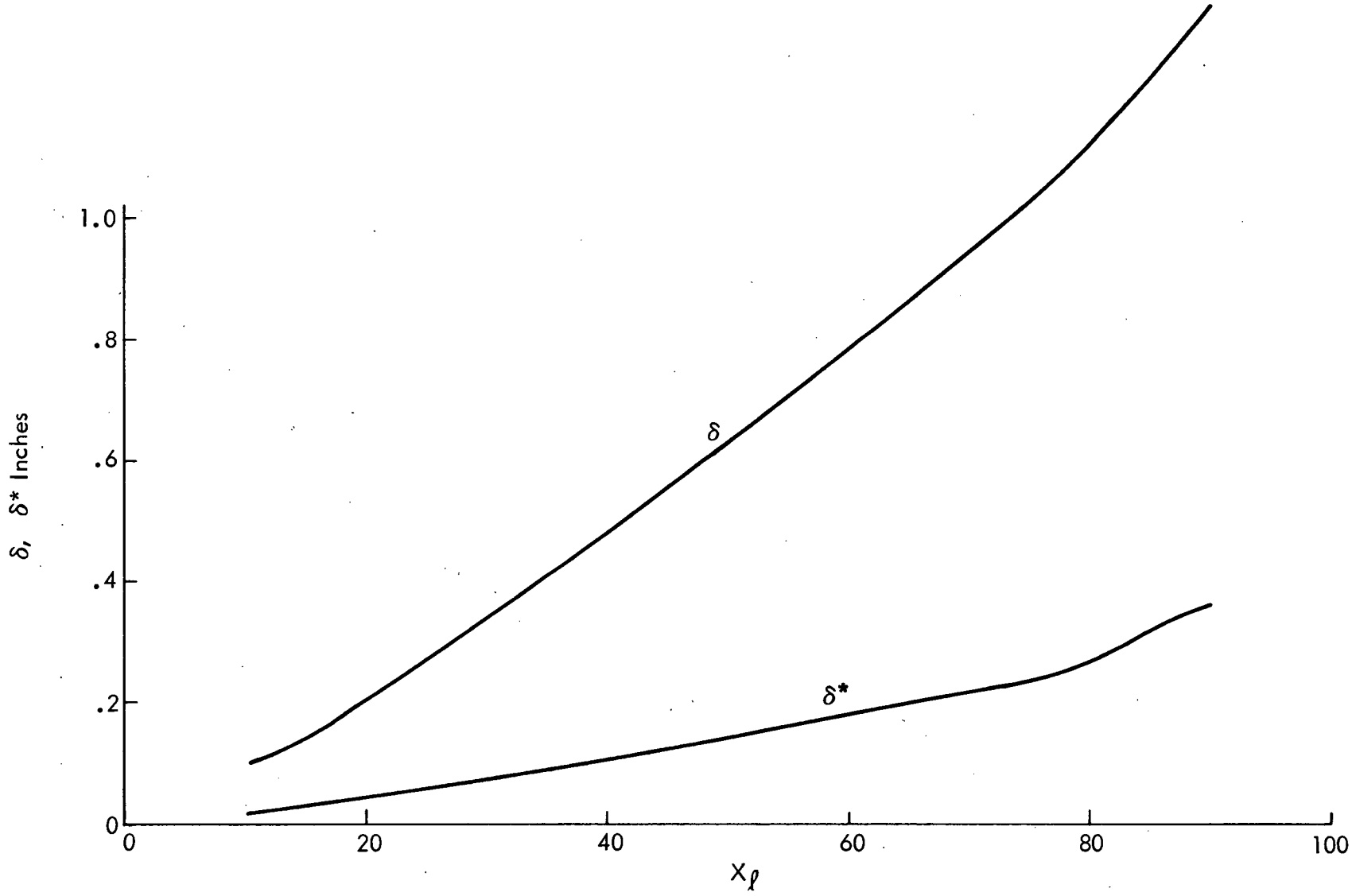

Figure 15. (Cont'd.) .307 Semispan

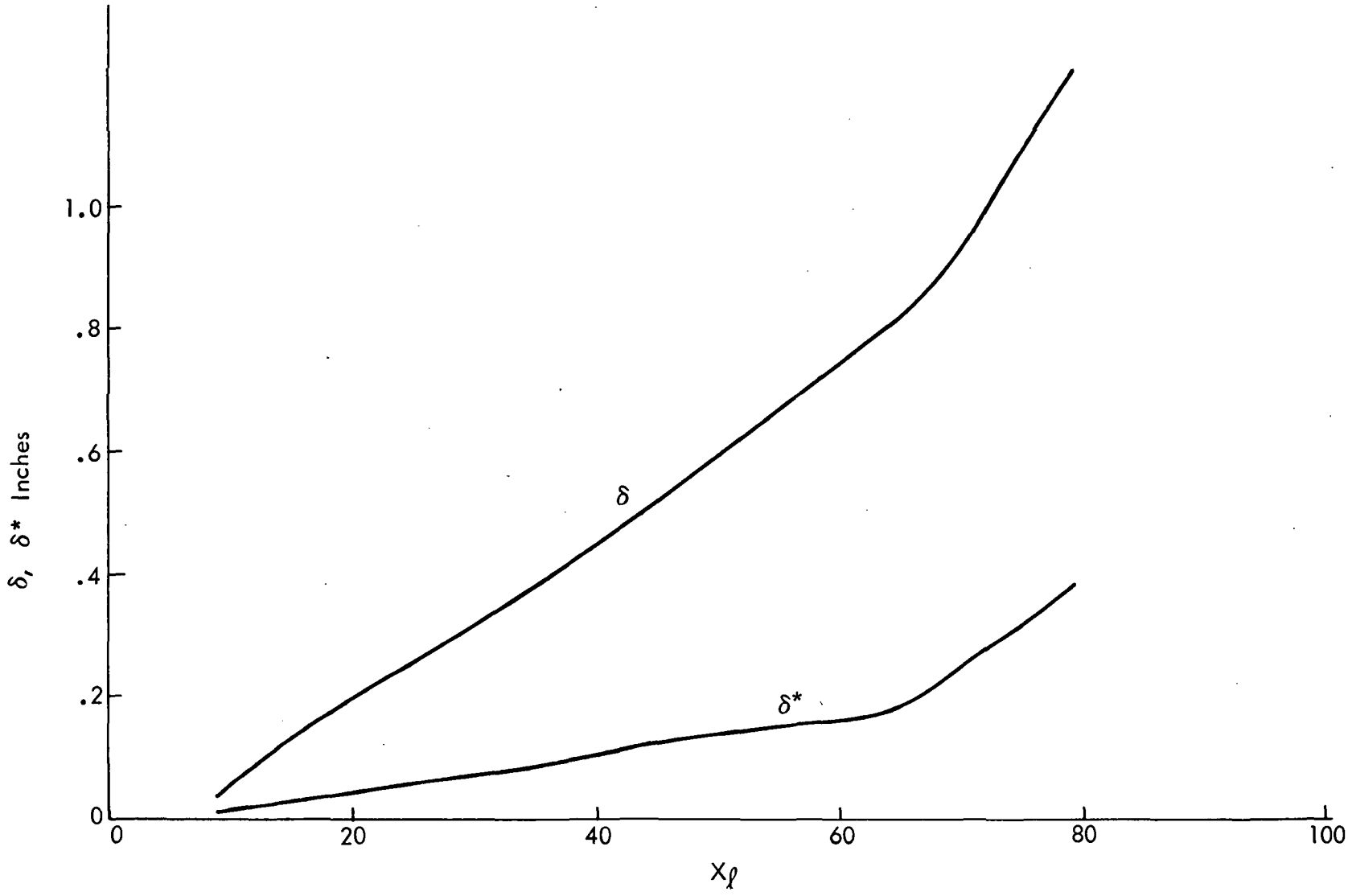

Figure 15. (Cont'd.) .458 Semispan

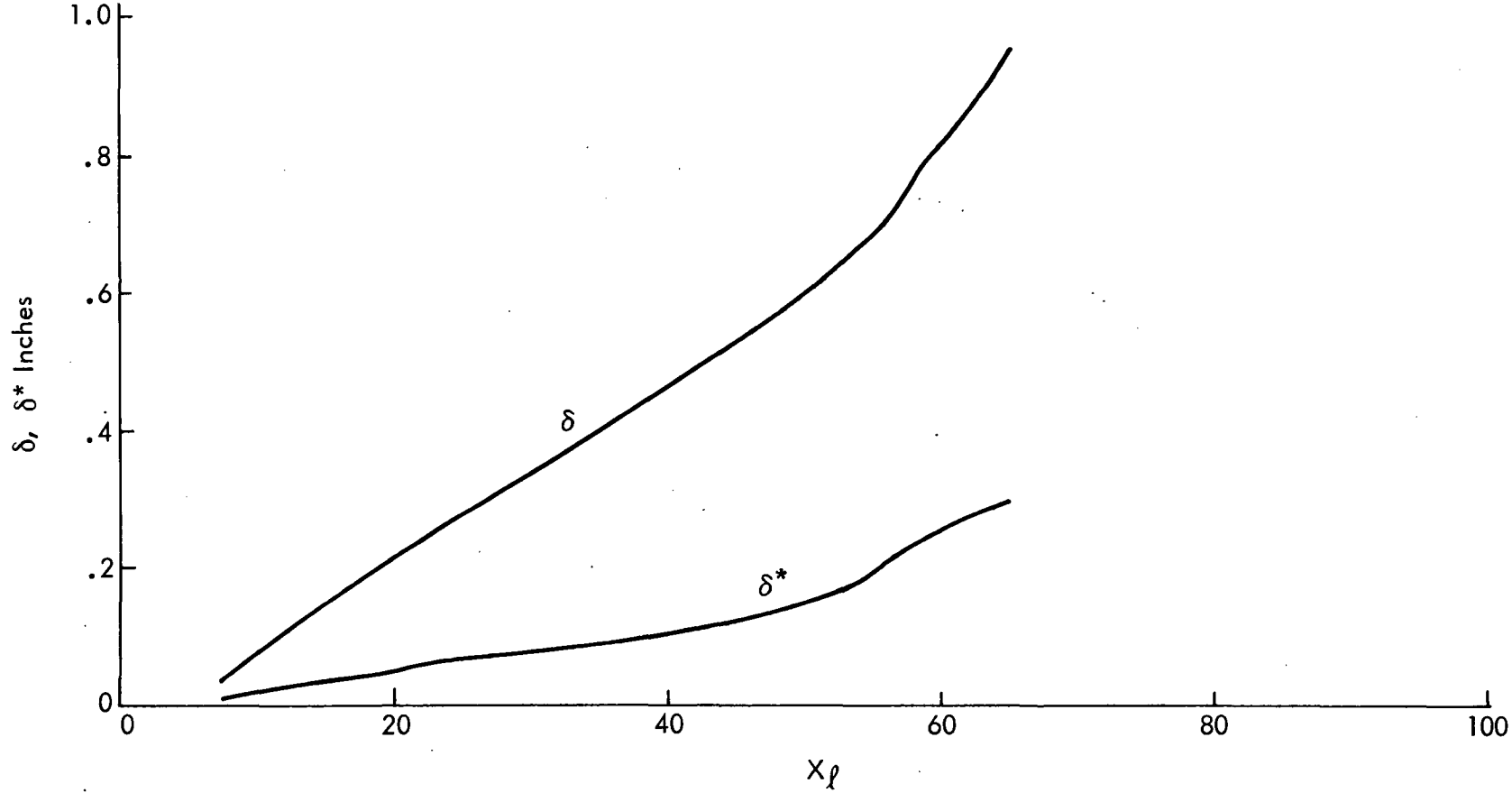

Figure 15. (Cont'd.) .653 Semispan

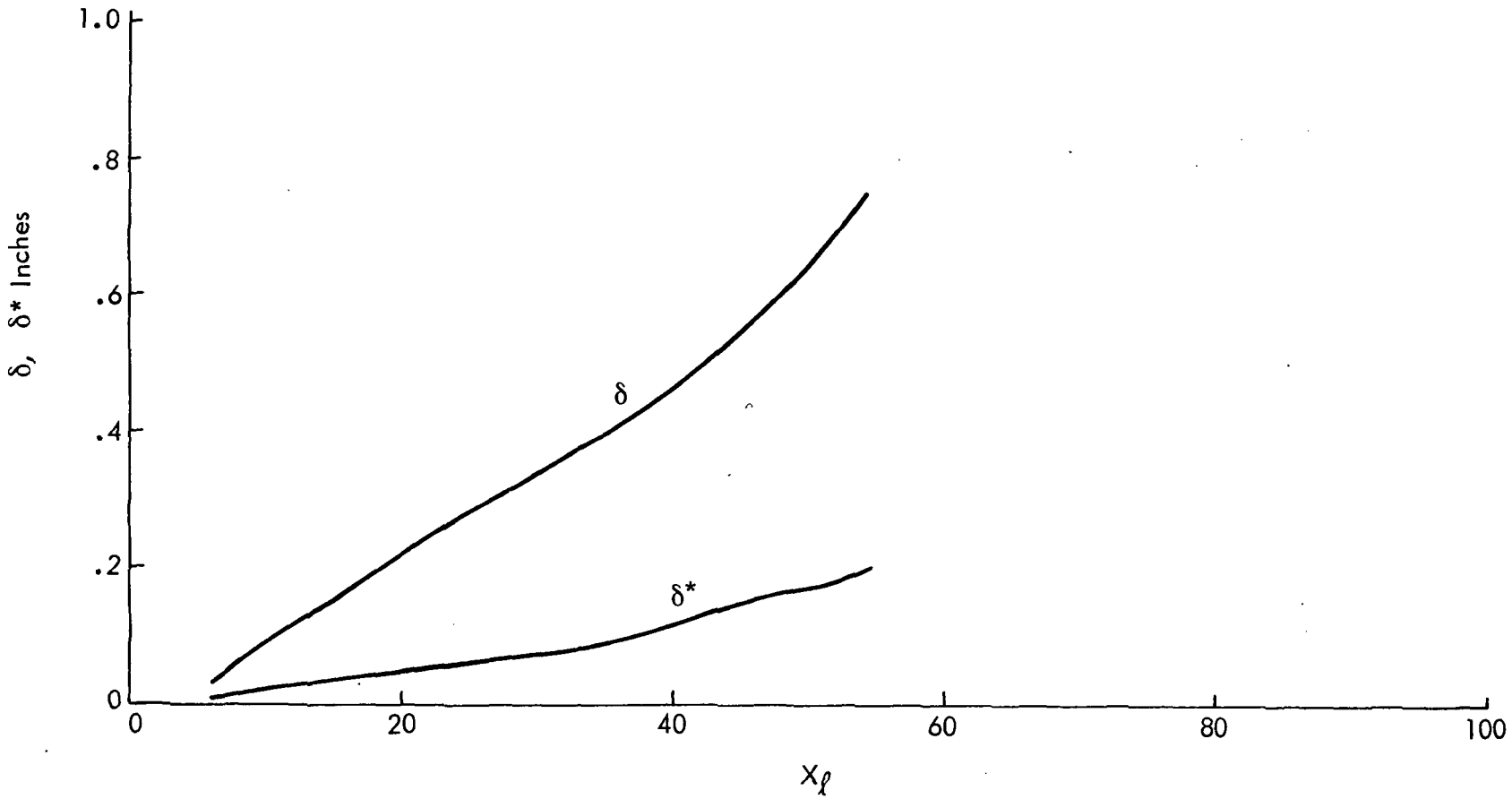

Figure 15. (Cont'd.) .804 Semispan

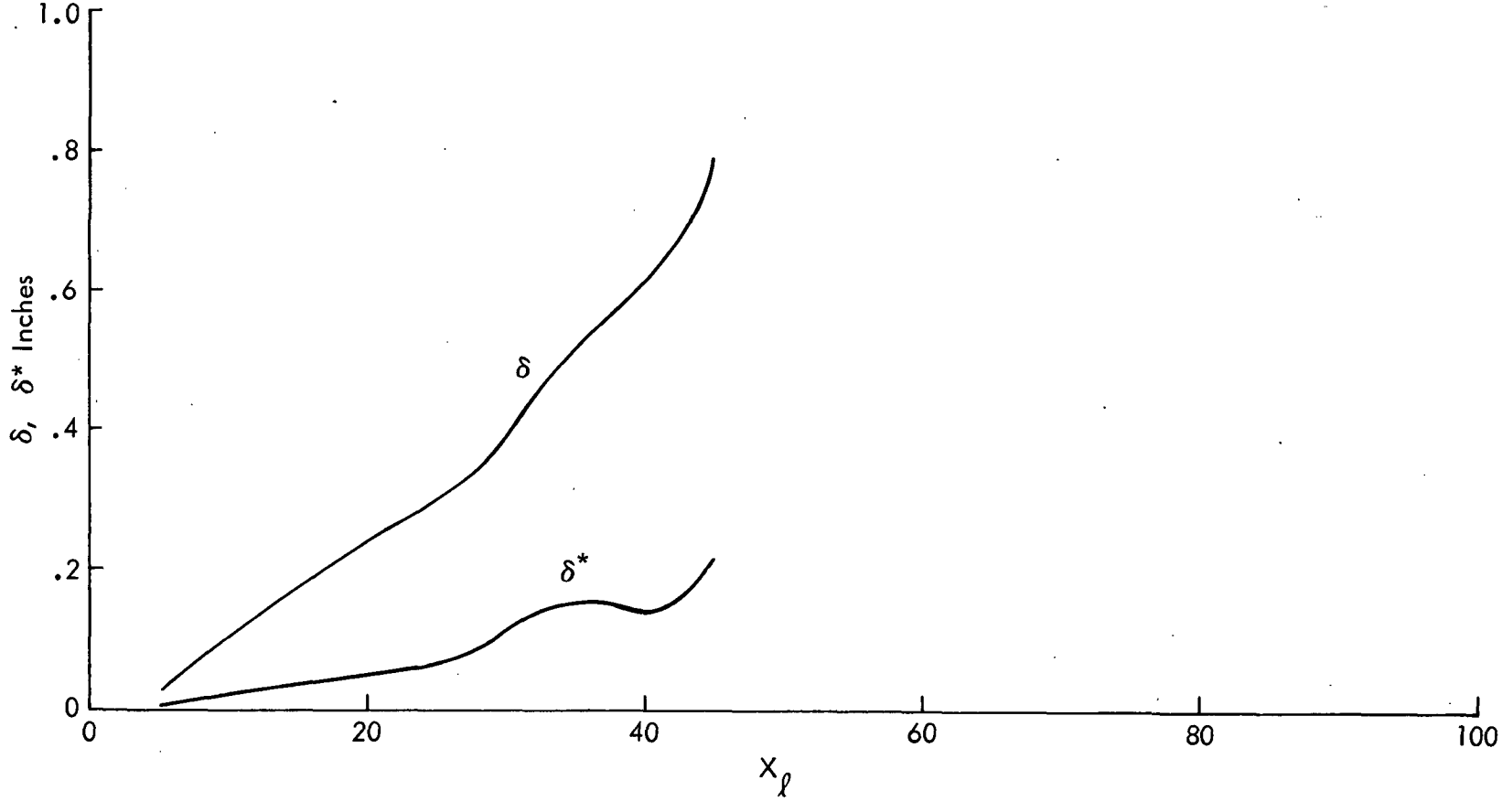

Figure 15. (Cont'd.) .933 Semispan

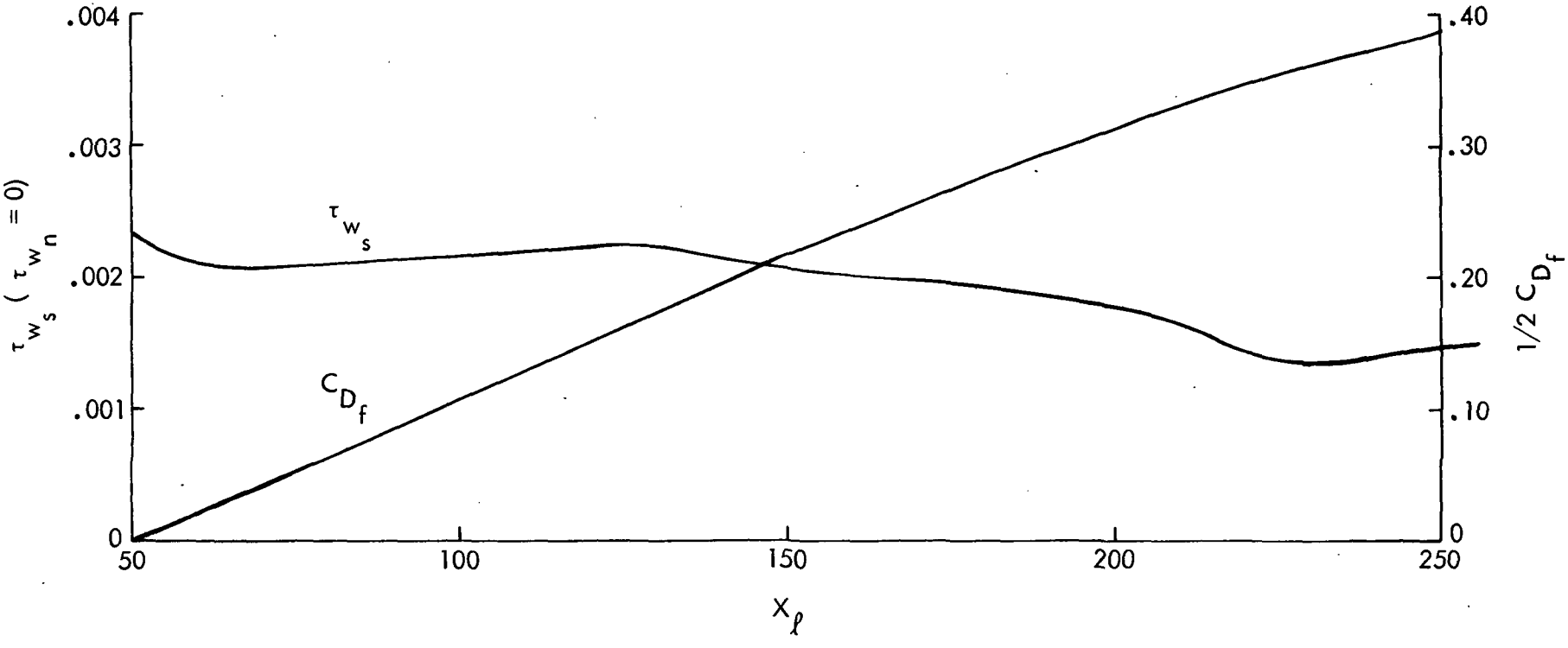

Figure 16. Skin Friction and Integrated Skin Friction, M = 0.99, Upper Surface, .044 Semispan

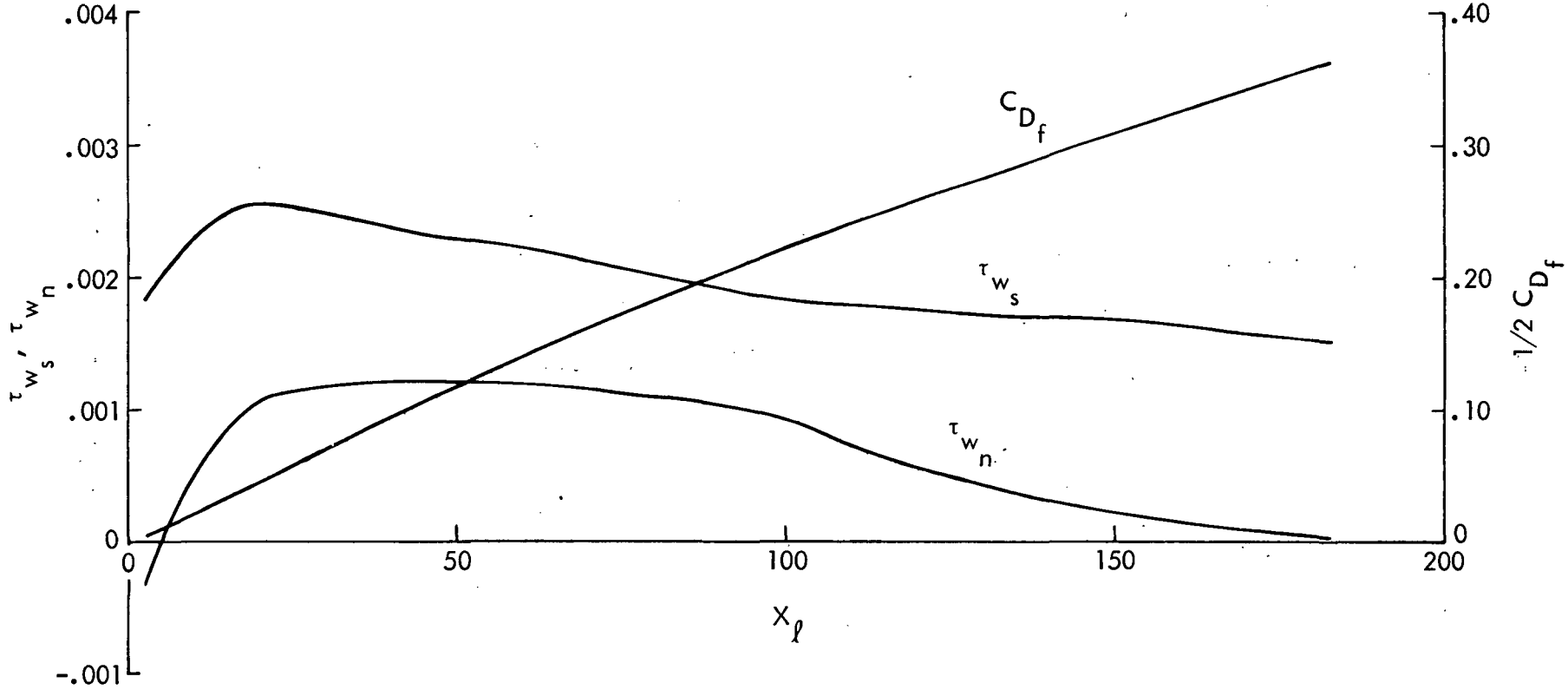

Figure 16. (Cont'd.) .133 Semispan

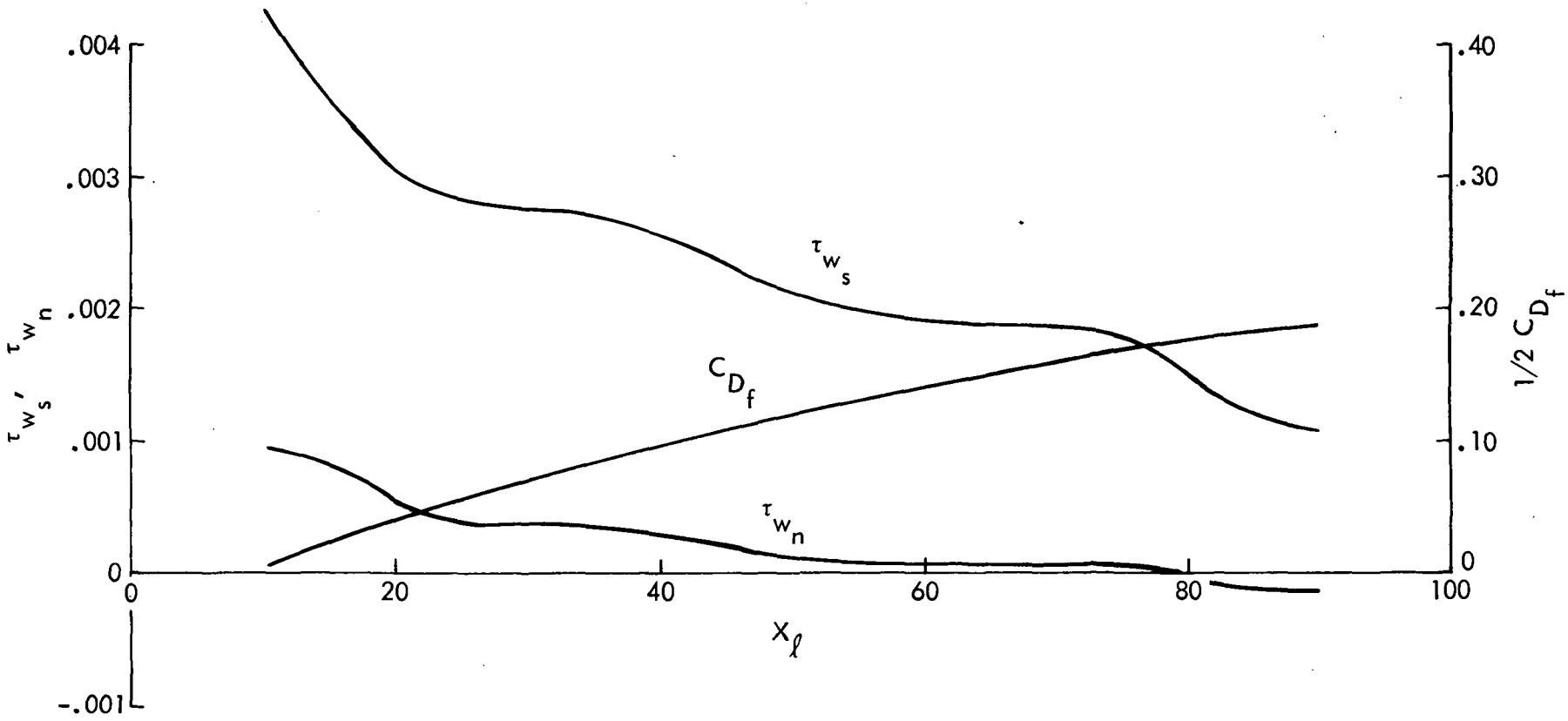

Figure 16. (Cont'd.) .307 Semispan

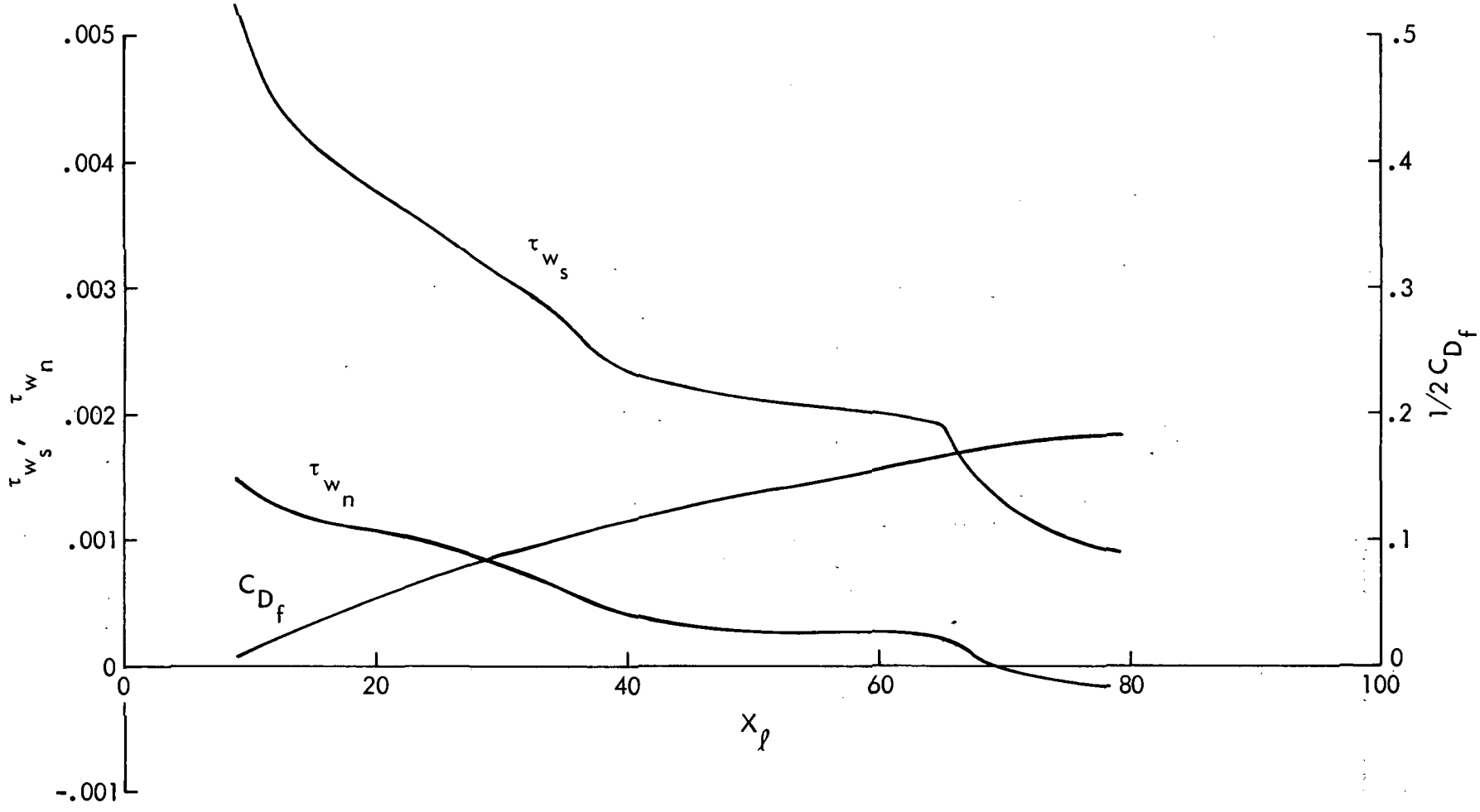

Figure 16. (Contld.) .458 Semispan

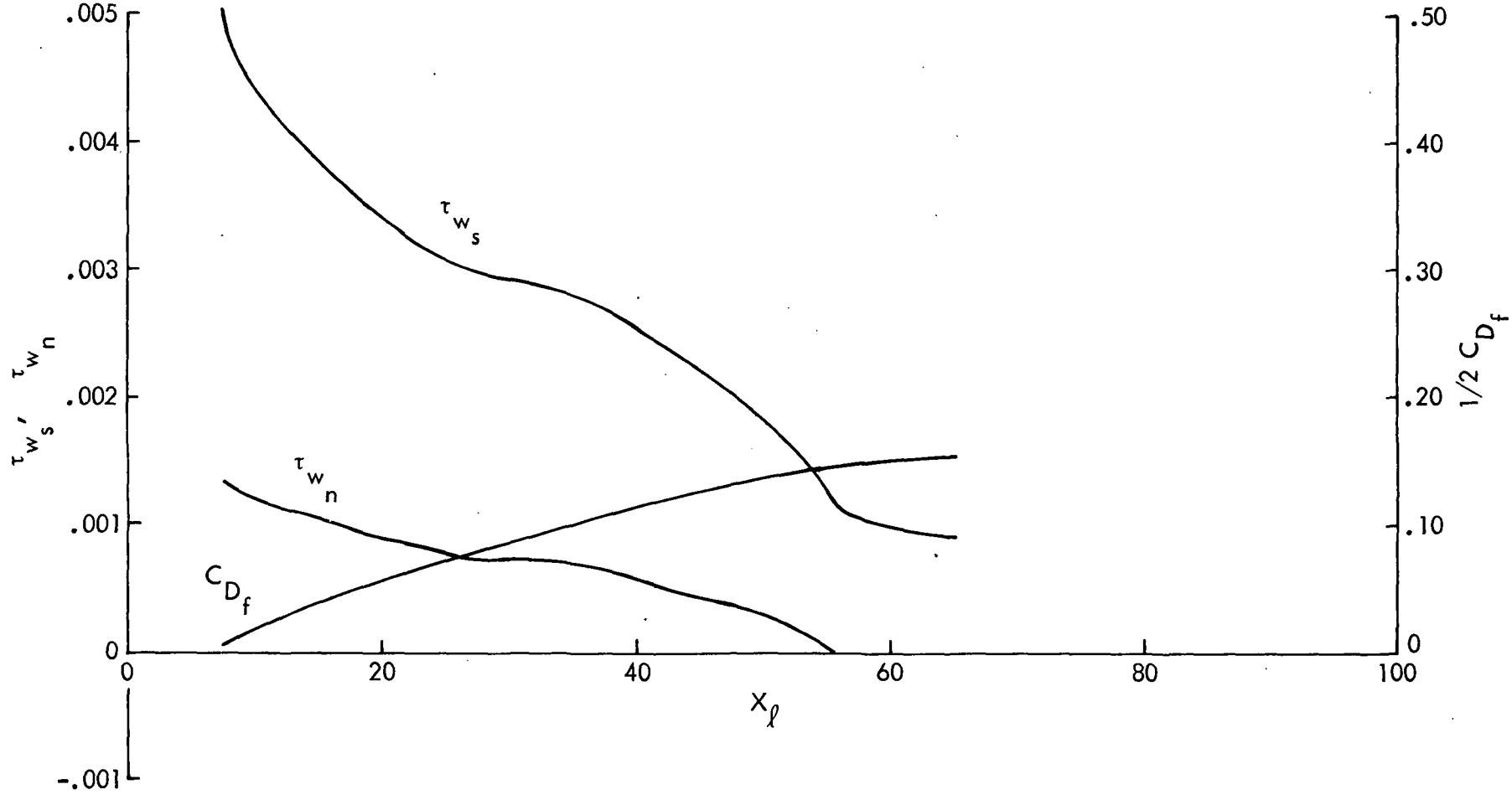

Figure 16. (Cont'd.) .653 Semispan

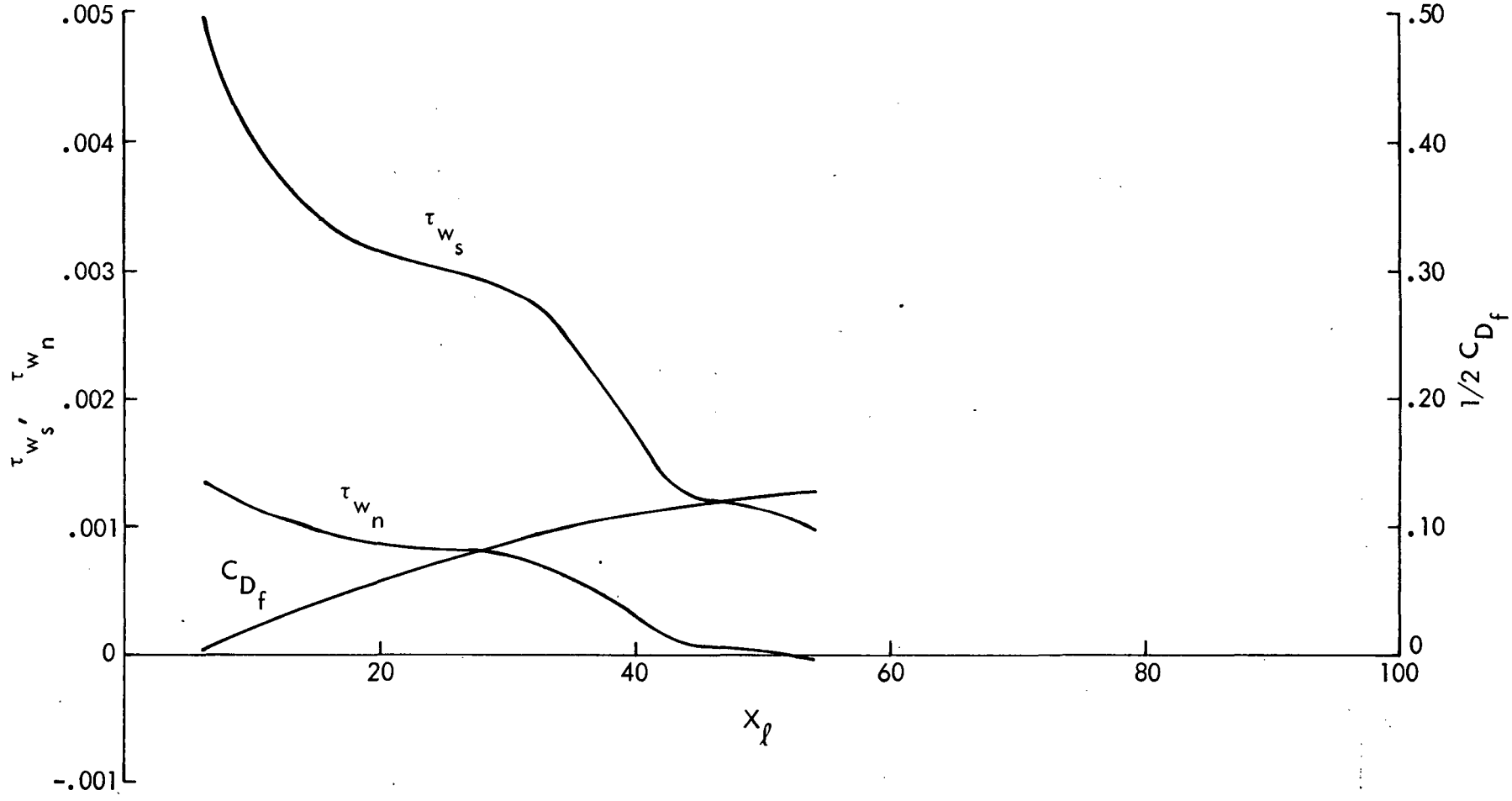

Figure 16. (Cont'd.) .804 Semispan

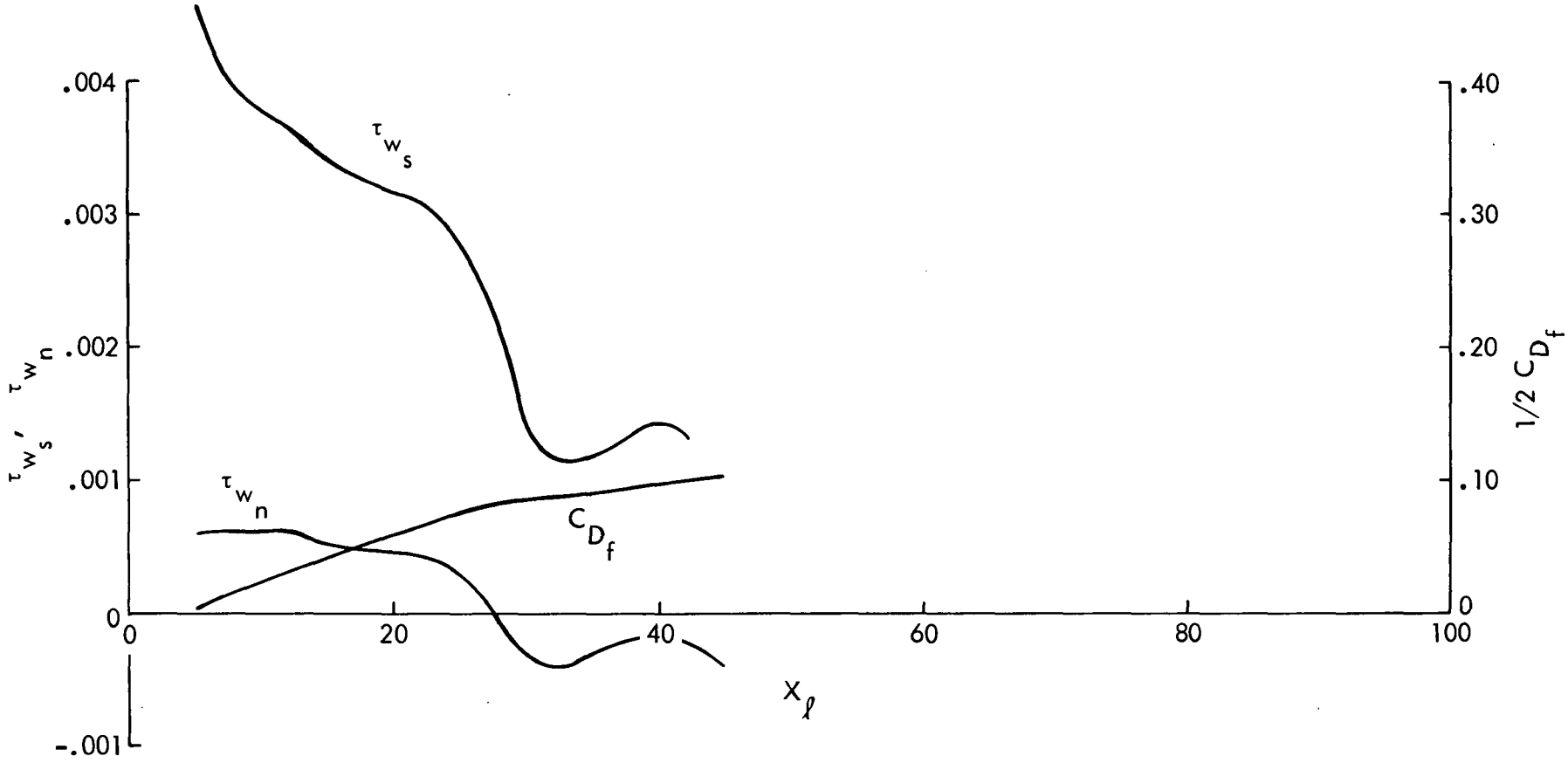

Figure 16. (Cont'd.) .933 Semispan

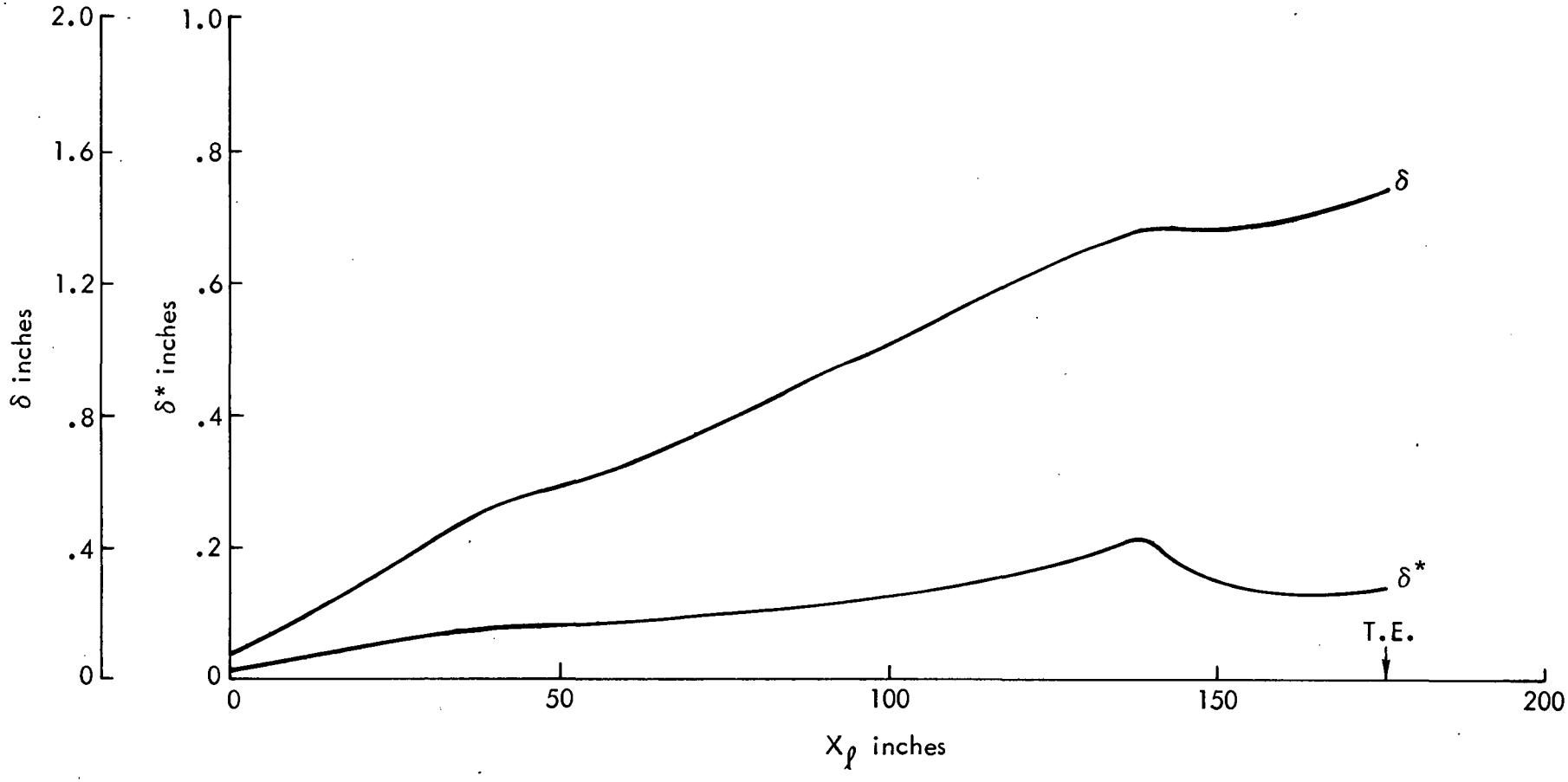

Figure 17. Boundary-Layer Thickness and Displacement Thickness,
M = 0.99, Lower Surface: .133 Semispan

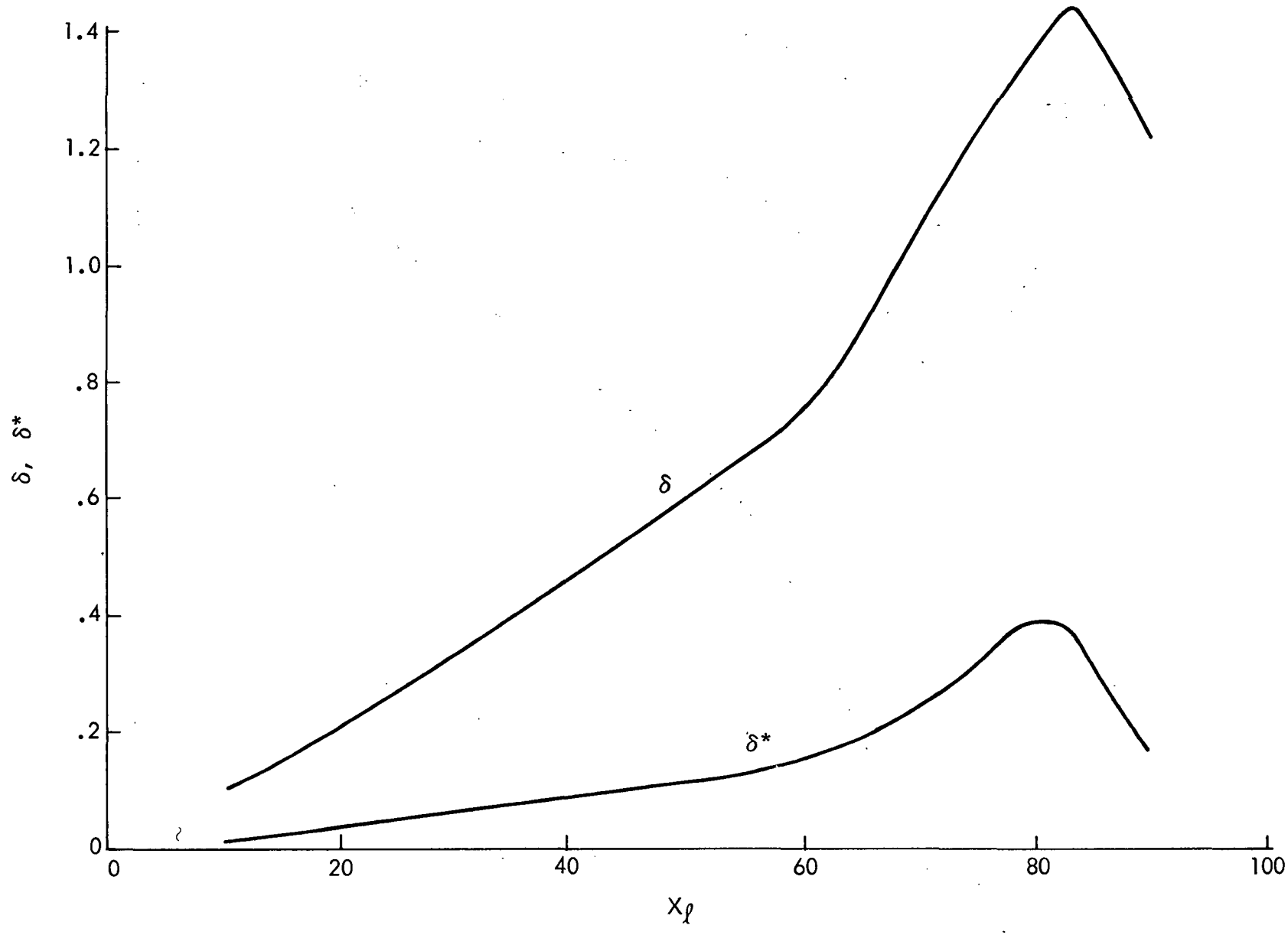

Figure 17. (Cont'd.) .307 Semispan

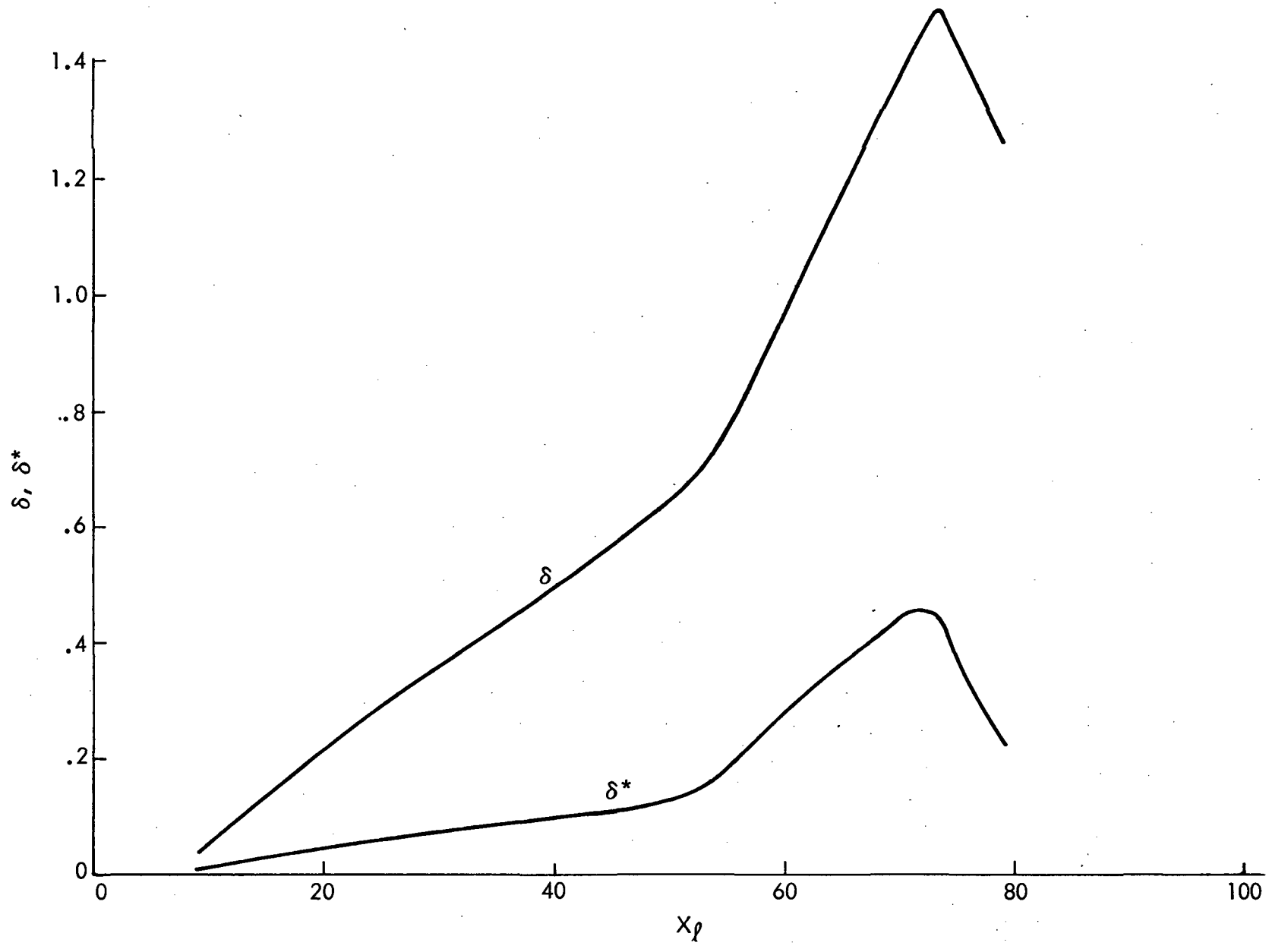

Figure 17. (Cont'd.) .458 Semispan

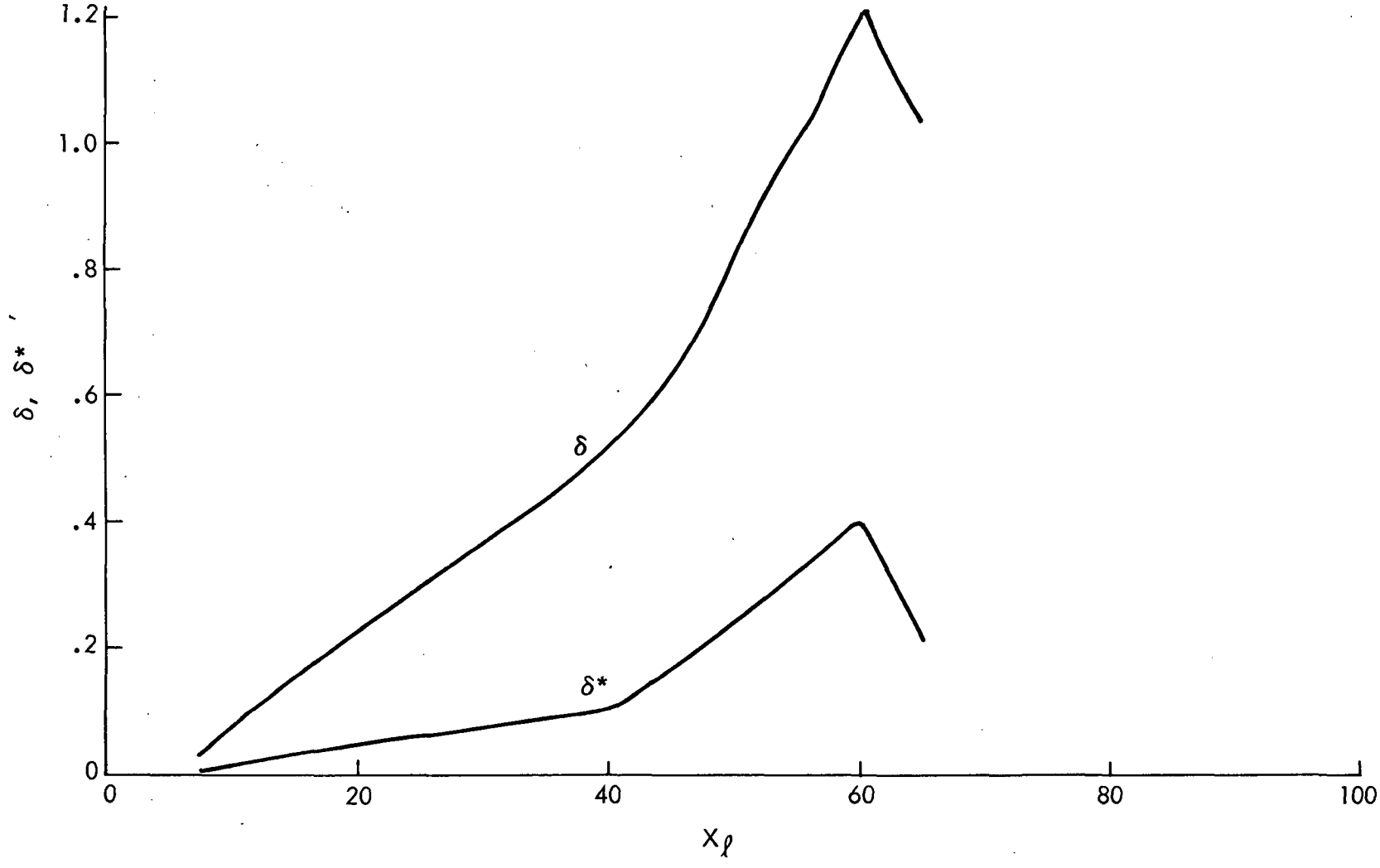

Figure 17. (Cont'd.) .653 Semispan

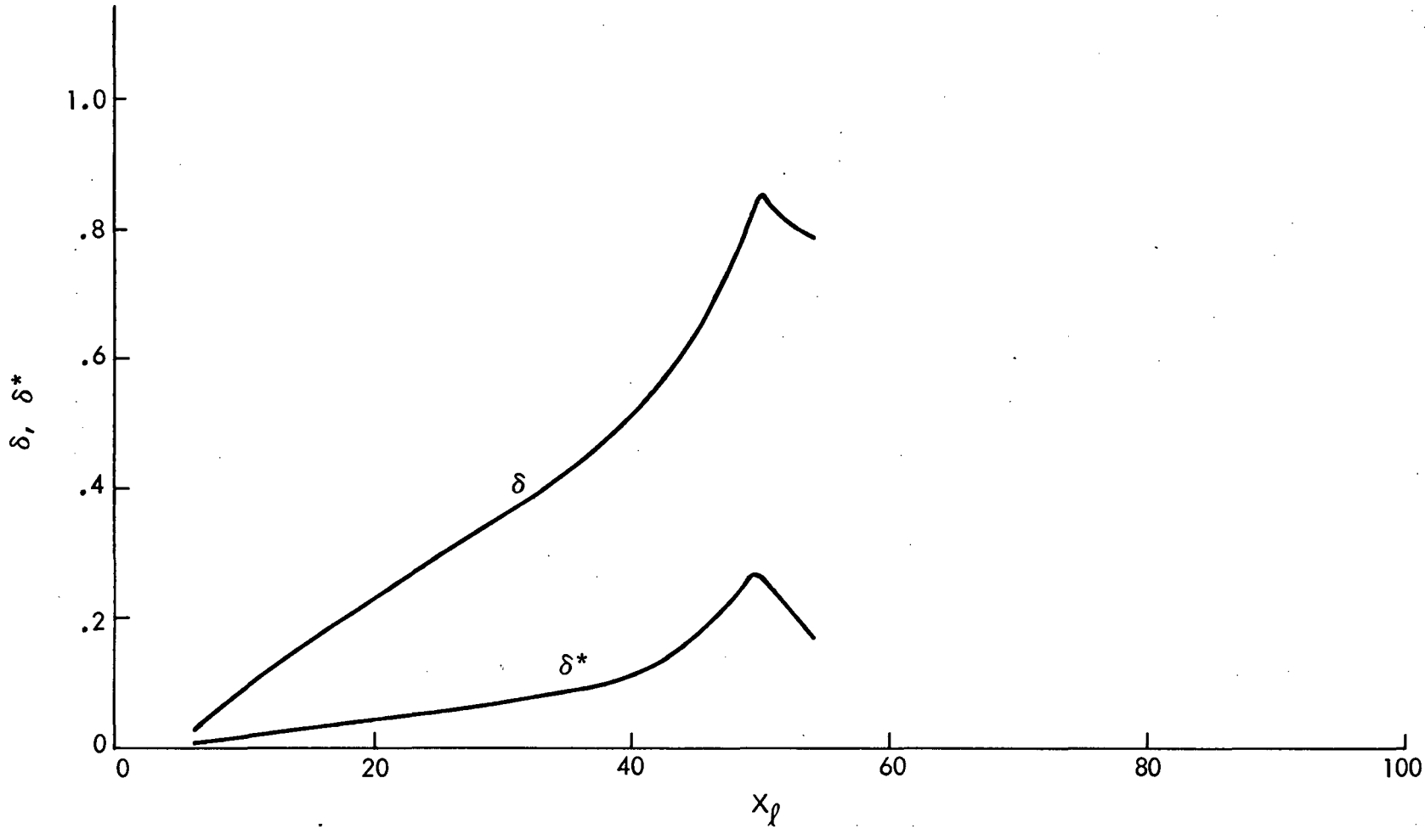

Figure 17. (Cont'd.) .804 Semispan

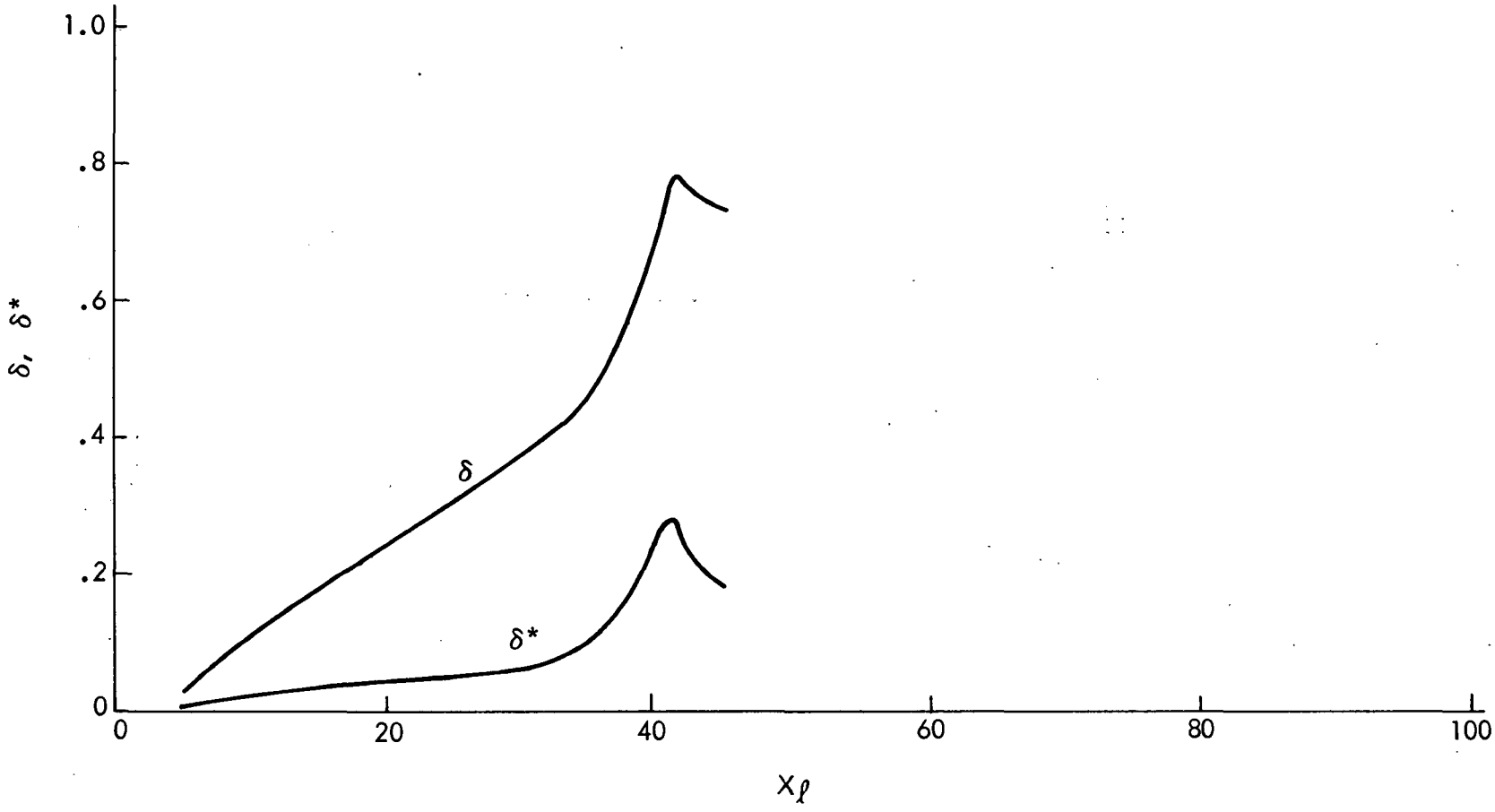

Figure 17. (Cont'd.) .933 Semispan

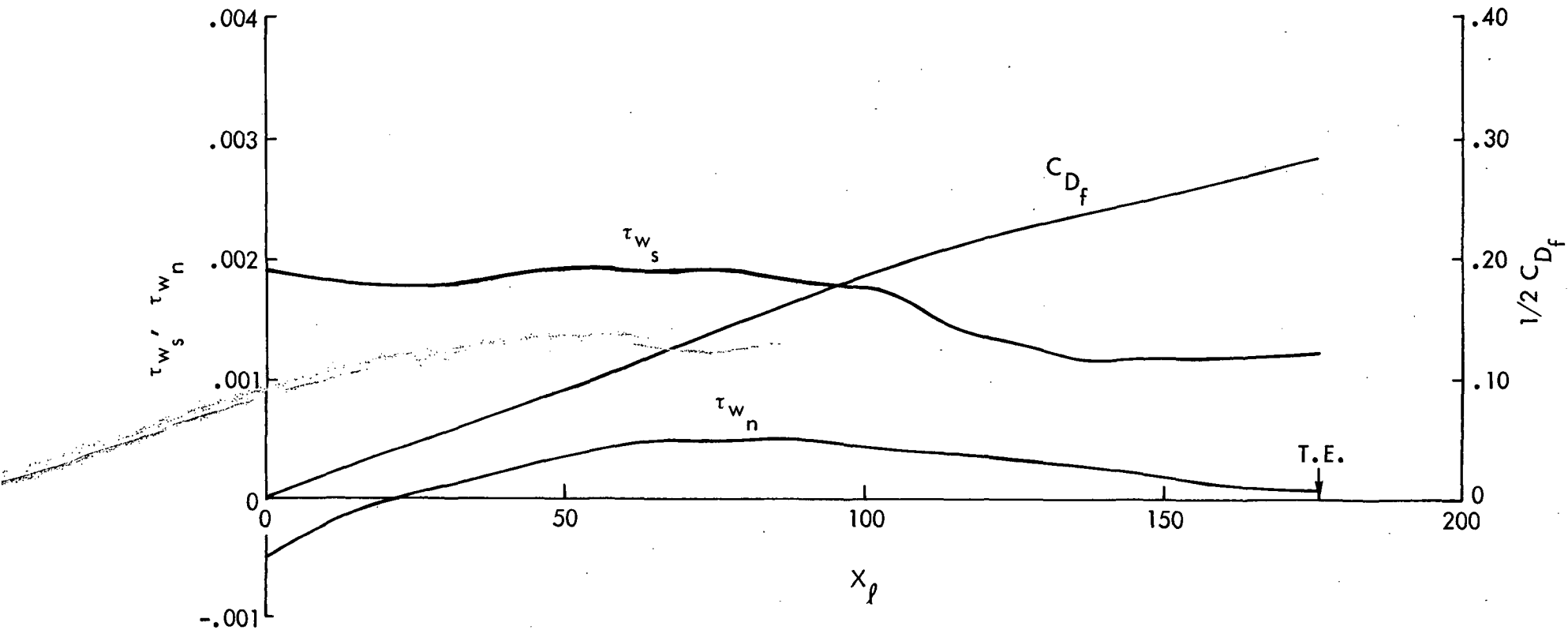

Figure 18. Skin Friction Components and Integrated Skin Friction
M = 0.99, Lower Surface, .133 Semispan

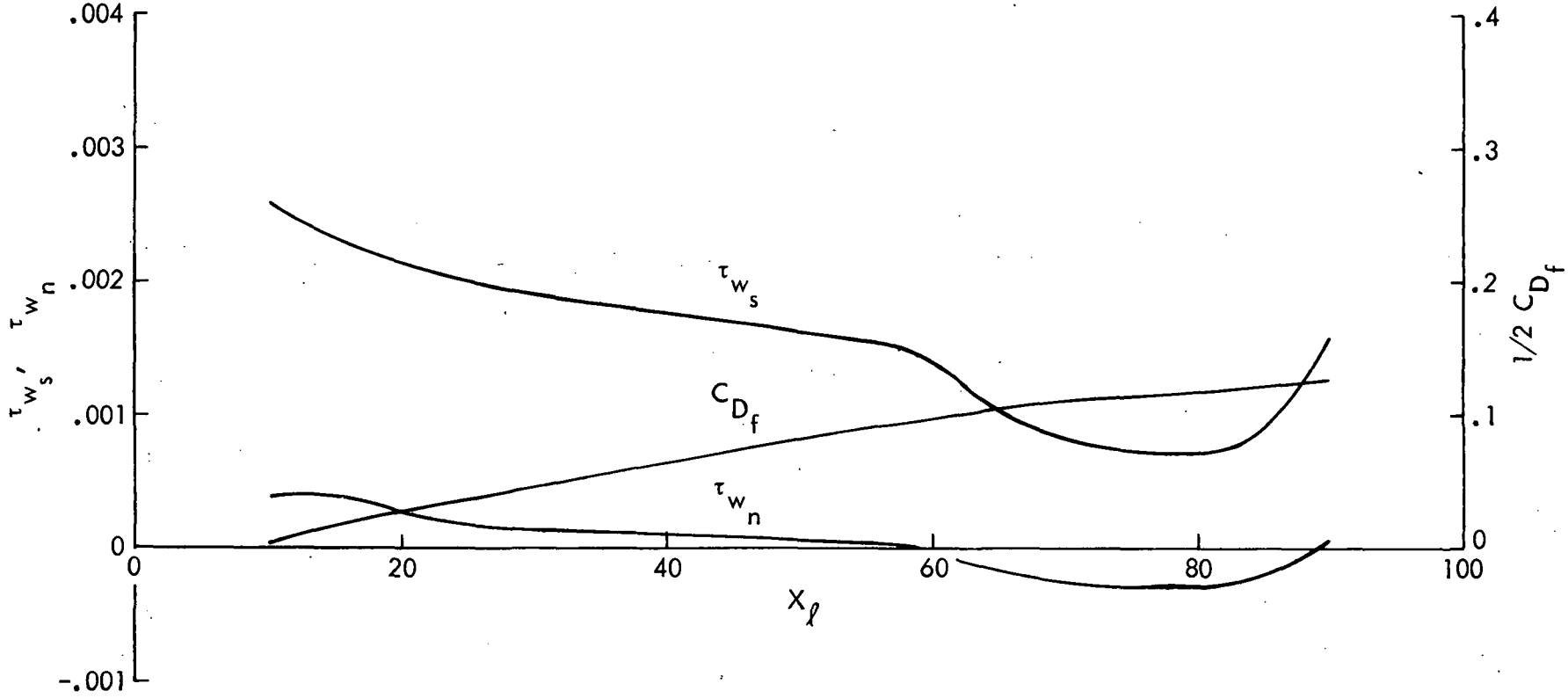

Figure 18. (Cont'd.) .307 Semispan

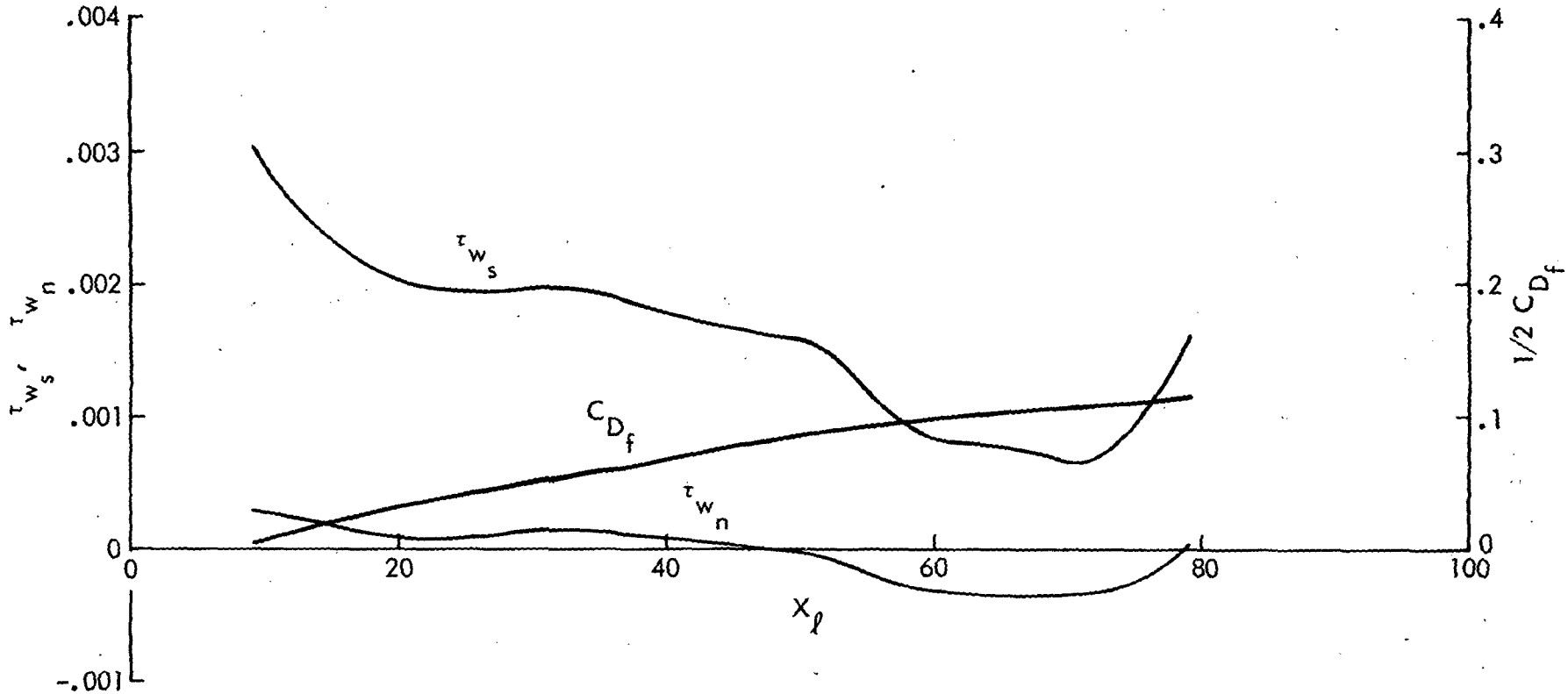

Figure 18. (Cont'd.) .458 Semispan

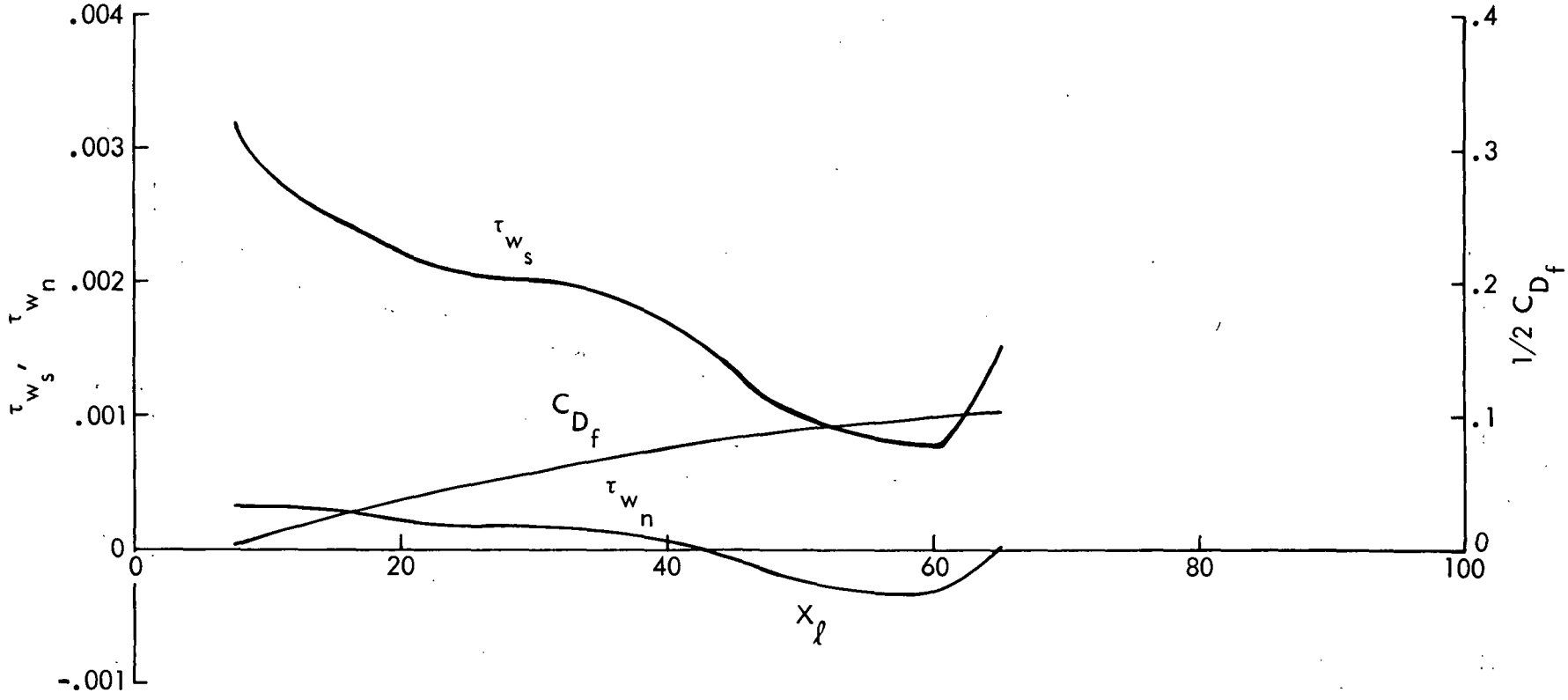

Figure 18. (Cont'd.) .653 Semispan

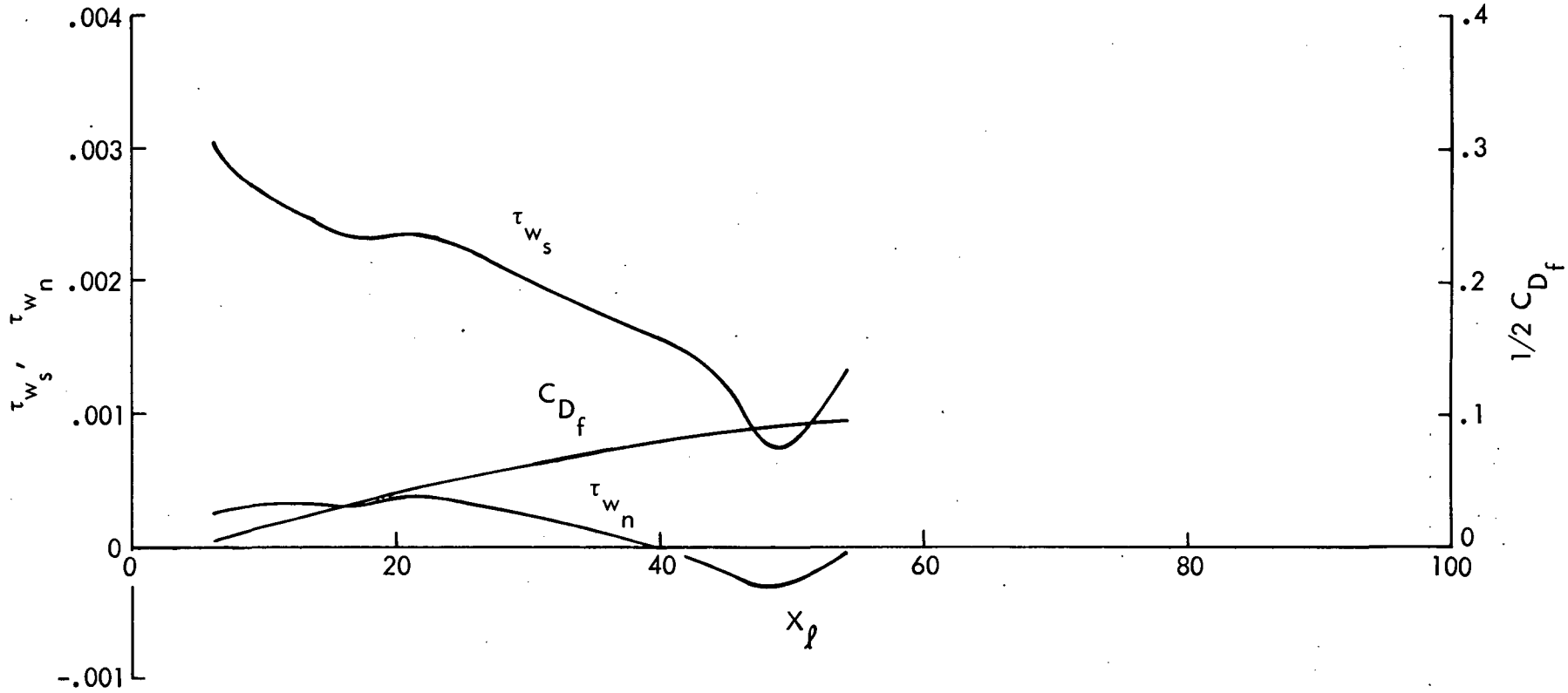

Figure 18. (Cont'd.) .804 Semispan

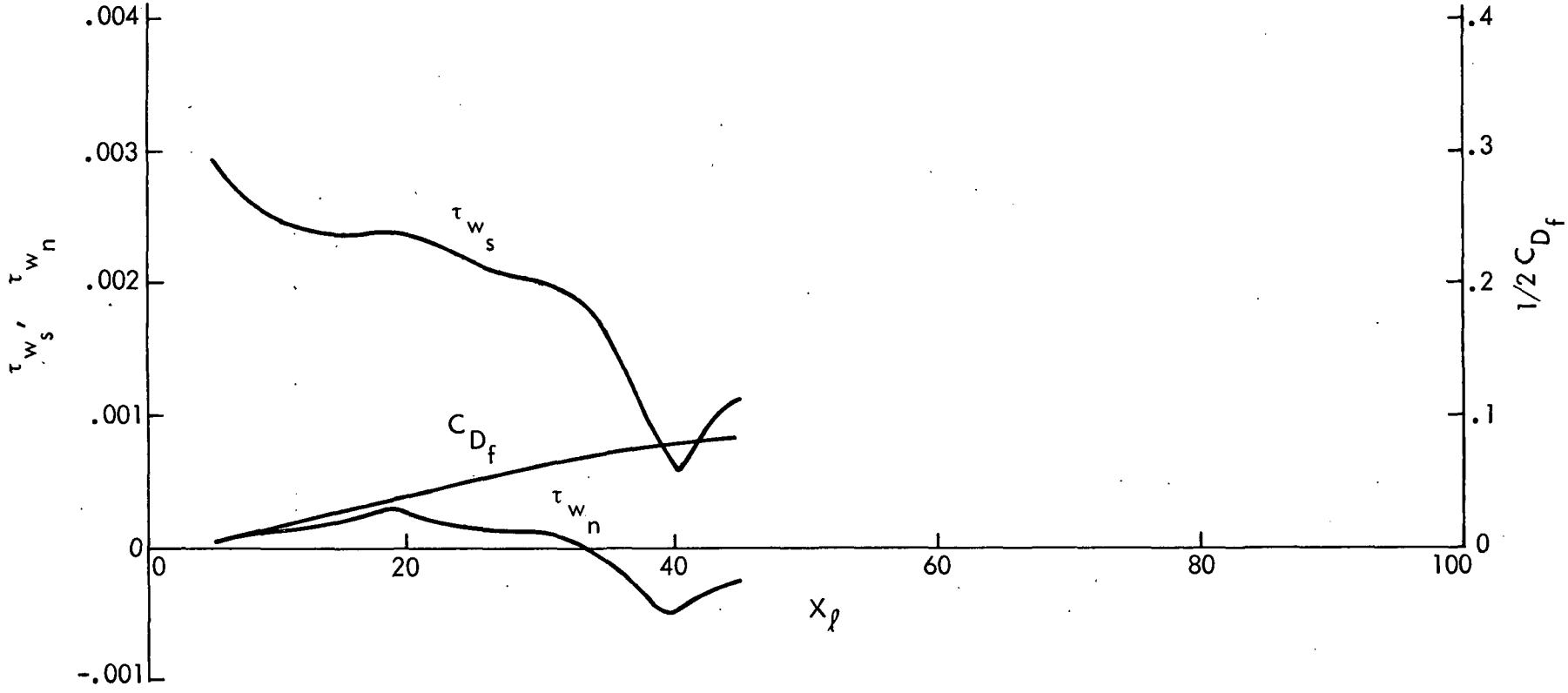

Figure 18. (Cont'd.) .933 Semispan

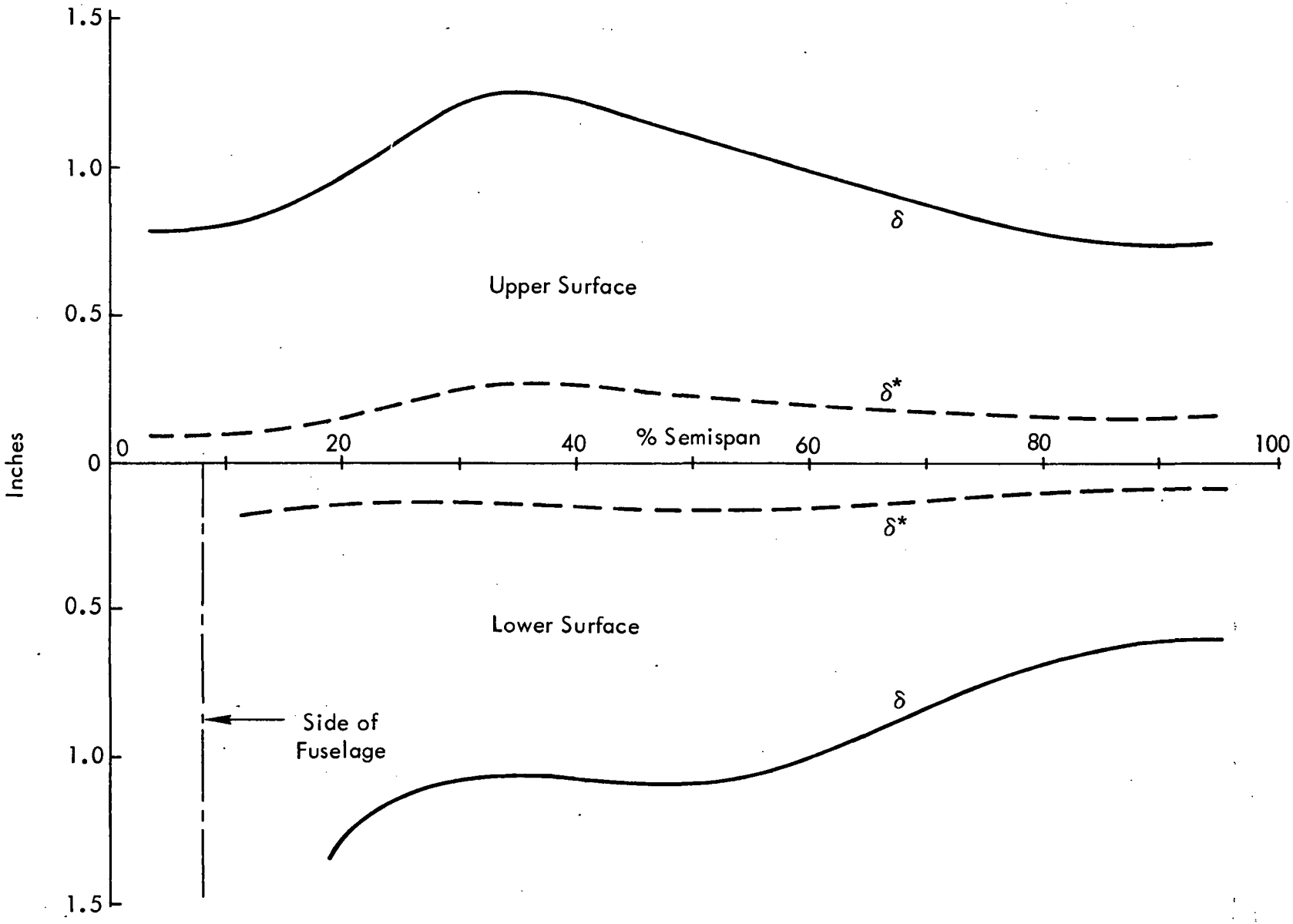

Figure 19. Boundary-Layer Thickness and Displacement Thickness at the Trailing Edge Versus Spanwise Position (M = 0.5)

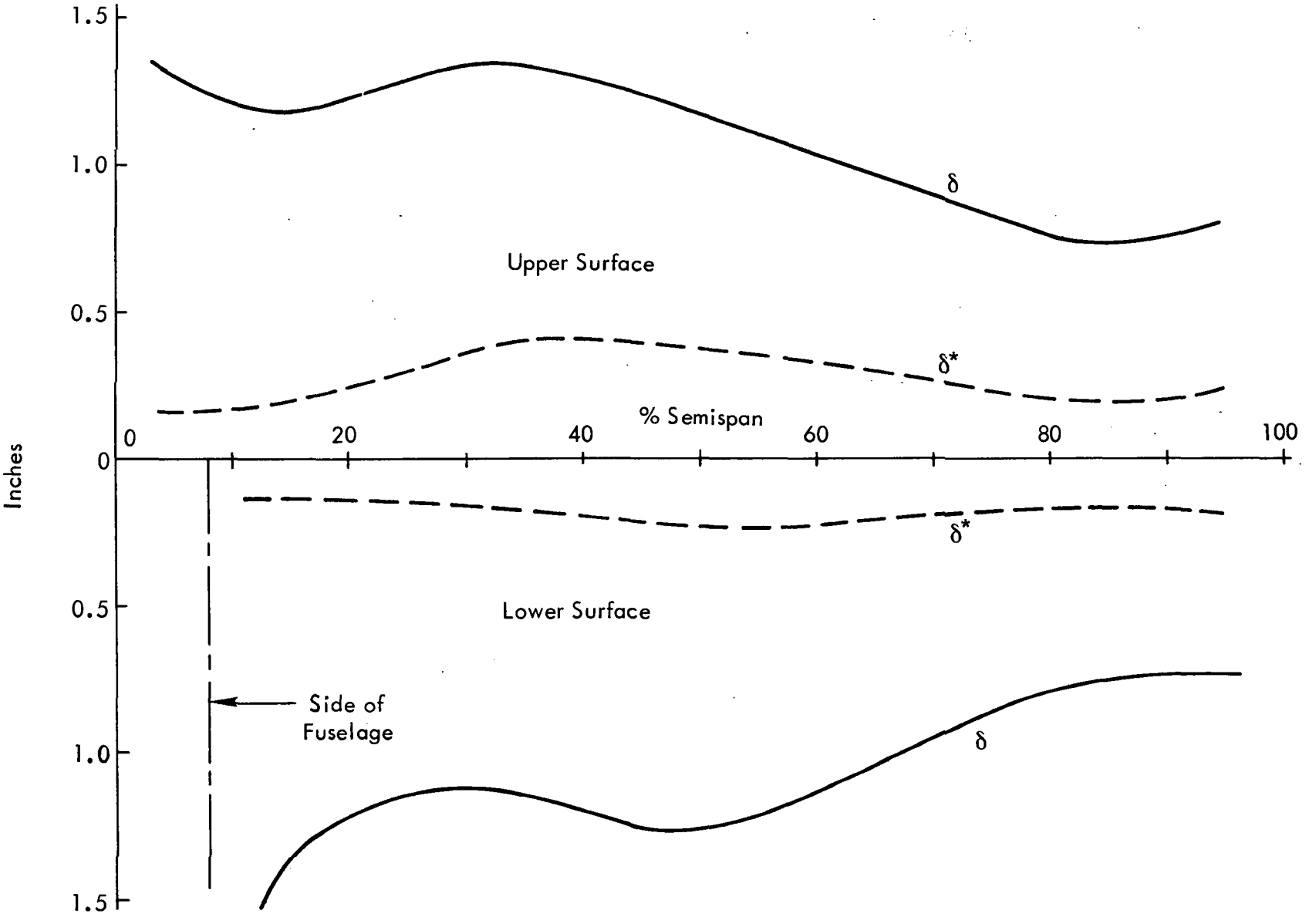

Figure 19. (Cont'd) Boundary-Layer Thickness and Displacement Thickness at the Trailing Edge Versus Spanwise Position (M = 0.99)

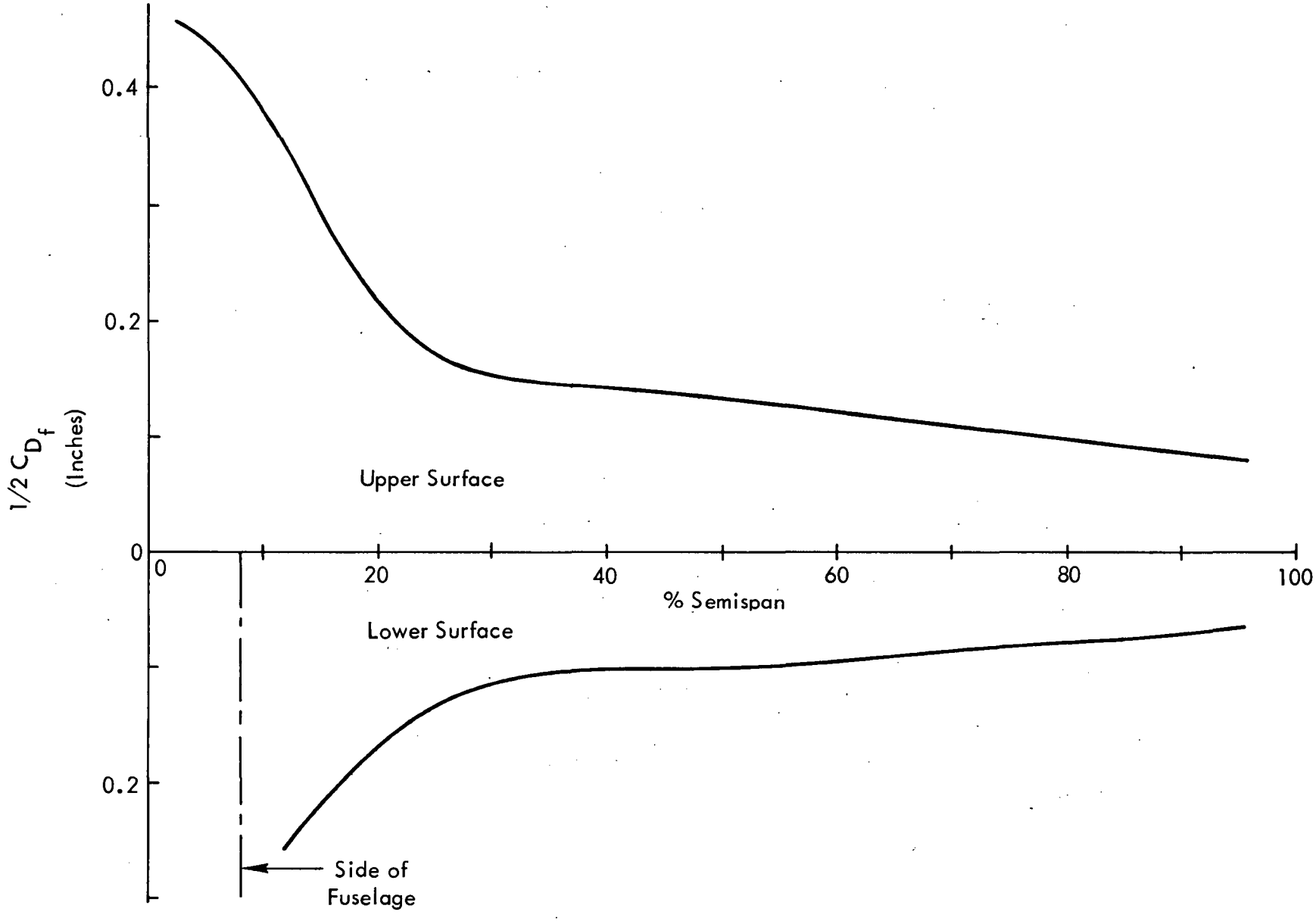

Figure 20. Sectional Integrated Skin Friction Versus Spanwise Position (M = 0.5)

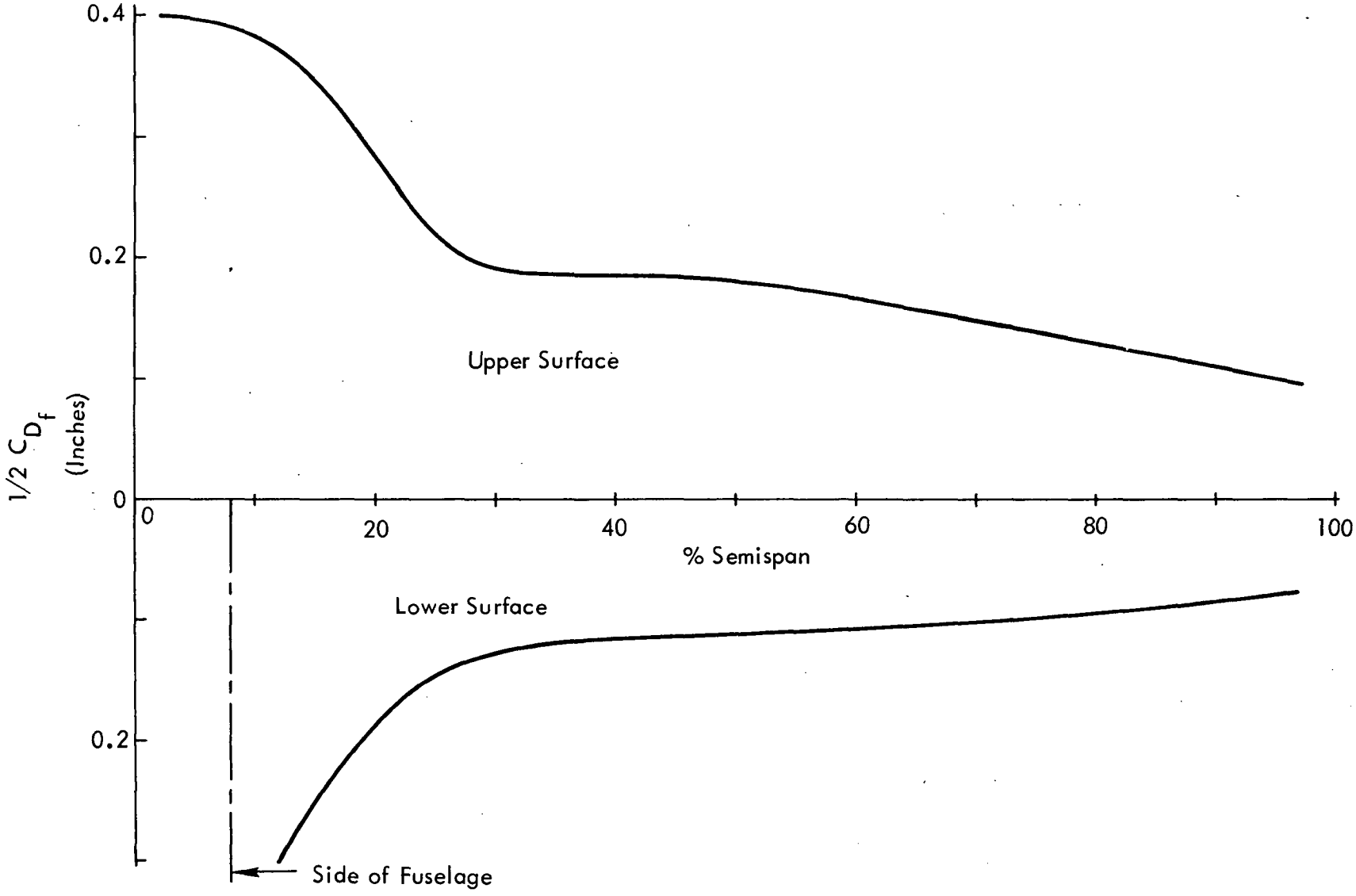

Figure 20. (Cont'd) Sectional Integrated Skin Friction Versus Spanwise Position (M = 0.99)

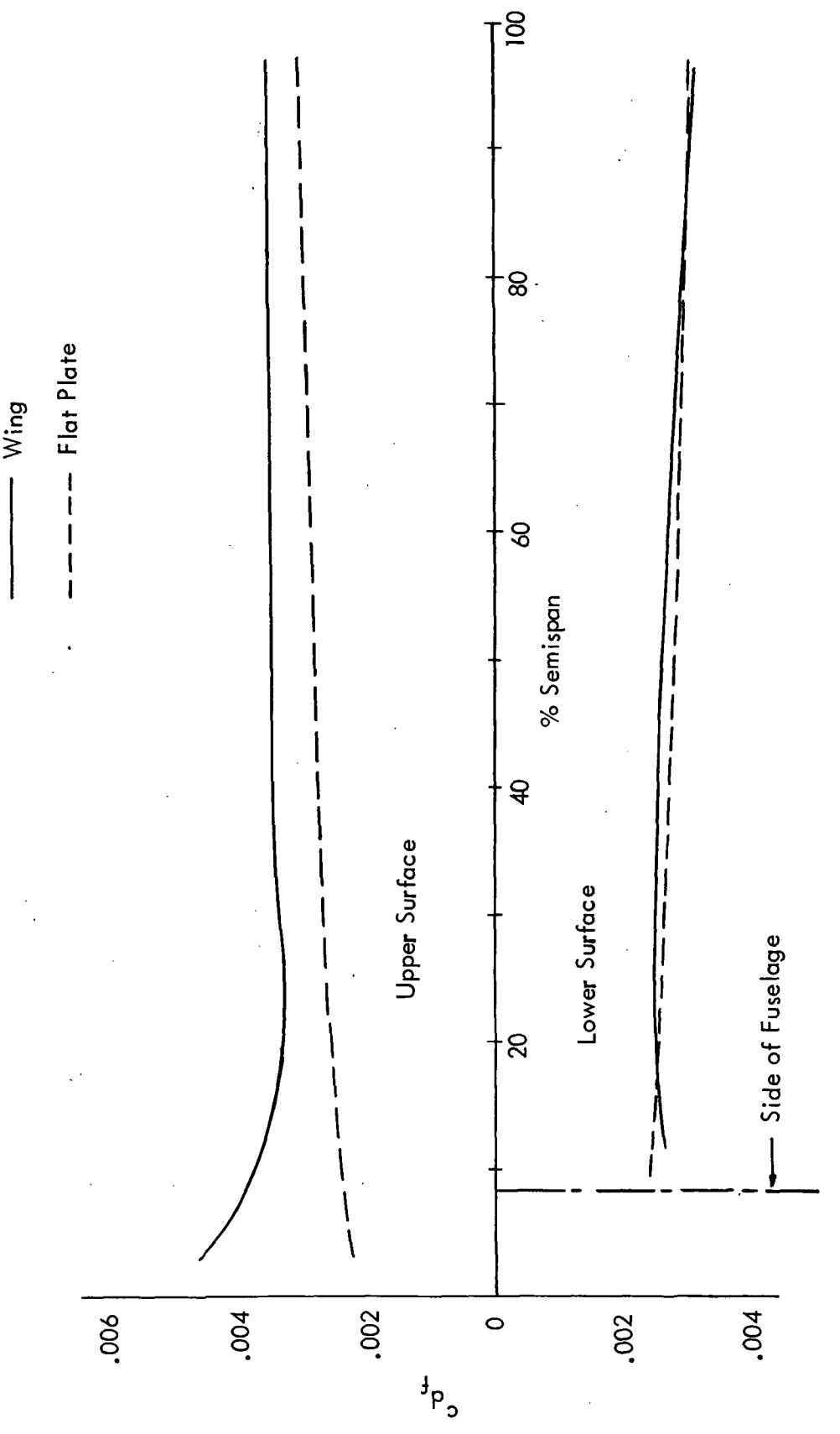

Figure 21. Sectional Skin Friction Drag Coefficient Versus Spanwise Position (M = 0.50)

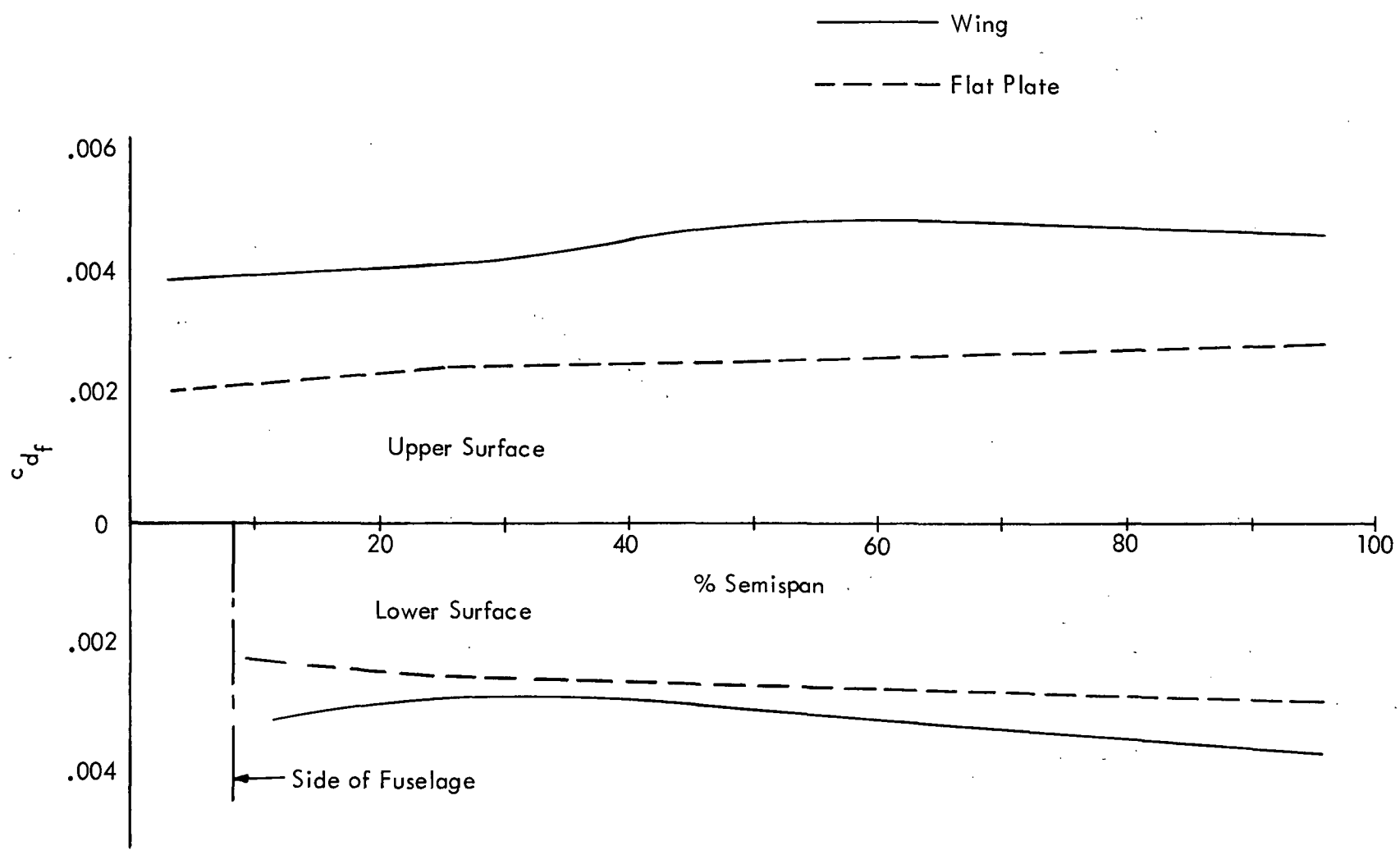

Figure 21. (Cont'd.) (M = 0.99)

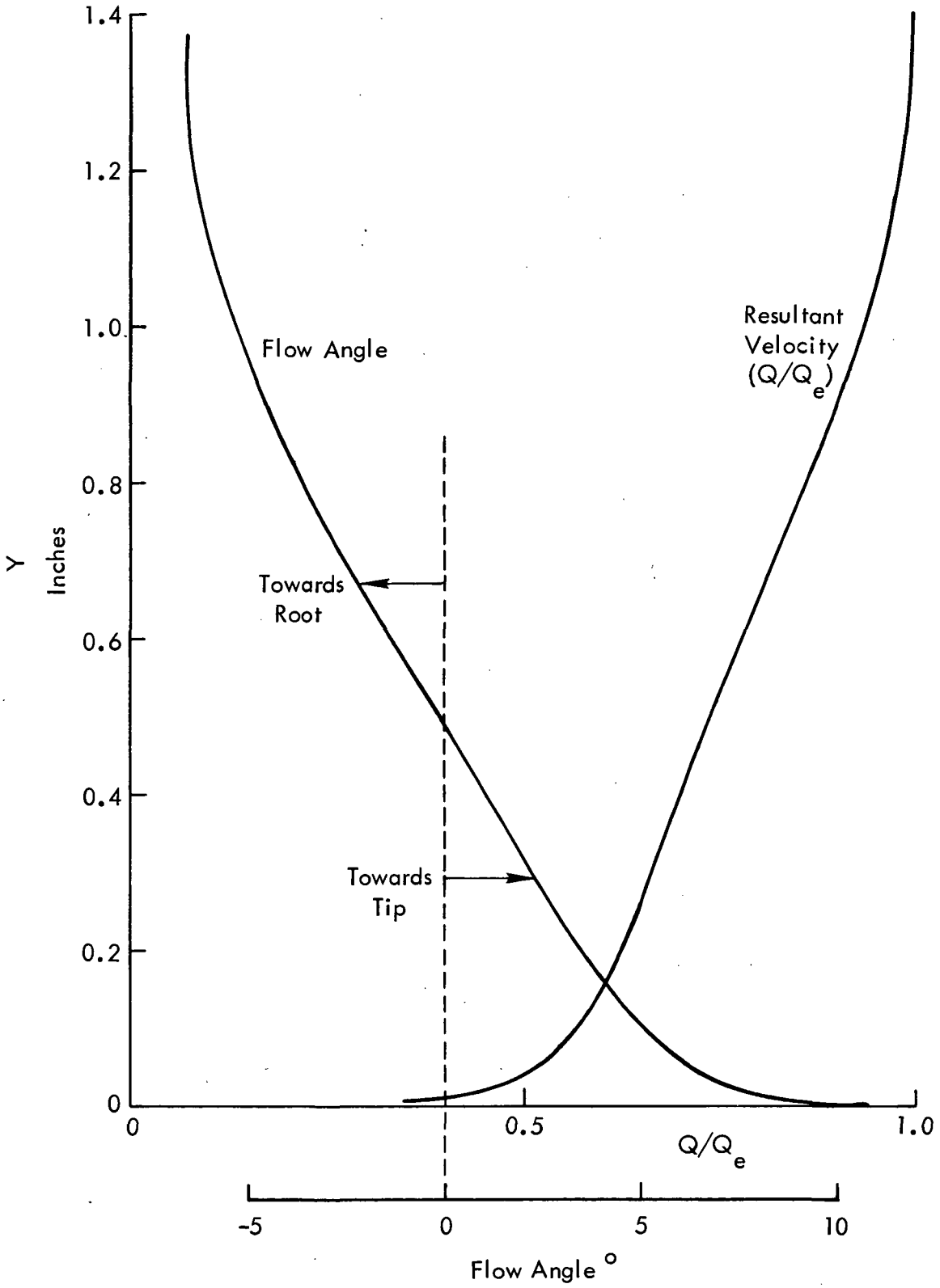

Figure 22. Velocity Profile at the Trailing Edge
(M = 0.99, Upper Surface, 0.458 Semispan)

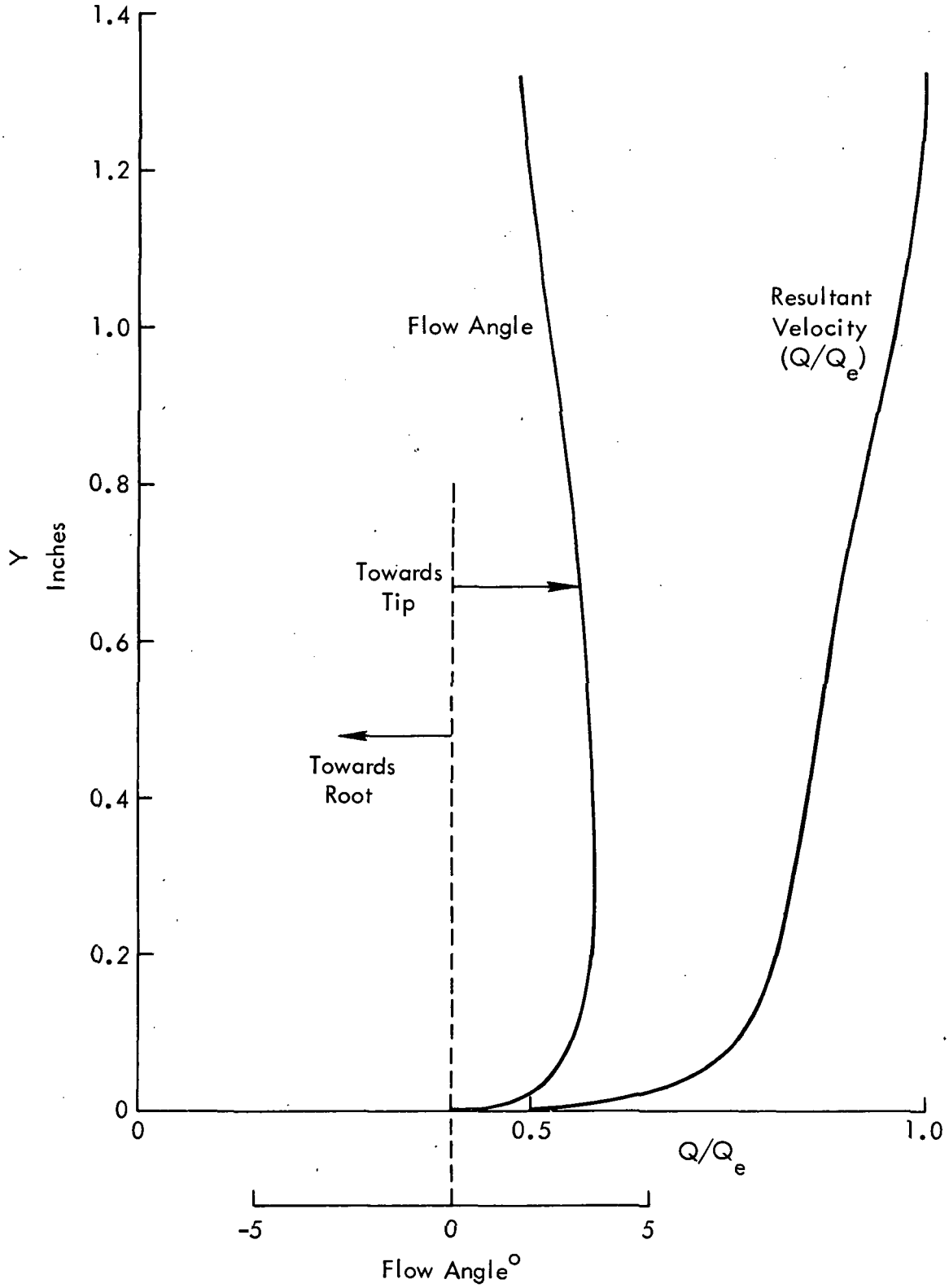

Figure 22. (Cont'd) Velocity Profile at the Trailing Edge
(M = 0.99, Lower Surface, 0.458 Semispan)

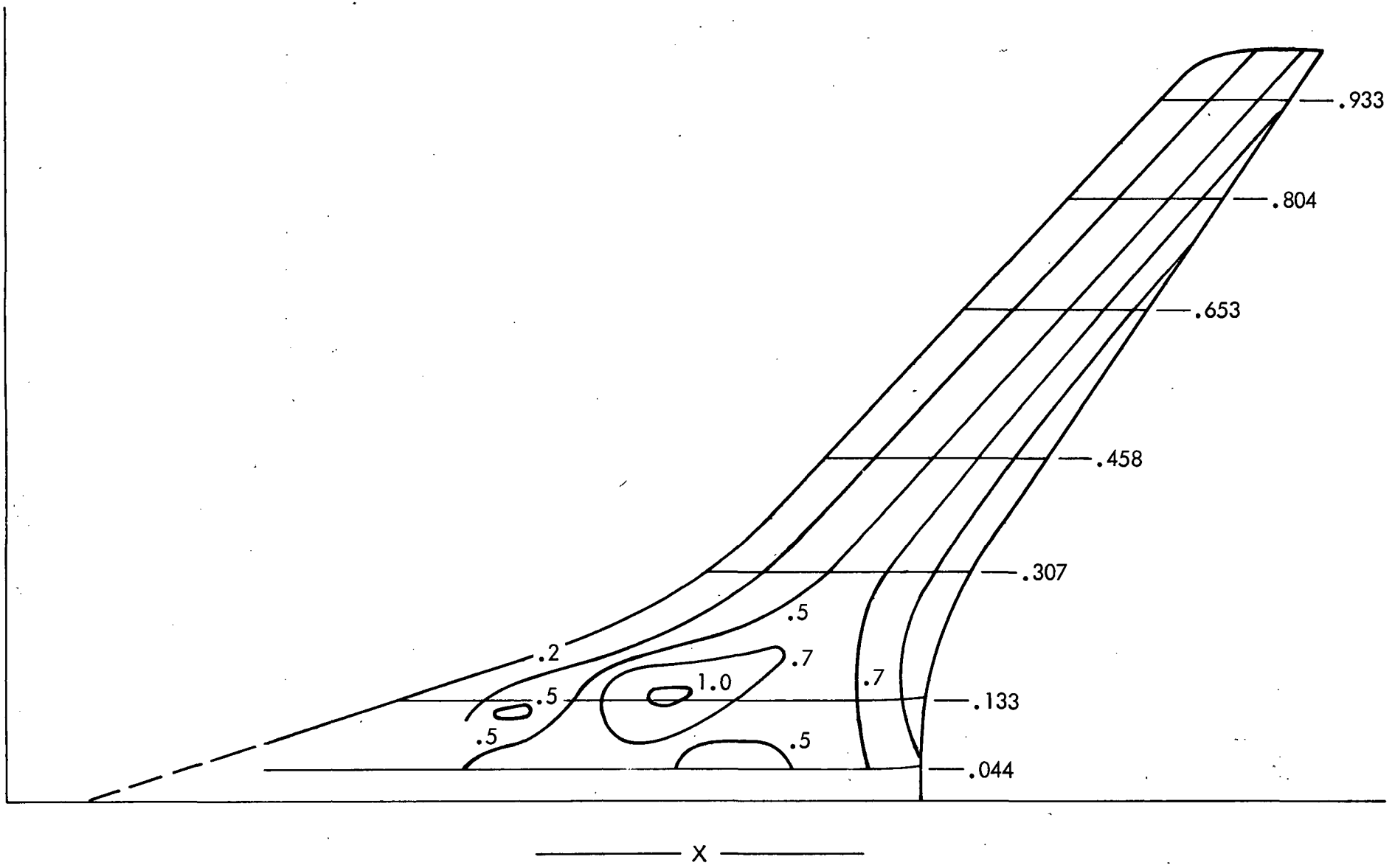

Figure 23. Boundary-Layer Thickness Contours (δ in inches)
M = 0.50, Upper Surface

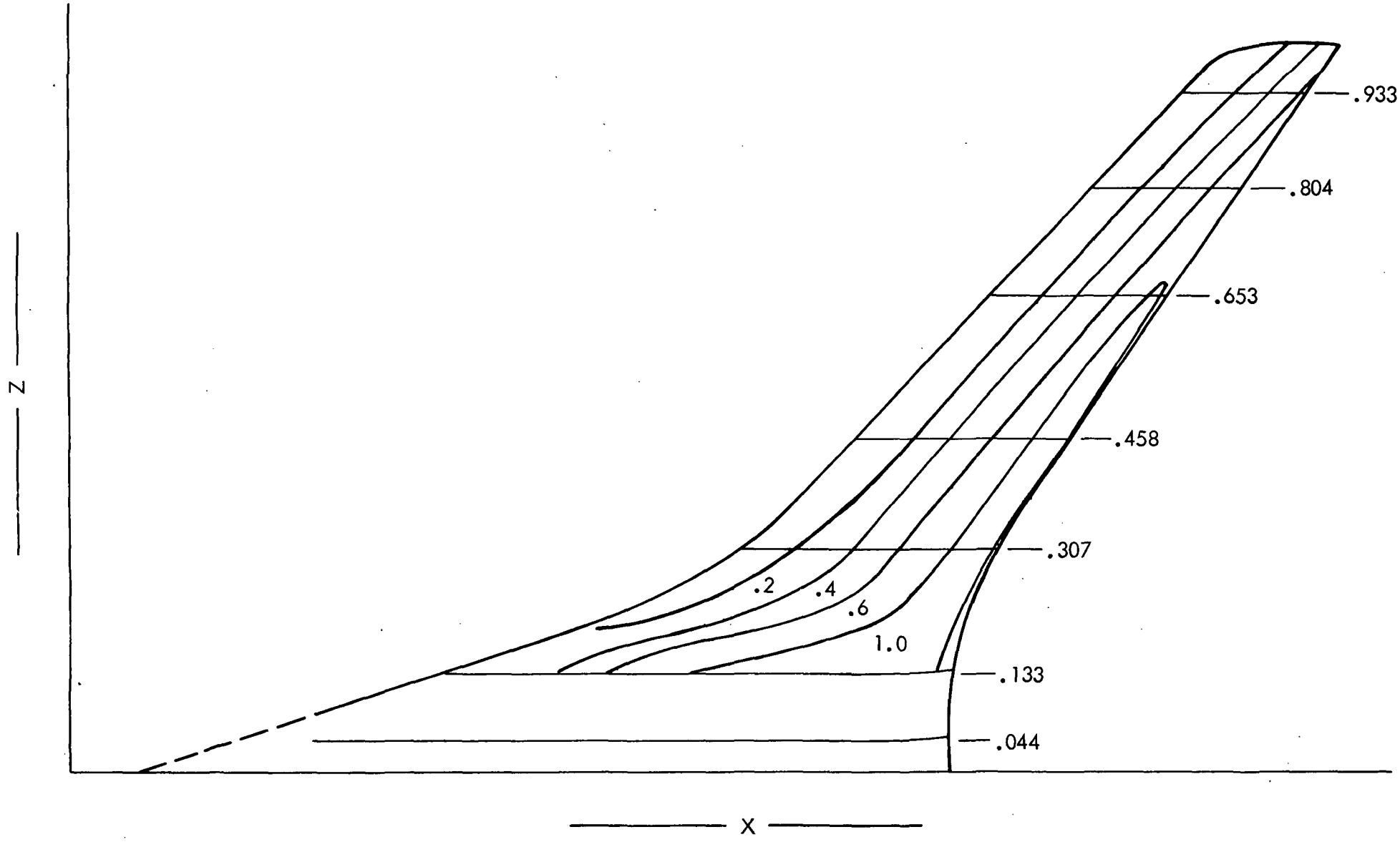

Figure 23. (Cont'd.) M = 0.50, Lower Surface

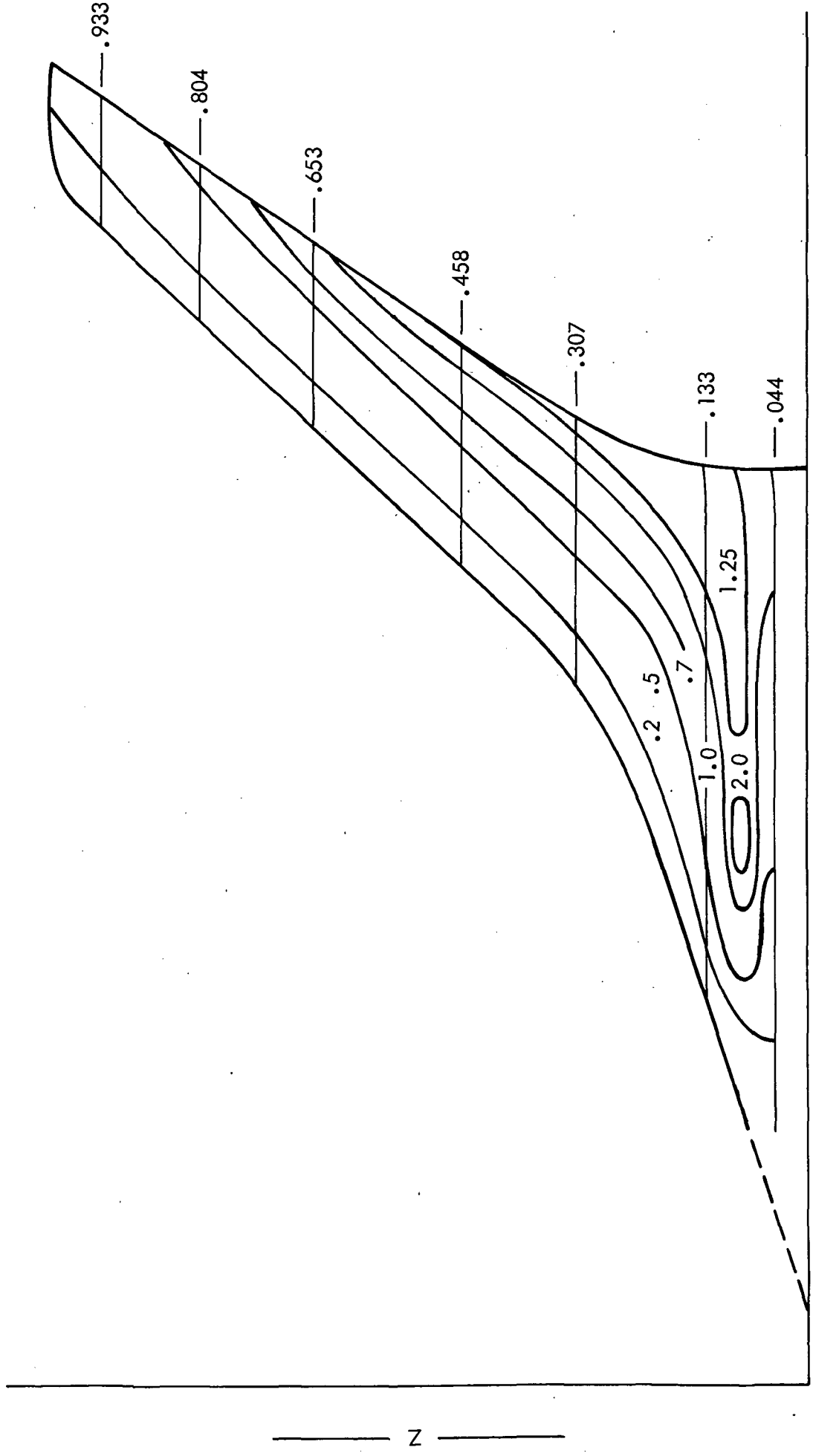

Figure 23. (Cont'd.) M = 0.99, Upper Surface

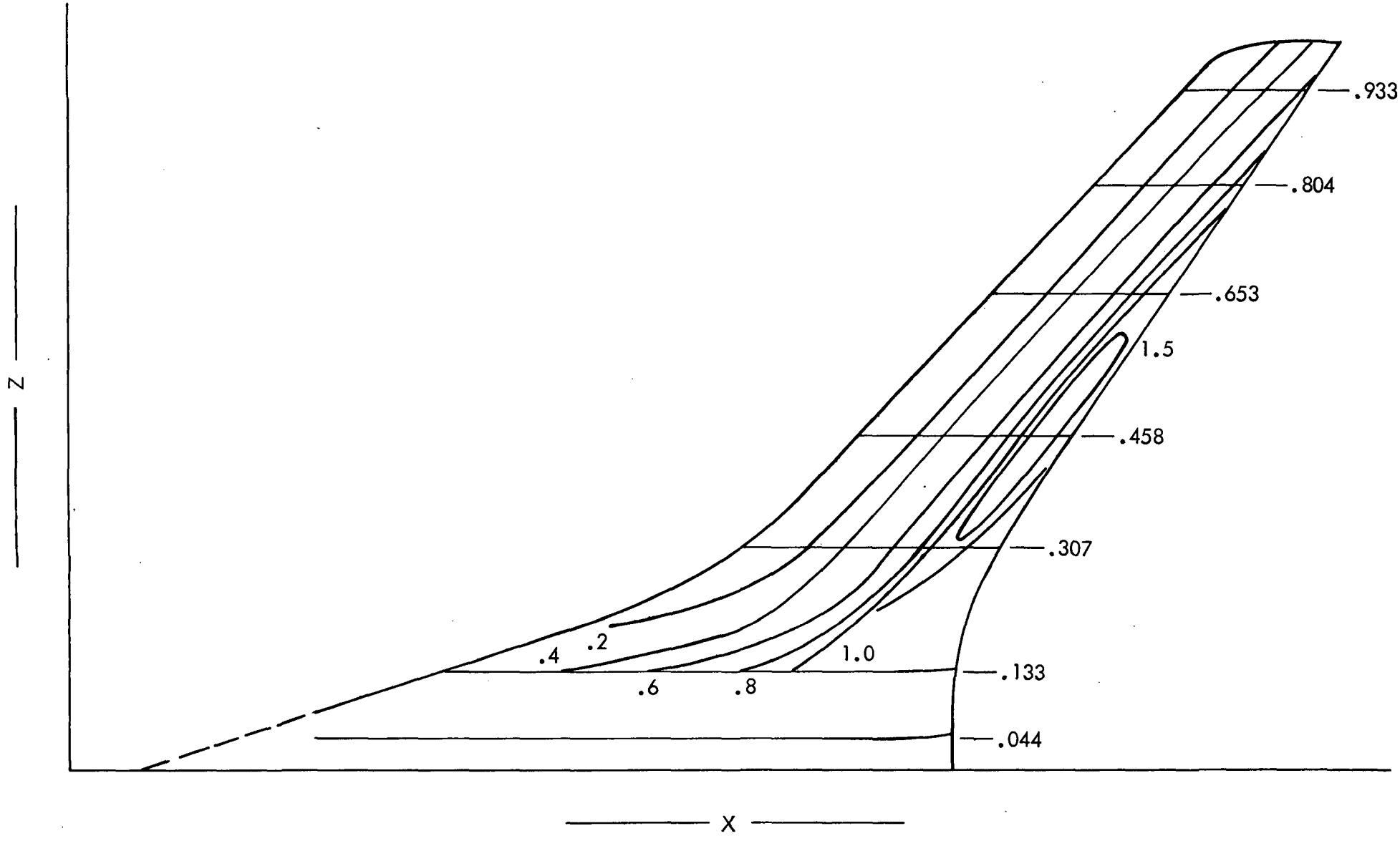

Figure 23. (Cont'd.) M = 0.99, Lower Surface

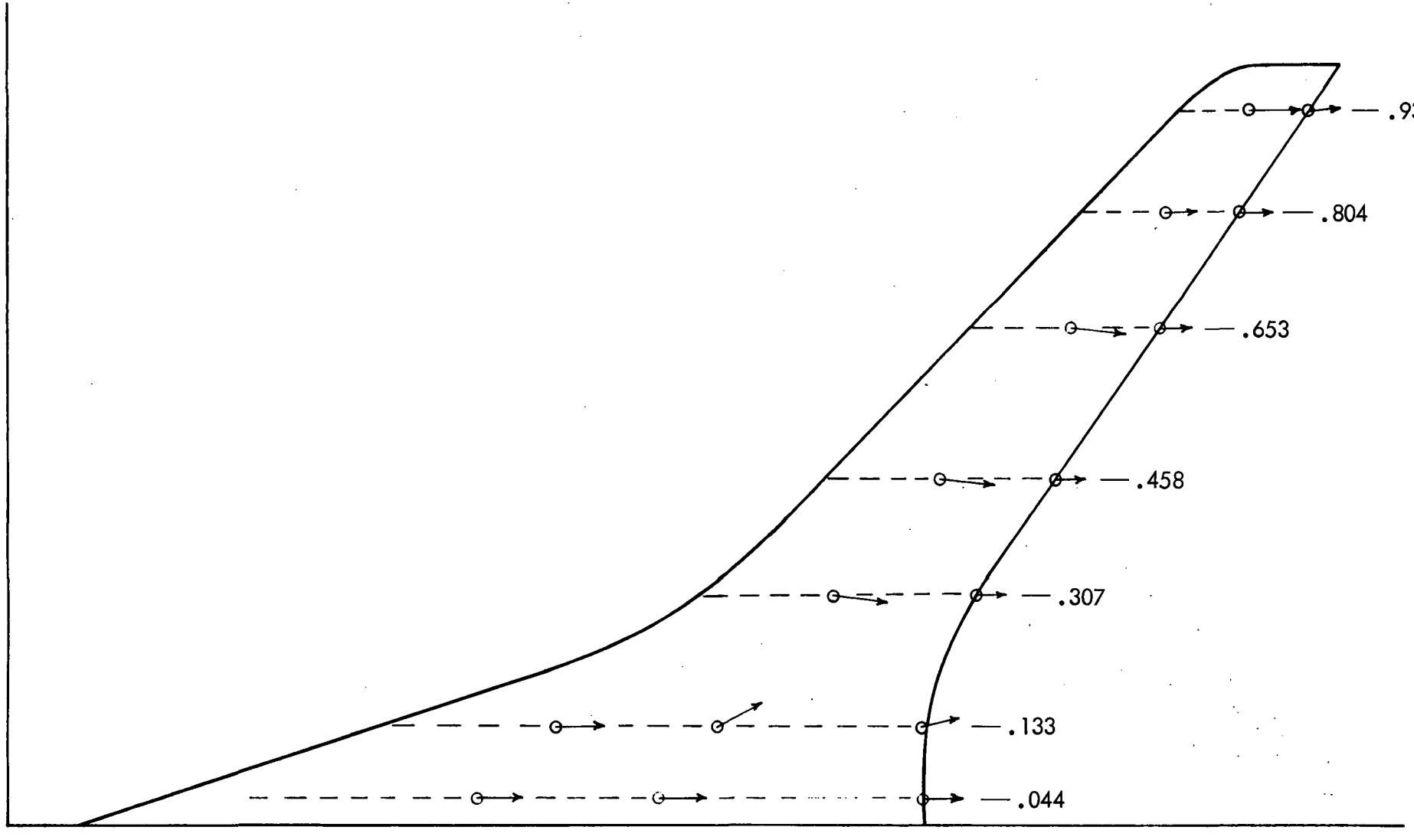

Figure 24. Skin-Friction Vectors
M = 0.50, Upper Surface

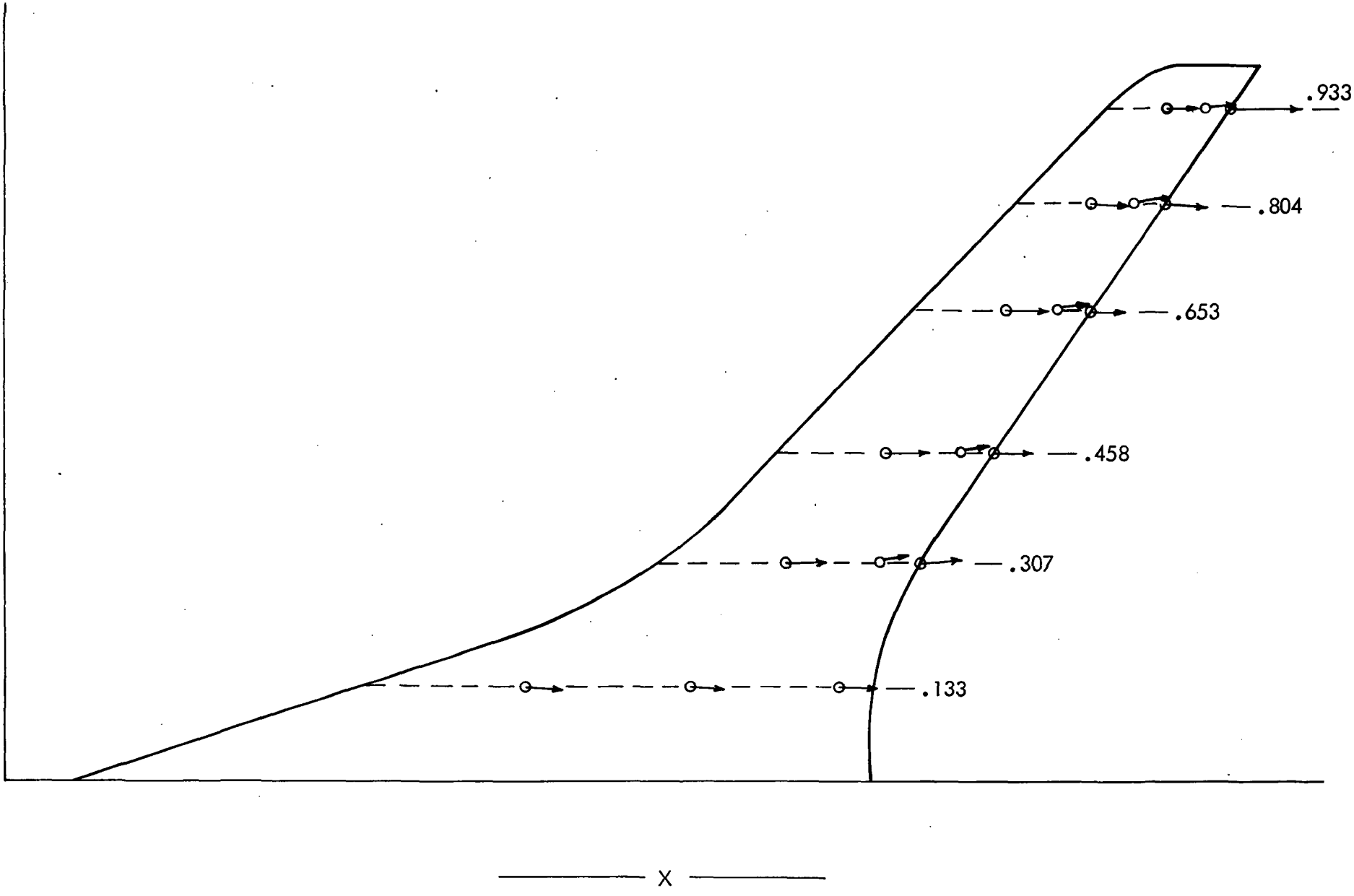

Figure 24. (Cont'd.) M = 0.50, Lower Surface

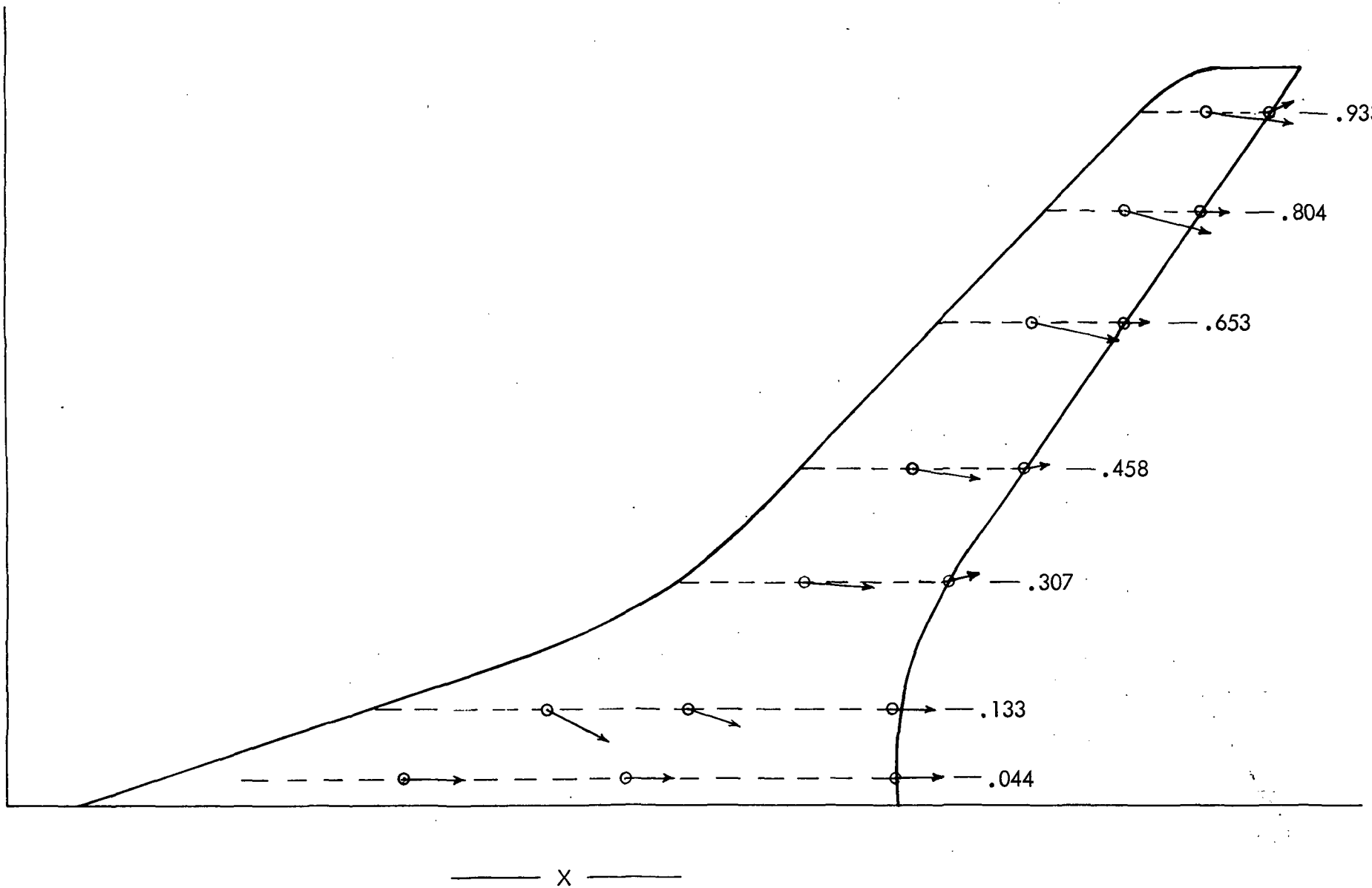

Figure 24. (Cont'd.) M = 0.99, Upper Surface

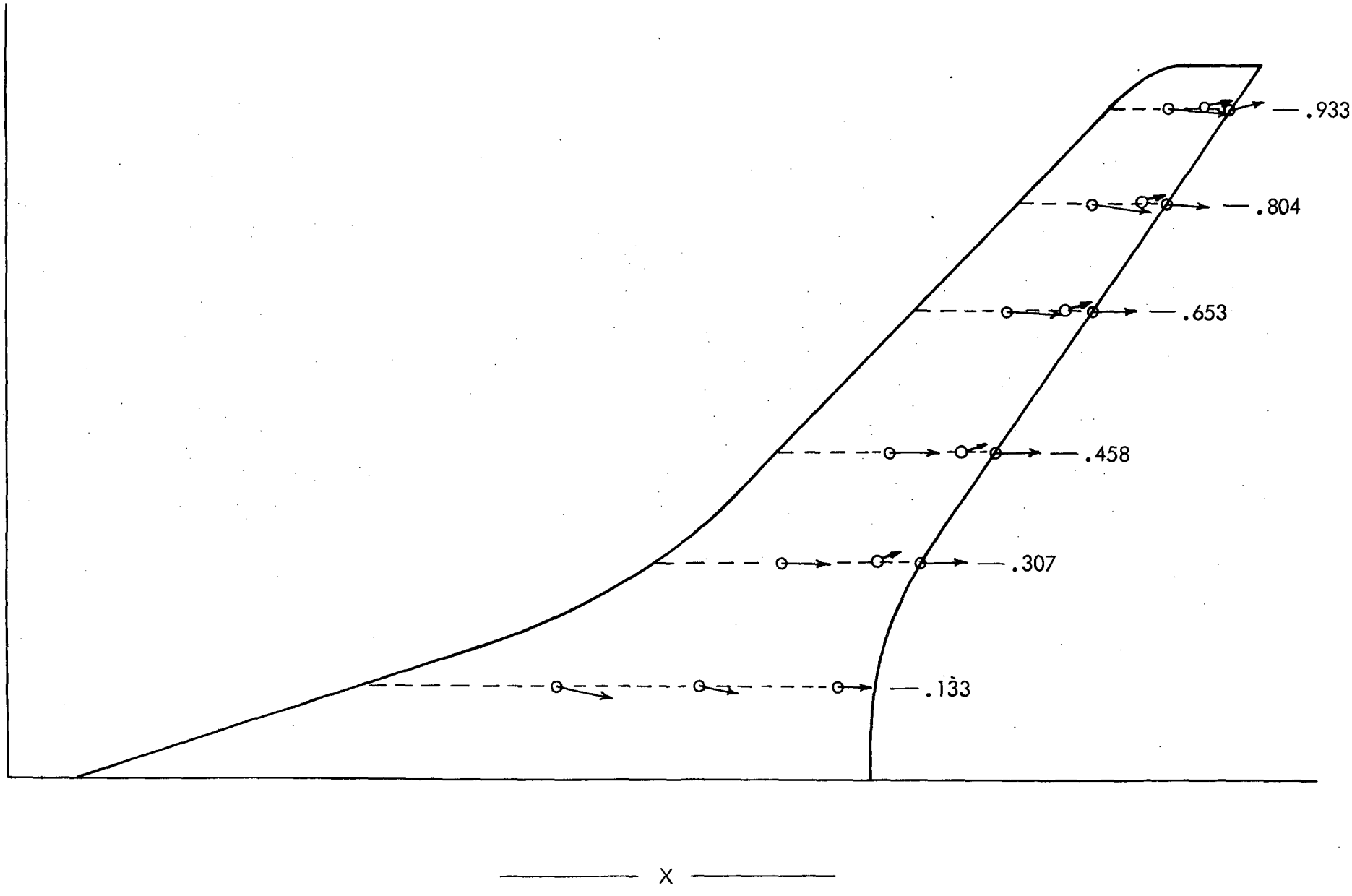

Figure 24. (Cont'd.) M = 0.99, Lower Surface